1-1-2018

Applications Of Effective Field Theories To New Physics

Derek Edward Hazard
Wayne State University,

APPLICATIONS OF EFFECTIVE FIELD THEORIES TO NEW PHYSICS

by

DEREK E. HAZARD

DISSERTATION

Submitted to the Graduate School

of Wayne State University

in partial fulfillment of the requirements

for the degree of

DOCTOR OF PHILOSOPHY

2018

MAJOR: Physics

Approved By:

_____

Advisor

_____

_____

_____

DEDICATION

In dedication to my friends and family
who have always believed in and encouraged me
even when I did not believe in myself ...

... and to my grandmother, Phyllis Trundle;
may you always be with me in spirit.

ACKNOWLEDGEMENTS

I would like to thank my adviser, Prof. Alexey A. Petrov, for his patient guidance during the past six years. Without you this would certainly not be possible. I am thankful you asked me to be your protégé. I also would like to thank Prof. Gil Paz who has taught many of the courses that set me up for future success. It is hard to say how many countless hours I spent in your office asking questions about quantum field theory. I am grateful to the other members of my committee, Prof. Sean Gavin, Prof. Edward Cackett, and Prof. Ruben Hayraptyan, your participation and help through this process will not be forgotten. Special thanks in particular goes to Prof. Hayrapetyan. Your enthusiastic teaching of Calculus II was integral in setting an awkward high school senior on the path to Doctor of Philosophy in Physics.

TABLE OF CONTENTS

LIST OF FIGURES

LIST OF TABLES

CHAPTER 1: INTRODUCTION AND MOTIVATION

In this chapter we will briefly review the current state of particle physics and our motivations to look for new physics (NP). We begin with a historical overview of particle physics. Then we introduce the Standard Model (SM) and the mechanisms it provides for lepton flavor violating (LFV) decays. After that we introduce the topic of effective field theory (EFT), which will be our tool chest for exploration of NP. Finally we will introduce our specific approach to constraining NP with LFV decays of mesons. The first three sections are included to give a complete and thorough picture, but the reader, especially if (s)he is familiar with the topic may skip straight to Section 1.4 without loss in continuity if desired.

1.1 Historical Overview of Particle Physics

The foundations of modern particle physics that lead to the development of the Standard Model can be traced back to turn of the 20th century [1]; a time even before physicists discovered quantum mechanics. J. J. Thompson's discovery of the electron in 1897 ignited a fire of particle physics discovery that has burned for over a century. Next came Rutherford's scattering experiments that proved the existence of a tiny massive and positively charged atomic core, the nucleus, which was assumed to consist of protons. An atomic model of the hydrogen atom as a single proton orbited by a single electron in 1914 by Niels Bohr was able to predict its spectrum and opened the door for quantum mechanics. Attempts to explain heavier atoms in a similar fashion ran into a problem. The masses of heavier atoms were heavier than could be accounted for by the proton mass alone. Helium is four times the mass of Hydrogen, but should only have two protons. Chadwick solved the problem with the discovery of the neutron in 1932.

Our understanding of the nature of light was also seeing a revolution at this time. In 1900 Planck was working on an explanation of the electromagnetic radiation emitted by a hot object, the so-called black-body radiation, but was left baffled by the results of statistical mechanics. It predicted that an infinite amount of power should be radiated and lead to

what physicists called "the ultraviolet catastrophe." Planck was able to avert disaster by assuming the quantization of electromagnetic radiation, which lead to his empirical rule that the energy of the emitted photons, E, equals a constant h times the radiation frequency ν. Here $h = 6.626 \times 10^{-17}$ is Planck's constant. The quantization of light was explained in 1905 by Einstein. Einstein put forth that when an incoming quantum of light hits a metal surface, it gives up its energy ($h\nu$) to an electron which breaks free. This electron loses an energy w, the work-function of the material, when breaking through the metal surface and emerges with energy $E \leq h\nu - w$. The implication of Einstein's discovery was that maximum electron energy is independent of light intensity, but depends solely on its frequency. Einstein argued that light was quantized by nature. This view was not well received, as the particle theory of light was widely discredited in the 19th century. In 1916 Millikan experimentally proved Einstein's photoelectric effect correct [2], but the issue would not be settled until 1923 when Compton found that the wavelength of light is shifted when scattered from a particle at rest. Compton showed that the shift was governed by $\lambda' = \lambda + \lambda_c(1 - \cos\theta)$, where $\lambda_c = \frac{h}{mc}$ is the Compton wavelength, θ is the scatering angle, λ is the incident wavelength, and λ' is the scattered wavelength. This formula may be found by applying the conservation of four-momentum of the photon and scattering particle before and after the interaction and using Planck's formula for the quantization of energy for light. This was a direct proof of the particle nature of light.

At this point physicists still could not explain how a nucleus of positively charged protons could stay together. The positive charges should repel each proton away from the other. It was assumed there must be another force greater than electromagnetism that binds the protons and neutrons together in the nucleus called the *strong force* (otherwise known as the nuclear force). This force would not be as apparent at macroscopic scales like the electromagnetic force because it has a very short range that limits its influence to the size a nucleus. Yukawa proposed the first significant theory for the strong force in 1934. He assumed that the proton and neutron were attracted to each other by a field and that this

field should be quantized. He predicted that in analogy to the photon there should be a particle that would account for the features of the strong force when exchanged. This particle would have to be heavy because of the short range of the strong force. He calculated that it should be about 300 times the electron mass. Yukawa's particle would come to be known as the meson and by 1937 a candidate fitting his description was found in cosmic ray experiments. Further work would identify that there were not one, but two particles [3, 4]. The first was the pion π, which was indeed Yukawa's meson and the strong force mediator in his theory, but the second was the muon μ, which we now know is a lepton.

A quantum theory of interactions of relativistic particles is now known as quantum field theory. It finds its roots in the 1927 work of Dirac whose famous Dirac Equation, which describes free electrons, had a disturbing problem. For every positive energy solution of the electron, $E = +\sqrt{\vec{p}^2 + m^2}$, there was a corresponding negative solution, $E = -\sqrt{\vec{p}^2 + m^2}$. If a system were to evolve naturally to its lowest energy state, an electron should simply continue on to increasingly negative energy states. Dirac rescued his equation by proposing that there was an infinite sea of electrons occupying the negative energy states and Pauli's exclusion principle prevented the observed electrons from occupying the same negative energy states. Furthermore if enough energy was imparted to a sea electron, then a hole would be formed which might be interpreted as a positive particle. There was no candidate particle to account for these holes, but in 1931 the positron was discovered by Anderson and it had the properties Dirac needed [5]. The infinite electron sea interpretation of the negative energy states eventually gave way to a simpler and more compelling interpretation by Feynman and Stuckelberg. Their formulation interpreted the negative energy electron solutions as the positive energy states of the positron. This dual energy solution in Dirac's equation is an important universal feature of quantum field theory. It means that for every particle there exists an anti-particle with the same mass and opposite electric charge.

The discovery of neutrinos took a parallel track to that of the aforementioned pion, muon, and anti-particles. In 1930 the study of beta decays had a problem. Beta decay is

the transition of a nucleus to a lighter nucleus with one more unit of positive charge and an electron. It is now known that this is actually the conversion of a neutron in the nucleus into a proton, but in 1930 the neutron had not been discovered yet. In a two-body decay such as this, given the rest frame of the decaying nucleus, the decay products should have equal and opposite momenta and the energy of the emitted electrons would be constant. Experiments showed that the electron energies were significantly variable. Pauli proposed that there must be another particle emitted with the electron that was electrically neutral and carried away the missing energy. Fermi presented a successful theory of beta decay that incorporated Pauli's particle and named it the *neutrino*[1]. We now know this beta decay process is a neutron transitioning to a proton, an electron, and an anti-neutrino ($n \rightarrow p^+ e^- \bar{\nu}$).

The neutrino also turned out to be of great importance in understanding the decays of Yukawa's pion π to a muon μ. In the cosmic ray experiments that discovered these two particles Powell's picture of the decaying pion tracks showed the muon moving away in a direction perpendicular to the original pion momentum. This is only kinematically possible if another particle were emitted back-to-back with the muon that would not leave a track (electric charge neutral). It was assumed to be the neutrino and so $\pi \rightarrow \mu + \nu$. Soon thereafter Powell's group announced the discovery of the decay of a muon to an electron and what would turn out to be two neutrinos ($\mu \rightarrow e + \nu_e + \nu_\mu$). They were able to determine that it must be a decay product of at least three particles due to the variability in the electron's momentum and by 1949 the accepted explanation was the emission of two neutrinos with the electron.

The need for direct experimental evidence for the neutrino was still necessary to confirm its existence and quiet skeptics. In 1950 direct evidence was found by Cowan and Reines using nuclear reactor experiments at the Savannah River reactor in South Carolina. They observed inverse beta decay reactions $\bar{\nu} + p^+ \rightarrow n + e^+$ and their results provided clear proof of the neutrino's existence [6]. There was a question as to whether or not the neutrino was

[1] In modern terminology this is actually an anti-neutrino.

its own anti-particle and if so, what was the disinguishing property? The crossed reaction of $\nu + n \rightarrow p^+ + e^-$ would occur at around the same rate as the inverse beta decay reaction. Davis looked at a similar reaction but with the anti-neutrino ($\bar{\nu} + n \rightarrow p^+ + e^-$) and found a null result [7] leading to the conclusion that the neutrino and anti-neutrino are distinct. This conclusion is still under debate as Davis's experiment does not preclude the Majorana fermion model which allows for the neutrino ν to be its own anti-neutrino $\bar{\nu}$ [8].

These results were expected as the law of lepton number conservation was previously proposed by Konopinski and Mahmoud in 1934 [9]. This law states that there is a quantum number L assigned to each lepton. $L = +1$ was for leptons: e^-, μ^-, and ν and $L = -1$ was assigned to anti-leptons: e^+, μ^+, and $\bar{\nu}$. The sum of the lepton numbers before an interaction must equal the sum after. Thus the simplest explanation for the property that distinguishes neutrinos from anti-neutrinos is the lepton number, L. Lepton number was relatively successful, but it could not explain why there was no experimental observation of $\mu \rightarrow e\gamma$, which was allowed under this formulation of lepton conservation and charge conservation. In the late 1950s and early 1960s it was proposed that there were actually electron neutrinos ν_e and muon neutrinos ν_μ and that law of lepton conservation should be extended such that there was electron number conservation L_e and muon number conservation L_μ. This allowed for an accounting of all forbidden and allowed processes.

The two neutrino hypothesis was tested in 1962 at Brookhaven. Lederman, Schwartz, Steinberg, et. al. used the anti-neutrinos from the decay of $\pi^- \rightarrow \mu^- + \nu_\mu$ to register 29 counts of the interaction $\nu_\mu + p^+ \rightarrow \mu^+ + n$ and zero for $\nu_\mu + p^+ \rightarrow e^+ + n$ [10]. If there was only one neutrino there should be equal rates for both decays and this proved there was more than one neutrino.

The years between 1947 and 1961 also saw a great number of experimental discoveries of both mesons (e.g. K, ρ, ω, ϕ, η, etc.) and baryons (e.g. Λ, Σ, Ξ, Δ, etc.). This period saw the introduction of the conservation of baryon number B by Stückelberg. Similar to lepton number it assigns a value of $B = +1$ to baryons (i.e. p, n) and $B = -1$ to anti-baryons (i.e.

$\bar{p}$, $\bar{n}$). These heavy baryons and mesons became known as strange particles first because they were unexpected, but also because they were produced in great numbers on the timescale of 10^{-23} seconds and decayed slowly on the scale of 10^{-10} seconds. The difference in time scales suggested a different mechanism of production and decay to Pais and the others [11]. We now know that their production is due the the strong force and their decay is the action of the weak force.

In 1953 Gell-Mann [12] and Nishijima [13] proposed another conservation law to provide a simple explanation for the production of strange particles in pairs. Each particle was assigned a new property of strangeness, S, that was conserved in strong interactions, but not in weak ones.

The situation for particle physics in 1960 seemed quite disorganized and physicists were looking for a way to organize all of the particles they found. Order was achieved by Gell-Mann and Ne'eman with the eight-fold way in 1961. They ordered baryons and mesons into their own hexagonal arrays of eight particles based on their electric charges and strangeness. Hexagonal arrays are only one example. Other geometric shapes were allowed such as the triangular array for organizing the heavier baryons (Δ, Σ, Ξ, and Ω) known as the bayron decuplet. When Gell-Mann organized the decuplet it lead him to predict a missing particle, the Ω^-, which was later found in experiment and reinforced the correctness of the eight-fold way. As more particles were discovered, they all found their place into an eight-fold way supermultiplet.

People still wondered why hadrons[2] should be organized in these geometric patterns. The explanation would come in 1964 from Gell-Mann and Zweig independently. They each proposed that hadrons were composed of elementary constituent particles to which Gell-Mann gave the name *quark*. There were three different flavored quarks in the theory (u, d, s) and they formed a triangular eight-fold way pattern. The u and d quarks had a strangeness of zero and the s quark had a strangeness of one. The d and s quarks had an electric charge

[2]A particle that experiences strong force interactions. Baryons and mesons are hadrons.

of $Q = -\frac{1}{3}$, while the u quarks had charge $Q = \frac{2}{3}$. Each of these quarks has an anti-quark counterpart with opposite charge and strangeness.

It is these quarks and anti-quarks that form baryons and mesons. Baryons (anti-baryons) are constructed of three quarks (anti-quarks). Mesons consist of a quark and an anti-quark. Using these three quarks one can generate the ten Δ, Σ, Ξ, and Ω type baryons in the baryon decuplet or the eight baryons in the baryon octet of type n, p, Σ, Λ, and Ξ and maintain the appropriate charge and strangeness. One can also form the eight mesons of the meson octet of type π, η, and K plus a ninth meson, η', to form a meson nonet. The quark model can reproduce all of the eight-fold way supermultiplets. Despite this success the quark model had a flaw. Experiments could not produce an individual quark, which lead to the ad hoc assumption that quarks are confined within baryons and mesons. The mechanism of this confinement is still an open question today.

Despite the difficulty of being confined inside hadron, quarks are not completely inaccessible to experiment. The interior of hadrons may be explored the same way Rutherford explored the interior of the atom. Deep inelastic scattering experiments that fired high energy electrons, neutrinos, and eventually protons were performed in the late 1960s and early 1970s and found that hadrons were mostly empty space. Ocassionally the incident partical would back scatter indicating they hit a small lump of matter. Protons appeared to have three lumps, which supports the quark model hypothesis.

The last point of contention for the quark model was the appearance that quarks violated the Pauli exclusion principle. The principle states that two identical fermions cannot occupy the same state, but hadrons such as the Δ^{++} consist of three u quarks in the same state. As u quarks are fermions and can only have spin $\pm 1/2$, this would imply a violation of the Pauli exclusion principle. It was proposed by Greenberg in 1964 that quarks come in three "colors" (r = red, g = green, and b =blue) in addition to three flavors [14]. The colors are an analogy to the optical spectrum. To form a hadron, one must use a colorless combination of quarks. This can be a combination of quarks with equal parts of color (rgb) which form baryons,

anti-color ($\bar{r}\bar{g}\bar{b}$) which form anti-baryons, or color and anti-color ($r\bar{r}$, $g\bar{g}$, $b\bar{b}$) which form the mesons. By introducing color we are able to avoid violating Pauli's exclusion principle in the Δ^{++} for example because the two u quarks are not identical due to their difference in color. The same concept applies to the all hadrons.

Because of the seemingly thin arguments for quark confinement and color, physicists were skeptical of the the quark model. This would begin to change with the discovery of the extremely heavy neutral J/ψ meson in 1974 by two independent groups [15]. The first was lead by Ting who named it J and the second was lead by Richter who called it ψ. What made the J/ψ particularly remarkable was that its lifetime was of order 10^{-20}; a thousand times longer than hadrons in a similar range of mass. They had clear evidence of some new physics.

This new physics was explained in terms of a fourth quark, the charm c quark and its anti-quark, from which the bound state $J/\psi = (c\bar{c})$ is made. The idea of a fourth quark had been put forth in previous years by Bjorken and Glashow [16] for various reasons. One of these reasons was the creation of an aesthetically pleasing parallel between the number of quarks and leptons. At that time there were four known leptons: μ, ν_μ, e, and ν_e; and three known quarks: u, d, and s. The c quark would make this four. This ready made explanation of J/ψ and the implication that there should be other charmed hadrons did much to legitimize the quark model. This lead to a period of new baryon and meson discoveries in the 1970s-1980s such as the D^0 and D^+ in 1976 [17] and the D_s^+ in 1977 [18].

In 1975, the τ lepton and its associated neutrino were discovered increasing the number of leptons to six [19]. Glashow's lepton quark symmetry was ruined, but not for long because the heavy neutral Υ meson was discovered in 1977 [20]. The quark model explained this as a quark anti-quark bound state composed of a fifth quark, the beauty b quark. In 1983 the first beauty mesons, $\bar{B}_0$ and B^- were found by CLEO. [21]. B-physics studied at B-factories such as Belle and BaBar has been a very rich area of study ever since and as we will see important to our research as well.

Finally in 1995 the much anticipated top t quark was found by the Tevatron [22] and restored Glashow's symmetry with a total of six quarks and six leptons. This is not the last part of the story before we reach modern day physics and the Standard Model (SM).

The last part of our tale is the story of the intermediate vector bosons. When Fermi first provided his theory of beta decays in 1933, he treated it as a contact interaction. He used an effective interaction approach not dissimilar to the one we will use later. Because this interaction occurred in the theory at a single point, no mediator particle was necessary. This approximation approach worked well at low energies, but would need to be replaced by a full theory at high-energies. This would require a mediator particle called an intermediate vector boson.

The electro-weak theory of Glashow, Weinberg, and Salam also called the GWS theory was able to predict that there are three intermediate vector bosons for the weak force ($W^{\pm}$ and Z) with masses of $m_W = 82 \pm 2$ GeV and $m_Z = 92 \pm 2$ GeV [23]. These W and Z bosons were discovered in 1983 at the European Organization for Nuclear Research (CERN) by Carlo Rubbia's group with measured masses of $m_W = 80.403 \pm 0.029$ GeV and $m_Z = 91.188 \pm 0.002$ GeV. This was a great achievement for physicists and further confirmed the validity of what had become known as the Standard Model.

We had the photon γ as the the mediator of the electromagnetic force, the $W^{\pm}$ and Z to mediate the weak force, but what about the strong force? In view of the quark model and the fact that mesons are not elementary particles, but rather composite structures, Yukawa's pion no longer looked like the fundamental mediator candidate we needed to mediate the strong force. Physicists instead asked what is the mediator of the strong force that binds quarks together to form hadrons? This intermediate vector boson was the gluon, which also carries color and therefore cannot exist as an isolated particle. Despite this they can and have been probed indirectly via deep inelastic scattering experiments and studies of inelastic scattering at high energies.

There was still one very important part of the SM that was missing. That was the Higgs

mechanism and its associated Higgs boson; the only scalar particle in the Standard Model. The Higgs mechanism was developed by Peter Higgs as well as Anderson, Brout, Englert, Guralnik, Hagen, Kibble, Landau, and 't Hooft between 1962 and 1971 [24, 25]. It was of great importance in completing the SM as it is the mechanism by which the intermediate gauge bosons and SM fermions attain their masses. Without the Higgs mechanism the SM Lagrangian would not contain the mass terms for the gauge bosons and SM fermions, which we know are massive from experiment and would represent a major flaw in the SM if not present. The experimental discovery of a 125 GeV scalar particle now believed to be the Higgs boson at CERN's Large Hadron Collider (LHC) provided experimental verification of the existence of the Higgs boson and completed the SM in 2012 [26].

The work of the past century has given us today's Standard Model, which consists of six leptons, six quarks, four mediators, and the Higgs boson from which we may build the universe. There are clear indications that the SM is not a complete theory. It has difficulty explaining baryonogenesis, which is the process that produced the imbalance of matter an anti-matter in the Universe, and provides no viable candidate for dark matter. These are a couple of reasons why we search for new physics. It is possible that the the SM is itself an effective theory; a low-energy approximation of a more fundamental and complete theory [27]. It is with this idea in mind that we can attempt to probe NP.

1.2 The Standard Model

The Standard Model is the culmination of particle physicists' hard work throughout the 20th Century and is based on the $SU(3) \otimes SU(2) \otimes U(1)$ gauge group. From the view of the SM, all matter is made from three categories of particles: leptons, quarks, and mediators. The particle content of the SM is summarized in Table 1.1. The quarks and leptons are both separated into three generations or families. Each generation is organized by the mass of the particles with the lowest masses in the first generation and the highest masses in the third generation [1].

In the lepton sector we have six distinct spin-1/2 fermion particles. Each generation

	generations of fermions			gauge	scalar
	I	II	III	bosons	bosons
quarks	u	c	t	g	h
	up	charm	top	gluon	Higgs
	d	s	b	γ	
	down	strange	bottom	photon	
leptons	e	μ	τ	Z	
	electron	muon	tauon	Z-boson	
	ν_e	ν_μ	ν_τ	W	
	e-neutrino	μ-neutrino	τ-neutrino	W-boson	

Table 1.1: Elementary particles of the Standard Model [1]

contains a $Q = -1$ electrically charged lepton (e.g. e, μ, τ) and its associated neutral neutrino partner. The quark sector also contains six different flavored spin-1/2 fermion particles. The quarks have electric charges of $Q = -1/3$ for d, s, and b; and $Q = 2/3$ for u, c, and t. For each of these quarks and leptons there are antiparticles of opposite charge. In addition to having six flavors, the quarks come with three different color charges: red, green, and blue, which are named in analogy to the primary colors of visible light [1].

There are four mediator particles that mediate the electromagnetic, weak, and strong forces. The electromagnetic force is mediated by the photon γ, which is an electrically neutral massless spin one vector boson. The weak force is mediated by the massive spin one W and Z vector bosons. The W boson can have an electric charge of $Q = \pm 1$ while the Z boson is electrically neutral. The final spin one vector boson mediator particle is the massless and electrically neutral gluon g, which mediates the strong force. While the gluon is electrically neutral, it is not color neutral. It is a bi-colored particle which carries both color and anti-color. Ultimately this means that gluons come in eight different possible color states. The gluon makes for a more complicated (some might say more interesting) mediator than the photon as it not only mediates the strong force, but also interacts with the strong

force (i.e. itself).

The final piece of the SM puzzle is the scalar Higgs boson. The Higgs boson comes as a consequence of the Higgs mechanism, the means by which the W and Z gauge bosons and all of the SM fermions obtain mass. The SM is able to predict the masses of the W and Z gauge bosons, but not the fermions, which must be determined empirically from experimental data.

All of the particle interactions may be mathematically described by the Lagrangian of the Standard Model [24, 25, 28]

$$\begin{aligned}\mathcal{L}_{SM} = &-\frac{1}{4}\left(\vec{W}^{\mu\nu}\cdot\vec{W}_{\mu\nu} + B^{\mu\nu}B_{\mu\nu} + G_a^{\mu\nu}G^a_{\mu\nu}\right)\\ &+\bar{L}\gamma^\mu\left(i\partial_\mu - g\frac{1}{2}\vec{\tau}\cdot\vec{W}_\mu - g'\frac{Y}{2}B_\mu\right)L + \bar{R}\gamma^\mu\left(i\partial_\mu - g'\frac{Y}{2}B_\mu\right)R\\ &+\left|\left(i\partial_\mu - g\frac{1}{2}\vec{\tau}\cdot\vec{W}_\mu - g'\frac{Y}{2}B_\mu\right)\phi\right|^2 - V(\phi)\\ &+g_s\bar{Q}G^a_\mu t^a Q - G_1\bar{L}\phi R - G_2\bar{L}\phi_c R + h.c.\ .\end{aligned} \tag{1.1}$$

The first line of Eq. (1.1) represents the kinetic energies and self interactions of the W, Z, γ and g mediators. Where $\vec{W}^{\mu\nu}$, $B^{\mu\nu}$, and $G_a^{\mu\nu}$ are the field strength tensors for the weak isospin, weak hypercharge, and QCD respectively. The second line of Eq. (1.1) represents the kinetic energies of the quarks and leptons and their interactions with the W, Z, γ mediators. $\vec{W}_\mu$ and B_μ are the $SU(2)$ and $U(1)$ gauge fields. Y is the hypercharge for $U(1)$, $\vec{\tau}$ are the Pauli matrices, and g and g' are the electroweak coupling constants. The L and R represent the left-handed doublets and right-handed singlets for leptons and quarks

$$\begin{aligned}L &= \begin{pmatrix}e\\ \nu_e\end{pmatrix}_L, \begin{pmatrix}\mu\\ \nu_\mu\end{pmatrix}_L, \begin{pmatrix}\tau\\ \nu_\tau\end{pmatrix}_L, \begin{pmatrix}u\\ d\end{pmatrix}_L, \begin{pmatrix}c\\ s\end{pmatrix}_L, \begin{pmatrix}t\\ b\end{pmatrix}_L,\\ R &= e_R,\ \mu_R,\ \tau_R,\ u_R,\ d_R,\ c_R,\ s_R,\ t_R,\ b_R.\end{aligned} \tag{1.2}$$

In line three of Eq. (1.1) are the terms that represent the couplings and masses of the

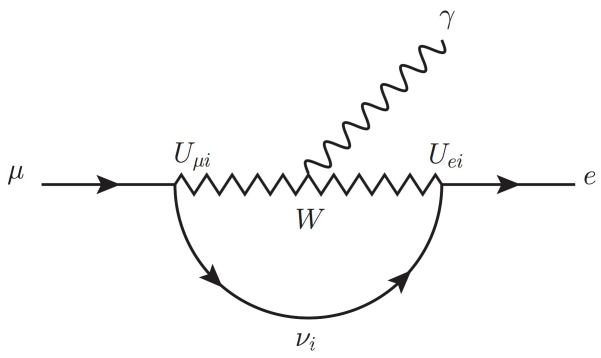

Figure 1.1: One loop diagram for the $\mu \to e\gamma$ decay mediated by neutrinos [30].

W, Z, γ, and the Higgs. Here ϕ is that Higgs scalar doublet and $V(\phi)$ is the Higgs potential. The last line of the SM Lagrangian describes the interactions of the quarks and gluons and the mass terms of fermions as well as their couplings to the Higgs boson. The constant g_s is the strong coupling constant, Q is the quark field spinor, and t^a represents the Gell-Mann matrices where $a = 1$–8. Finally, G_1 and G_2 represent the appropriate Yukawa couplings and ϕ_c is another Higgs doublet constructed from ϕ by $\phi_c = -i\tau_2\phi^*$. The ϕ_c Higgs doublet is required to generate the masses of the upper members of the quark doublets.

Using this Lagrangian one may in principle calculate any physically allowed interaction for the SM degrees of freedom. This of course is not a complete picture of particle physics as there is much evidence for new physics. One clear and important example is neutrino oscillations, which imply massive neutrinos [1, 29]. In a pure SM neutrinos are massless and this leads to lepton family number conservation and therefore no neutrino oscillations or flavor changing neutral currents (FCNCs) for charge leptons (e.g. $\mu \to e$). This is not the case and so with a small extension of the SM to include neutrino masses, we generate FCNCs for charged leptons at loop level, Fig. (1.1) [30, 31, 32].

The branching ratio of this transition is [33]

$$\mathcal{B}(\mu \to e\gamma) \simeq \frac{\Gamma(\mu \to e\gamma)}{\Gamma(\mu \to e\nu\bar{\nu})} = \left(\frac{3\alpha}{32\pi}\right)\left(U_{\mu 3}U_{e3}^*\frac{\Delta m_{31}^2}{M_W^2} + U_{\mu 2}U_{e2}^*\frac{\Delta m_{21}^2}{M_W^2}\right)^2 \lesssim 10^{-54} \qquad (1.3)$$

Here α is the electromagnetic coupling constant, $U_{\ell i}$ is a Pontecorvo-Maki-Nakagawa-Sakata (PMNS) matrix element, and $\Delta m_{ij}^2/m_W^2$ is the ratio of the difference between squared neutrino masses, $\Delta m_{ij}^2 \equiv m_{\nu_i}^2 - m_{\nu_j}^2$, and the W-boson mass squared. From solar neutrino and reactor experiments we know $\Delta m_{31}^2 \simeq 2 \times 10^{-3}$ eV^2 and $\Delta m_{21}^2 \simeq 8 \times 10^{-5}$ eV^2 [34]. Taking the ratio of this to m_W^2, where $m_W = 80$ GeV, reveals that $\Delta m_{31}^2/m_W^2 \sim 10^{-25}$ and $\Delta m_{21}^2/m_W^2 \sim 10^{-26}$. Therefore it is ultimately the ratio $\Delta m_{ij}^2/m_W^2$ that causes this mechanism of charged lepton flavor violation (CLFV) to be highly suppressed as shown in Eq. (1.3). If we see CLFV, it will not be a SM process, but instead some form of new physics (NP).

1.3 Effective Field Theory

The effective field theory (EFT) approach is a rich and interesting topic with applications throughout physics. Entire books have been written about it (e.g. [27]). Here we summarize only the most general and relevant details required for the reader to gain a basic understanding of its application in the following Chapters.

EFTs take advantage of the naturally occurring separation of scales that appear in physics. One would not find it practical to describe the position and velocity of an automobile using quantum mechanics, which is best equipped to describe these observables on the scale of particles not cars. That is not to say that quantum mechanical principles are not present at macroscopic scales, just that their effects are averaged over so much that we do not perceive them. EFT uses this separation of scales to its advantage [27].

The only degrees of freedom that are relevant to the problem one is attempting to understand are the ones necessary to perform the calculation. For our work this means that only fields that are below the scale of particle physics that we probe should remain in the theory. The removed particles are said to be integrated out in reference to the formal procedure from the path integral formulation of quantum field theory. In practical calculations, such as our work, the formal procedure is unnecessary. The integrated out particles do not disappear in entirety. Their participation in interactions is limited by quantum theory to creation and

destruction on very short distance scales. A classic example of an EFT is the Fermi theory of beta decay $n \to pe\nu_e$ in which the W-boson is integrated out of the theory [25, 27].

Our application of effective field theory will deal with infrared or low energy degrees of freedom. The EFT is mathematically described by an effective Lagrangian, which contains local operators that are written in terms of the available infrared degrees of freedom. So long as this Lagrangian contains the most general set of operators allowed under the symmetries of the full theory, the S-matrix elements derived from it will also be the most general possible. This would be a great number of operators (infinite in general) and so we must employ a proper power counting scheme to organize the operators to avoid calculating an infinite number of contributions [27].

The relevant power counting scheme for our purposes is simply to count the operator dimension. These operators form an infinite series of increasingly higher dimension with each term in the series associated with increasing powers of $1/\Lambda$. Λ being the scale associated with the UV complete theory described at low energies by the effective Lagrangian

$$\mathcal{L} = \mathcal{L}_{\text{dim } 4} + \frac{\mathcal{L}_{\text{dim } 5}}{\Lambda} + \frac{\mathcal{L}_{\text{dim } 6}}{\Lambda^2} + \cdots . \tag{1.4}$$

Because the scale Λ is much larger than the low energy scale at which we are working with the effective theory, we may neglect the higher dimension terms as corrections. Although the series in Eq. (1.4) is infinite, the individual terms $\mathcal{L}_{\text{dim } i}$ contain a finite number of operators of dimension i. Each of these operators would be multiplied by an unknown coefficient called a Wilson coefficient (WC). If the complete UV theory is known, these coefficients may be calculated by a process known as *matching*. This is because one sets equal or matches the results of the full and effective theories.

In many cases the full UV complete theory is unknown and although we may not be able to find the Wilson coefficients through matching, we do know that the higher scale physics is encoded upon them. We can therefore learn about the UV complete theory using empirical data from experiments to calculate or constrain the numerical values of the WCs.

1.4 Lepton Flavor Violating Decays Using Standard Model Effective Field Theory

Flavor-changing neutral current (FCNC) interactions serve as a powerful probe of physics beyond the standard model (BSM). Since no operators generate FCNCs in the Standard Model at tree level, new physics degrees of freedom can effectively compete with the SM particles running in the loop graphs, making their discovery possible. Of course this is only true provided the BSM models include flavor-violating interactions [35, 36][3].

The observation of charged lepton flavor violating (CLFV) transitions would provide especially clean probes for new physics. This is because as we saw in Sect. 1.2 in the Standard Model with massive neutrinos, the CLFV transitions are suppressed by the powers of $\Delta m_{ij}^2/m_W^2$, which renders the predictions for their transition rates vanishingly small, e.g. $\mathcal{B}(\mu \to e\gamma)_{\nu SM} \sim 10^{-54}$ [33]. There are indeed many well-established new physics models (see, e.g. [37, 38, 39, 40, 41]) that meet this opportunity and predict charged lepton flavor violating (CLFV) transition rates that are significantly larger than the Standard Model rates [37].

Currently operating and future B-factories, such as LHCb and Belle-II, will be accumulating significant amounts of beauty and charm decay data. These large data sets will be quite useful in studies of the decay rates of bottomonium and charmonium and the extremely small decay rates of B and D mesons, which could probe new physics (NP) at unprecedentedly high energy scales. In particular, studies of vector and pseudoscalar meson ($M = V, P$) decays such as: $V = \Upsilon$, J/ψ, and excited states; and $P = \eta_b$, η_c, B_q^0, $\bar{D}^0$, and K^0 into the final states containing charged leptons of different flavors such as $M \to \ell_1\bar{\ell}_2$ and $M \to \gamma\ell_1\bar{\ell}_2$ could be performed.

A convenient way to describe CLFV transitions in low energy experiments is by introducing an effective Lagrangian, $\mathcal{L}_{\rm eff}$. Such a Lagrangian is a convenient parameterization

[3]The remainder of this document draws directly from journal papers written with Alexey A. Petrov in Refs. [35, 36]

of all new physics models that include lepton flavor violation with the details of the models encoded in the Wilson coefficients of $\mathcal{L}_{\rm eff}$, which are obtained by matching the effective Lagrangian to a given BSM model at the new physics scale Λ [27]. This Lagrangian is required to be invariant under the unbroken symmetry groups $SU(3)_c \otimes U(1)_{\rm em}$ below the electroweak symmetry breaking scale. At the low scale for which a given process occurs the effective operators would exhibit the relevant Standard Model degrees of freedom with the effective operators written completely using quarks ($q_i = b, c, s, u$, and d) and leptons ($\ell_i = \tau, \mu$, and e). In what follows, we assume that top quarks are integrated out of the theory, and we do not consider neutrinos. The effective Lagrangian $\mathcal{L}_{\rm eff}$ that involves CLFV may be written as

$$\mathcal{L}_{\rm eff} = \mathcal{L}_{\ell q} + \mathcal{L}_D + \mathcal{L}_G + \cdots, \tag{1.5}$$

where $\mathcal{L}_D$ is a dipole part, $\mathcal{L}_{\ell q}$ is the part that contains four-fermion interactions, and $\mathcal{L}_G$ is the gluonic part. Here the ellipses denote effective operators that are not relevant for the following analysis. We are interested in the decays of electrically-neutral vector, pseudo-scalar, and scalar mesons to flavor-off-diagonal lepton pairs and other particles. This includes decays of quarkonia, which are $q\bar{q}$ mesons, and the pseudo-scalar mesons B_q^0, $\bar{D}^0$, and K^0, which are composed of one heavy quark and one light quark. The transitions for the B_q^0, $\bar{D}^0$, and K^0 mesons involve FCNC interactions on both quark and lepton sides, while quarkonia only have a FCNC on the lepton side.

The dipole part of Eq. (1.5), which could contribute to two-body vector decays, $V \to \ell_1 \bar{\ell}_2$ and radiative decays $M \to \gamma \ell_1 \bar{\ell}_2$ is written as [42]

$$\mathcal{L}_D = -\frac{m_2}{\Lambda^2} \left[\left(C_{DR}^{\ell_1 \ell_2} \; \bar{\ell}_1 \sigma^{\mu\nu} P_L \ell_2 + C_{DL}^{\ell_1 \ell_2} \; \bar{\ell}_1 \sigma^{\mu\nu} P_R \ell_2 \right) F_{\mu\nu} + h.c. \right]. \tag{1.6}$$

The WCs of $\mathcal{L}_D$ have been well constrained in leptonic LFV decays [37].

Note that it is known that the quark FCNC transitions, at least in the decays of down-type quarks, are dominated by the SM contributions. For instance, the dipole operator

describing $q_1 \to q_2\gamma$ can be written as [46]

$$\mathcal{L}_{\rm peng} = \frac{G_F}{\sqrt{2}} \sum_q \lambda_q^P C_{7\gamma} \frac{\sqrt{4\pi\alpha}}{\pi^2} \frac{m_{q_1}}{2} \bar{q}_1 \sigma_{\mu\nu} \left(1+\gamma_5\right) F^{\mu\nu} q_2 + h.c. \tag{1.7}$$

Here $\lambda_q^P = V_{qq_2} V_{qq_1}^*$ denotes the appropriate Cabibbo-Kobayashi-Maskawa (CKM) matrix elements, m_{q_1} is the heavier quark, and $C_{7\gamma}$ is the corresponding Wilson coefficient [46].

The four-fermion dimension-six lepton-quark part of the effective Lagrangian, Eq. (1.5), takes the form [42]:

$$\begin{aligned}
\mathcal{L}_{\ell q} = -\frac{1}{\Lambda^2} \sum_{q_1,q_2} \Big[& \left(C_{VR}^{q_1 q_2 \ell_1 \ell_2} \ \bar{\ell}_1 \gamma^\mu P_R \ell_2 + C_{VL}^{q_1 q_2 \ell_1 \ell_2} \ \bar{\ell}_1 \gamma^\mu P_L \ell_2 \right) \ \bar{q}_1 \gamma_\mu q_2 \\
& + \left(C_{AR}^{q_1 q_2 \ell_1 \ell_2} \ \bar{\ell}_1 \gamma^\mu P_R \ell_2 + C_{AL}^{q_1 q_2 \ell_1 \ell_2} \ \bar{\ell}_1 \gamma^\mu P_L \ell_2 \right) \ \bar{q}_1 \gamma_\mu \gamma_5 q_2 \\
& + m_2 m_{q_{\rm H}} G_F \left(C_{SR}^{q_1 q_2 \ell_1 \ell_2} \ \bar{\ell}_1 P_L \ell_2 + C_{SL}^{q \ell_1 \ell_2} \ \bar{\ell}_1 P_R \ell_2 \right) \ \bar{q}_1 q_2 \\
& + m_2 m_{q_{\rm H}} G_F \left(C_{PR}^{q_1 q_2 \ell_1 \ell_2} \ \bar{\ell}_1 P_L \ell_2 + C_{PL}^{q_1 q_2 \ell_1 \ell_2} \ \bar{\ell}_1 P_R \ell_2 \right) \ \bar{q}_1 \gamma_5 q_2 \\
& + m_2 m_{q_{\rm H}} G_F \left(C_{TR}^{q_1 q_2 \ell_1 \ell_2} \ \bar{\ell}_1 \sigma^{\mu\nu} P_L \ell_2 + C_{TL}^{q_1 q_2 \ell_1 \ell_2} \ \bar{\ell}_1 \sigma^{\mu\nu} P_R \ell_2 \right) \ \bar{q}_1 \sigma_{\mu\nu} q_2 \quad + \quad h.c. \Big].
\end{aligned} \tag{1.8}$$

Here $m_{q_{\rm H}}$ is the mass of the heavier quark ($m_{q_{\rm H}} = \max[m_{q_1}, m_{q_2}]$) and $P_{\rm R,L} = (1 \pm \gamma_5)/2$ is the right (left) chiral projection operator. In general the Wilson coefficients would be different for different lepton flavors ℓ_i and quark flavors q_i. For a thorough discussion on how to form a complete operator basis see Refs. [42, 43, 44, 45].

We note that the tensor operators (see the last line of Eq. (1.8)) are often omitted when constraints on the Wilson coefficients in Eq. (1.8) are derived (see, e.g. [42]). It should be clarified that those operators are no less motivated than others in Eq. (1.8). For example, they would be induced from Fierz rearrangement of operators of the type $\mathcal{O} \sim (\bar{q}\ell_2)\left(\bar{\ell}_1 q\right)$ that often appear in leptoquark models. Also, as we shall see later, the experimental constraints on those coefficients follow from studying vector meson decays, where the best information on LFV transitions in quarkonia is available.

The dimension seven gluonic operators can be either generated by some high scale physics

or by integrating out heavy quark degrees of freedom [42, 47],

$$\mathcal{L}_G = -\frac{m_2 G_F}{\Lambda^2}\frac{\beta_L}{4\alpha_s}\Big[\Big(C_{GR}^{\ell_1\ell_2}\ \bar{\ell}_1 P_L \ell_2 + C_{GL}^{\ell_1\ell_2}\ \bar{\ell}_1 P_R \ell_2\Big) G^a_{\mu\nu} G^{a\mu\nu} + \Big(C_{\tilde{G}R}^{\ell_1\ell_2}\ \bar{\ell}_1 P_L \ell_2 + C_{\tilde{G}L}^{\ell_1\ell_2}\ \bar{\ell}_1 P_R \ell_2\Big) G^a_{\mu\nu} \widetilde{G}^{a\mu\nu} \quad + \quad h.c.\Big]. \tag{1.9}$$

Here $\beta_L = -9\alpha_s^2/(2\pi)$ is defined for the number of light active quark flavors, L, relevant to the scale of the process, which we take $\mu \approx 2$ GeV. All Wilson coefficients should also be calculated at the same scale. G_F is the Fermi constant and $\widetilde{G}^{a\mu\nu} = (1/2)\epsilon^{\mu\nu\alpha\beta} G^a_{\alpha\beta}$ is a dual to the gluon field strength tensor [42].

The experimental constraints on the Wilson coefficients of effective operators in $\mathcal{L}_{\rm eff}$ could be obtained from a variety of LFV decays (see e.g. [37] for a review). Deriving constraints on those Wilson coefficients usually involves an assumption that only one of the effective operators dominates the result. This is not necessarily so in many particular UV completions of the LFV EFTs, so certain cancellations among contributions of various operators are possible. Nevertheless, single operator dominance is a useful theoretical assumption in placing constraints on the parameters of $\mathcal{L}_{\rm eff}$.

In Chapters 2 and 3 we argue that most of the Wilson coefficients of the effective Lagrangian in Eq. (1.5) for different ℓ_i could be determined from experimental data on quarkonium and heavy pseudoscalar meson (B_q^0, $\bar{D}^0$, and K^0) decays. In particular, we consider two- and three-body decays of the mesons with differing quantum numbers and with quarks of various flavors such as $\Upsilon(nS) \to \ell_1\bar{\ell}_2$, $\Upsilon(nS) \to \gamma\ell_1\bar{\ell}_2$, etc. We highlight the fact that restricted kinematics of the two-body transitions would allow us to select operators with particular quantum numbers significantly reducing the reliance on the single operator dominance assumption. Finally, we shall argue that studies of radiative lepton flavor violating (RLFV) decays of vector quarkonia could provide important complementary access to study $\mathcal{L}_{\rm eff}$. Similarly RLFV decays of pseudoscalar mesons B_q^0, $\bar{D}^0$, and K^0, can provide complementary access to operators of type $\mathcal{O} \sim \left(\ell_1\bar{\ell}_2\right)(\bar{q}q)$, where there is only a FCNC on the

lepton side and primary access to vector and tensor operators of type $\mathcal{O} \sim \left(\ell_1 \bar{\ell}_2\right)(\bar{q}_1 q_2)$, where there are FCNCs on both the quark and lepton sides.

Note that here we only consider short distance effects in kaon decays. In the SM long distance effects on decays such as $K^0_{L(S)} \to \gamma\ell\bar{\ell}$ dominate the dynamics [48]. In light of this, our kaon results may be modified by long distance effects. Unlike K^0, the B^0_q and D^0 mesons are not expected to be greatly modified by long distance effects as they are not known to dominate their dynamics in rare SM decays.

We shall provide calculations of the relevant decay rates and establish constraints, where experimental data are available, on Wilson coefficients of effective operators of the Lagrangian $\mathcal{L}_{\text{eff}}$ of Eq. (1.5). In the following chapters we assume CP-conservation, which implies that all Wilson coefficients will be treated as real numbers. We also use the convention that the subscript of "1" denotes the lighter lepton and the subscript "2" denotes the heavier lepton. In studying branching ratios we assume that for a meson, M, the branching fraction $\mathcal{B}(M \to \ell_1\ell_2) = \mathcal{B}(M \to \bar{\ell}_1\ell_2) + \mathcal{B}(M \to \ell_1\bar{\ell}_2)$, unless specified otherwise. Finally, it is important to note that some of the two-body and all of the three-body transitions have yet to be experimentally studied. Numerical constraints on some Wilson coefficients of the effective Lagrangian, $\mathcal{L}_{eff}$, from these unstudied decays are not yet available.

CHAPTER 2: TWO-BODY LEPTON FLAVOR VIOLATING DECAYS

2.1 Vector Quarkonium Decays $V \to \ell_1 \overline{\ell}_2$

There is abundant experimental information on flavor off-diagonal leptonic decays of vector quarkonia, both from the ground and excited states [34]. This information can be effectively converted to experimental bounds on Wilson coefficients of vector and tensor operators in Eq. (1.8), as well as on those of the dipole operators of Eq. (1.6). Those Wilson coefficients can then be related to model parameters of explicit realizations of UV completions of effective Lagrangian in Eq. (1.5). The examples of particular new physics models that have been previously suggested to be constrained using vector meson decays $V \to \ell_1 \overline{\ell}_2$ include, e.g. [49, 50] (for Z' scenarios), [38, 39, 40] (for R-parity violating supersymmetric models), and [51, 52, 53] for other approaches.

One can find a general amplitude expression for $V \to \ell_1 \overline{\ell}_2$ by considering the initial and final states. The presence of the vector meson in the initial state implies the amplitude must contain an associated polarization vector $\varepsilon^\mu(p)$. The lepton and anti-lepton in the final state will require $\bar{u}(p_1, s_1)$ and $v(p_2, s_2)$ spinors to be present in the amplitude. There is a free index on the polarization vector that must be contracted with the matrix element between the spinors. We therefore conclude the amplitude must be of the form $\bar{u}(p_1, s_1) M_\mu v(p_2, s_2) \varepsilon^\mu(p)$.

Now we must consider what structures can contribute to the matrix M_μ. Our options are the meson momentum p^μ, the first lepton momentum p_1^μ, the second anti-lepton momentum p_2^μ, and the Dirac bilinears: 1, γ_5, γ^μ and $\gamma^\mu\gamma_5$. We know that $p^\mu \varepsilon_\mu(p) = 0$ for on-shell vector bosons, so we can drop terms associated with p^μ. When writing the general amplitude we should consider the $(p_2 + p_1)^\mu$ and $(p_2 - p_1)^\mu$ combinations of the final state momenta. The terms proportional to combination $(p_2 + p_1)^\mu$ can be dropped because it is equal to p^μ due to momentum conservation and $p^\mu \varepsilon_\mu(p) = 0$. This leads us to four possible composite structures built from the allowed momenta and Dirac bilinears: $(p_2 - p_1)^\mu$, $(p_2 - p_1)^\mu\gamma_5$, γ^μ, and $\gamma^\mu\gamma_5$.

$\ell_1\ell_2$	$\mu\tau$	$e\tau$	$e\mu$
$\mathcal{B}(\Upsilon(1S) \to \ell_1\ell_2)$	6.0×10^{-6}	$\cdots$	$\cdots$
$\mathcal{B}(\Upsilon(2S) \to \ell_1\ell_2)$	3.3×10^{-6}	3.2×10^{-6}	$\cdots$
$\mathcal{B}(\Upsilon(3S) \to \ell_1\ell_2)$	3.1×10^{-6}	4.2×10^{-6}	$\cdots$
$\mathcal{B}(J/\psi \to \ell_1\ell_2)$	2.0×10^{-6}	8.3×10^{-6}	1.6×10^{-7}
$\mathcal{B}(\phi \to \ell_1\ell_2)$	FPS	FPS	4.1×10^{-6}
$\mathcal{B}(\ell_2 \to \ell_1\gamma)$	4.4×10^{-8}	3.3×10^{-8}	5.7×10^{-13}

Table 2.1: Available experimental upper bounds on $\mathcal{B}(V \to \ell_1\ell_2)$ and $\mathcal{B}(\ell_2 \to \ell_1\gamma)$ [34, 54]. Center dots signify that no experimental constraints are available and "FPS" means that the transition is forbidden by available phase space. Charge averages of the final states are always assumed [35].

The most general expression for the $V \to \ell_1\overline{\ell}_2$ decay amplitude can be written as

$$\mathcal{A}(V \to \ell_1\overline{\ell}_2) = \overline{u}(p_1, s_1)\left[A_V^{\ell_1\ell_2}\gamma_\mu + B_V^{\ell_1\ell_2}\gamma_\mu\gamma_5 + \frac{C_V^{\ell_1\ell_2}}{m_V}(p_2 - p_1)_\mu + \frac{iD_V^{\ell_1\ell_2}}{m_V}(p_2 - p_1)_\mu\gamma_5\right] v(p_2, s_2)\varepsilon^\mu(p). \tag{2.1}$$

$A_V^{\ell_1\ell_2}$, $B_V^{\ell_1\ell_2}$, $C_V^{\ell_1\ell_2}$, and $D_V^{\ell_1\ell_2}$ are dimensionless constants which depend on the underlying Wilson coefficients of the effective Lagrangian of Eq. (1.5) as well as on hadronic effects associated with meson-to-vacuum matrix elements or decay constants.

The amplitude of Eq. (2.1) leads to the branching fraction, which is convenient to represent in terms of the ratio:

$$\frac{\mathcal{B}(V \to \ell_1\overline{\ell}_2)}{\mathcal{B}(V \to e^+e^-)} = \left(\frac{m_V\,(1-y^2)}{4\pi\alpha f_V Q_q}\right)^2 \left[\left(\left|A_V^{\ell_1\ell_2}\right|^2 + \left|B_V^{\ell_1\ell_2}\right|^2\right) + \frac{1}{2}\left(1-2y^2\right)\left(\left|C_V^{\ell_1\ell_2}\right|^2 + \left|D_V^{\ell_1\ell_2}\right|^2\right) + y\ \mathrm{Re}\left(A_V^{\ell_1\ell_2}C_V^{\ell_1\ell_2 *} + iB_V^{\ell_1\ell_2}D_V^{\ell_1\ell_2 *}\right)\right]. \tag{2.2}$$

Here α is the fine structure constant, we set $y = m_2/m_V$, and we neglected the mass of the lighter of the two leptons. The form of the coefficients $A_V^{\ell_1\ell_2}$ to $D_V^{\ell_1\ell_2}$ depends on the initial

state meson. For example, for $V = \Upsilon(nS)$ ($b\bar{b}$ states), $\psi(nS)$ ($c\bar{c}$ states), or ϕ ($s\bar{s}$ state), the coefficients are:

$$
\begin{aligned}
A_V^{\ell_1\ell_2} &= \frac{f_V m_V}{\Lambda^2}\Bigg[\sqrt{4\pi\alpha}\,Q_q y^2\left(C_{DL}^{\ell_1\ell_2}+C_{DR}^{\ell_1\ell_2}\right)+\kappa_V\left(C_{VL}^{q\ell_1\ell_2}+C_{VR}^{q\ell_1\ell_2}\right)\\
&\qquad\qquad +2y^2\kappa_V\frac{f_V^T}{f_V}G_F m_V m_q\left(C_{TL}^{q\ell_1\ell_2}+C_{TR}^{q\ell_1\ell_2}\right)\Bigg],\\
B_V^{\ell_1\ell_2} &= \frac{f_V m_V}{\Lambda^2}\Bigg[-\sqrt{4\pi\alpha}\,Q_q y^2\left(C_{DL}^{\ell_1\ell_2}-C_{DR}^{\ell_1\ell_2}\right)-\kappa_V\left(C_{VL}^{q\ell_1\ell_2}-C_{VR}^{q\ell_1\ell_2}\right)\\
&\qquad\qquad -2y^2\kappa_V\frac{f_V^T}{f_V}G_F m_V m_q\left(C_{TL}^{q\ell_1\ell_2}-C_{TR}^{q\ell_1\ell_2}\right)\Bigg],\\
C_V^{\ell_1\ell_2} &= \frac{f_V m_V}{\Lambda^2}y\Bigg[\sqrt{4\pi\alpha}\,Q_q\left(C_{DL}^{\ell_1\ell_2}+C_{DR}^{\ell_1\ell_2}\right)+2\kappa_V\frac{f_V^T}{f_V}G_F m_V m_q\left(C_{TL}^{q\ell_1\ell_2}+C_{TR}^{q\ell_1\ell_2}\right)\Bigg],\\
D_V^{\ell_1\ell_2} &= i\frac{f_V m_V}{\Lambda^2}y\Bigg[-\sqrt{4\pi\alpha}\,Q_q\left(C_{DL}^{\ell_1\ell_2}-C_{DR}^{\ell_1\ell_2}\right)-2\kappa_V\frac{f_V^T}{f_V}G_F m_V m_q\left(C_{TL}^{q\ell_1\ell_2}-C_{TR}^{q\ell_1\ell_2}\right)\Bigg].
\end{aligned}
\tag{2.3}
$$

Here $Q_q = (2/3, -1/3)$ is the charge of the quark q and $\kappa_V = 1/2$ is a constant for pure $q\bar{q}$ states. The κ constants are introduced purely for the purpose of writing concise equations. Different meson states have different quark flavor mixing which contribute to the different numerical factors of κ for various initial states. It is a good approximation to drop terms proportional to y^2 in Eq. (2.3) for the heavy quarkonium states. Inspecting the ratio in Eq. (2.2), one immediately infers that the best constraints could be placed on the four-fermion coefficients, $C_{VL}^{q\ell_1\ell_2}$ and $C_{VR}^{q\ell_1\ell_2}$, as no final state lepton mass suppression exists for those coefficients. Yet, constraints on the the dipole coefficients, $C_{DL}^{\ell_1\ell_2}(C_{DR}^{\ell_1\ell_2})$, are also possible in this case. This would provide NP constraints that are complementary to the ones obtained from the lepton decay experiments, especially for $\ell = \tau$, obtained in the radiative $\tau \to \mu(e)\gamma$ decays.

The constraints on the Wilson coefficients of tensor operators, $C_{TL}^{q\ell_1\ell_2}(C_{TR}^{q\ell_1\ell_2})$, in Eq. (2.3)

State	$\Upsilon(1S)$	$\Upsilon(2S)$	$\Upsilon(3S)$	J/ψ	$\psi(2S)$	ϕ	$\rho\,(\omega)$
f_V, MeV	649 ± 31	481 ± 39	539 ± 84	418 ± 9	294 ± 5	241 ± 18	209.4 ± 1.5

Table 2.2: Vector meson decay constants used in the calculation of branching ratios $\mathcal{B}(V \to \ell_1\bar{\ell}_2)$. The transverse decay constants are set $f_V^T = f_V$ except for J/ψ, which has $f_{J/\psi}^T = 410 \pm 10$ MeV [35, 51, 55, 56, 57, 58, 59].

also depend on the ratio of meson decay constants,

$$\begin{aligned} \langle 0|\bar{q}\gamma^\mu q|V(p)\rangle &= f_V m_V \varepsilon^\mu(p)\,, \\ \langle 0|\bar{q}\sigma^{\mu\nu} q|V(p)\rangle &= i f_V^T\,(\varepsilon^\mu p^\nu - p^\mu \varepsilon^\nu)\,, \end{aligned} \tag{2.4}$$

where $\varepsilon^\mu(p)$ is the V-meson polarization vector, and p is its momentum [55].

While the decay constants, f_V, are known, both experimentally from leptonic decays and theoretically from lattice or QCD sum rule calculations, for a variety of states V, the tensor (transverse) decay constant, f_V^T, has only recently been calculated for the charmonium J/ψ state with the result $f_{J/\psi}^T(2\text{ GeV}) = (410 \pm 10)$ MeV [55]. In the absence of the estimate for f_V^T, we follow the suggestion made in Ref. [60] and assume that $f_V^T = f_V$. This seems to be the case for the J/ψ state [55] to better than 10 %. We present numerical values of the decay constants in Table 2.2. Note that the ratio of Eq. (2.2) is largely independent of the values of the decay constants due to the choice of normalization.

Choosing other initial states would make it possible to constrain other combinations of the Wilson coefficients in Eq. (1.5). This is important for the NP models where several LFV operators would contribute, especially in the case where no operator gives *a priori* dominant

contribution. For example, choosing $V = \rho$ meson with $\rho \sim \left(u\bar{u} - d\bar{d}\right)/\sqrt{2}$ gives:

$$\begin{aligned}
A_\rho^{e\mu} &= \frac{f_\rho m_\rho}{\Lambda^2} y^2 \sqrt{2\pi\alpha}\,(Q_u - Q_d)\left(C_{DL}^{\ell_1\ell_2} + C_{DR}^{\ell_1\ell_2}\right), \\
B_\rho^{e\mu} &= -\frac{f_\rho m_\rho}{\Lambda^2} y^2 \sqrt{2\pi\alpha}\,(Q_u - Q_d)\left(C_{DL}^{\ell_1\ell_2} - C_{DR}^{\ell_1\ell_2}\right), \\
C_\rho^{e\mu} &= \frac{f_\rho m_\rho}{\Lambda^2} y\ \sqrt{2\pi\alpha}\,(Q_u - Q_d)\left(C_{DL}^{\ell_1\ell_2} + C_{DR}^{\ell_1\ell_2}\right), \\
D_\rho^{e\mu} &= -i\frac{f_\rho m_\rho}{\Lambda^2} y\ \sqrt{2\pi\alpha}\,(Q_u - Q_d)\left(C_{DL}^{\ell_1\ell_2} - C_{DR}^{\ell_1\ell_2}\right).
\end{aligned} \tag{2.5}$$

Here we imposed isospin symmetry on the NP operators and their coefficients, which resulted in the cancellation of the four-fermion operator contribution. The ρ meson is kinematically restricted to decay to μe and no other LFV products, so only μe operators can be constrained in this channel. The corresponding results for $V = \omega \sim \left(u\bar{u} + d\bar{d}\right)/\sqrt{2}$ decay can be obtained from Eq. (2.3) by substituting $Q_q \to (Q_u + Q_d)/\sqrt{2}$ and using $\kappa_\omega = 1/\sqrt{2}$. Again, the restricted kinematics of the decay implies that only μe operators interacting with up and down quarks can be constrained. Since we imposed isospin symmetry, it is convenient to use $m_q = (m_u + m_d)/2$.

Contrasting Eq. (2.2) with the experimental data from Ref. [34] we can constrain the Wilson coefficients of the Lagrangian Eq. (1.5). Assuming single operator dominance, the results can be found in Table 2.3. The Wilson coefficients of dipole operators can be found in Table 2.4.

It is important to note that some of the bounds presented in Tables 2.3 and 2.4 are rather weak and might not even look physically meaningful, especially the ones coming from ϕ decays. In fact, assuming Wilson coefficients $C \sim 1$ seems to imply that new physics scale $\Lambda/\sqrt{C}$ only extends to several MeVs, clearly breaking the EFT paradigm that assumes local operators up to the scales of several TeVs! A correct interpretation of those entries in Tables 2.3 and 2.4 is that existing data simply does not allow to place strong constraints on the combination Wilson coefficients. This is rather common in EFT analyses of new physics phenomena, see e.g. [61].

Wilson coefficient (GeV^{-2})	Leptons $\ell_1\ell_2$	Initial state (quark) $\Upsilon(1S)$ (b)	$\Upsilon(2S)$ (b)	$\Upsilon(3S)$ (b)	J/ψ (c)	ϕ (s)
$\lvert C_{VL}^{q\ell_1\ell_2}/\Lambda^2\rvert$	$\mu\tau$	5.6×10^{-6}	4.1×10^{-6}	3.5×10^{-6}	5.5×10^{-5}	FPS
	$e\tau$	$\cdots$	4.1×10^{-6}	4.1×10^{-6}	1.1×10^{-4}	FPS
	$e\mu$	$\cdots$	$\cdots$	$\cdots$	1.0×10^{-5}	2×10^{-3}
$\lvert C_{VR}^{q\ell_1\ell_2}/\Lambda^2\rvert$	$\mu\tau$	5.6×10^{-6}	4.1×10^{-6}	3.5×10^{-6}	5.5×10^{-5}	FPS
	$e\tau$	$\cdots$	4.1×10^{-6}	4.1×10^{-6}	1.1×10^{-4}	FPS
	$e\mu$	$\cdots$	$\cdots$	$\cdots$	1.0×10^{-5}	2×10^{-3}
$\lvert C_{TL}^{q\ell_1\ell_2}/\Lambda^2\rvert$	$\mu\tau$	4.4×10^{-2}	3.2×10^{-2}	2.8×10^{-2}	1.2	FPS
	$e\tau$	$\cdots$	3.3×10^{-2}	3.2×10^{-2}	2.4	FPS
	$e\mu$	$\cdots$	$\cdots$	$\cdots$	4.8	1×10^{4}
$\lvert C_{TR}^{q\ell_1\ell_2}/\Lambda^2\rvert$	$\mu\tau$	4.4×10^{-2}	3.2×10^{-2}	2.8×10^{-2}	1.2	FPS
	$e\tau$	$\cdots$	3.3×10^{-2}	3.2×10^{-2}	2.4	FPS
	$e\mu$	$\cdots$	$\cdots$	$\cdots$	4.8	1×10^{4}

Table 2.3: Constraints on the Wilson coefficients of four-fermion operators. Center dots signify that no experimental data are available to produce a constraint; "FPS" means that the transition is forbidden by phase space. The vector operators will always be better constrained relative to the tensor operators via this decay channel due to the chiral suppression of the tensor operators. Note that no experimental data is available for higher excitations of ψ [35].

Wilson coefficient (GeV^{-2})	Leptons $\ell_1\ell_2$	Initial state $\Upsilon(1S)$	$\Upsilon(2S)$	$\Upsilon(3S)$	J/ψ	ϕ	$\ell_2 \to \ell_1\gamma$
$\lvert C_{DL}^{\ell_1\ell_2}/\Lambda^2\rvert$	$\mu\tau$	2.0×10^{-4}	1.6×10^{-4}	1.4×10^{-4}	2.5×10^{-4}	FPS	2.6×10^{-10}
	$e\tau$	$\cdots$	1.6×10^{-4}	1.6×10^{-4}	5.3×10^{-4}	FPS	2.7×10^{-10}
	$e\mu$	$\cdots$	$\cdots$	$\cdots$	1.1×10^{-3}	0.2	3.1×10^{-7}
$\lvert C_{DR}^{\ell_1\ell_2}/\Lambda^2\rvert$	$\mu\tau$	2.0×10^{-4}	1.6×10^{-4}	1.4×10^{-4}	2.5×10^{-4}	FPS	2.6×10^{-10}
	$e\tau$	$\cdots$	1.6×10^{-4}	1.6×10^{-4}	5.3×10^{-4}	FPS	2.7×10^{-10}
	$e\mu$	$\cdots$	$\cdots$	$\cdots$	1.1×10^{-3}	0.2	3.1×10^{-7}

Table 2.4: Constraints on the dipole Wilson coefficients from the 1^{--} quarkonium decays and radiative lepton transitions $\ell_2 \to \ell_1\gamma$. Center dots signify that no experimental data are available to produce a constraint; "FPS" means that the transition is forbidden by phase space [35].

$\ell_1\ell_2$	$e\mu$
$\mathcal{B}(\eta \to \ell_1\ell_2)$	6.0×10^{-6}
$\mathcal{B}(\eta' \to \ell_1\ell_2)$	4.7×10^{-4}
$\mathcal{B}(\pi^0 \to \ell_1\ell_2)$	3.6×10^{-10}

Table 2.5: Available experimental limits on $\mathcal{B}(P \to \ell_1\ell_2)$ [34]. Note that no constraints for the heavy quark pseudoscalar states such as $\eta_{b(c)}$ are available. Only phase space allowed transitions are shown [35].

Looking at Eq. (2.3) one sees that there is a practical limitation on the two-body vector meson decays. Only a subset of the Wilson coefficients is selected by the quantum numbers of the initial state and can be probed. This fact can be turned into virtue if experimental information on LFV decays of quarkonium states with other quantum numbers is available.

2.2 Pseudo-scalar Quarkonium Decays $P \to \ell_1\overline{\ell}_2$

Constraints on other Wilson coefficients of the effective Lagrangian in Eq. (1.5) could be obtained by considering decays of pseudoscalar mesons with quantum numbers $J^{PC} = 0^{-+}$, which include states like $\eta_{b(c)}$, $\eta^{(\prime)}$, and their excitations. These decays would be sensitive to axial and pseudoscalar operators without flavor changes in the quark currents, providing information about $C_{PL}^{q\ell_1\ell_2}(C_{PR}^{q\ell_1\ell_2})$ and/or $C_{AL}^{q\ell_1\ell_2}(C_{AR}^{q\ell_1\ell_2})$ in Eq. (1.8) as well as to gluonic operators of Eq. (1.9). The $\eta_{b(c)}$ states could be abundantly produced at the LHCb experiment directly in gluon-gluon fusion interactions [62]. In case of the η_c and its excitations, another production mechanism would include non-leptonic B-decays, as the corresponding branching ratios for non-leptonic B decays into η_c and kaons are reasonably large, of order of per mille [34].

Following a similar method to the decays of vector mesons considered in Sect. 2.1, one can write the most general expression for the $P \to \ell_1\overline{\ell}_2$ decay. In the case of the decay of a pseudoscalar, there is no polarization vector, but we still have the two spinors $\bar{u}(p_1, s_1)$ and $v(p_2, s_2)$ for the leptons $\ell_{1,2}$. This leads to a general amplitude of $\bar{u}(p_1, s_1)Mv(p_2, s_2)$. The matrix M has no Lorentz indices because there is nothing to contract with a free index. It

therefore can only depend on the Dirac bilinears 1 and γ_5 and some constants. One can then write the most general expression for the $P \to \ell_1 \bar{\ell}_2$ decay amplitude as

$$\mathcal{A}(P \to \ell_1 \bar{\ell}_2) = \overline{u}(p_1, s_1) \left[E_P^{\ell_1 \ell_2} + i F_P^{\ell_1 \ell_2} \gamma_5 \right] v(p_2, s_2) \tag{2.6}$$

with $E_P^{\ell_1 \ell_2}$ and $F_P^{\ell_1 \ell_2}$ being dimensionless constants which depend on the Wilson coefficients of operators in Eq. (1.5) and various decay constants.

The amplitude of Eq. (2.6) leads to the branching ratio for decays of pseudoscalar mesons to flavor off-diagonal lepton products:

$$\mathcal{B}(P \to \ell_1 \bar{\ell}_2) = \frac{m_P}{8\pi \Gamma_P} \left(1 - y^2\right)^2 \left[\left| E_P^{\ell_1 \ell_2} \right|^2 + \left| F_P^{\ell_1 \ell_2} \right|^2 \right]. \tag{2.7}$$

Here Γ_P is the total width of the pseudoscalar state. We have once again neglected the mass of the lighter lepton and set $y = m_2/m_P$. Calculating $E_P^{\ell_1 \ell_2}$ and $F_P^{\ell_1 \ell_2}$ for $P = \eta_b$ ($b\bar{b}$ state) and η_c ($c\bar{c}$ state), the coefficients are

$$\begin{aligned} E_P^{\ell_1 \ell_2} = \quad & \frac{y m_P}{4\Lambda^2} \Big[- i f_P \left(2 \left(C_{AL}^{q \ell_1 \ell_2} + C_{AR}^{q \ell_1 \ell_2} \right) - m_P^2 G_F \left(C_{PL}^{q \ell_1 \ell_2} + C_{PR}^{q \ell_1 \ell_2} \right) \right) \\ & \qquad + 9 G_F a_P \left(C_{\widetilde{G}L}^{\ell_1 \ell_2} + C_{\widetilde{G}R}^{\ell_1 \ell_2} \right) \Big], \\ F_P^{\ell_1 \ell_2} = -i \frac{y m_P}{4\Lambda^2} \Big[& - i f_P \left(2 \left(C_{AL}^{q \ell_1 \ell_2} - C_{AR}^{q \ell_1 \ell_2} \right) - m_P^2 G_F \left(C_{PL}^{q \ell_1 \ell_2} - C_{PR}^{q \ell_1 \ell_2} \right) \right) \\ & \qquad + 9 G_F a_P \left(C_{\widetilde{G}L}^{\ell_1 \ell_2} - C_{\widetilde{G}R}^{\ell_1 \ell_2} \right) \Big]. \end{aligned} \tag{2.8}$$

The hadronic matrix elements in Eq. (2.11) are defined as [47]

$$\begin{aligned} & \langle 0 | \bar{q}_1 \gamma^\mu \gamma_5 q_2 | P(p) \rangle = - i f_P p^\mu \,, \\ & \langle 0 | \frac{\alpha_s}{4\pi} G^{a \mu \nu} \widetilde{G}^a_{\mu \nu} | P(p) \rangle = a_P \,. \end{aligned} \tag{2.9}$$

Here p is the momentum of the meson. For heavy quarks $q = c, b$ one expects the matrix elements of gluonic operators in Eq. (2.9) to be quite small. This can be visualized by noting that in the heavy quark limit $\eta_{b(c)}$ is a small state of size $(m_{b(c)} v)^{-1}$ and has a small overlap

State	η_b	η_c	$\eta, u(d)$	η, s	$\eta', u(d)$	η', s	π
f_P^q, MeV	667 ± 6	387 ± 7	108 ± 3	-111 ± 6	89 ± 3	136 ± 6	130.41 ± 0.20

Table 2.6: Pseudoscalar meson decay constants used in the calculation of branching ratios $\mathcal{B}(P \to \ell_1 \overline{\ell}_2)$ [35, 34, 55, 63, 64].

with soft gluons, whose Compton wavelength is of the order of $\Lambda_{\rm QCD}^{-1}$, as $m_{b(c)} v \gg \Lambda_{\rm QCD}$. Here v is the velocity of heavy quarks. Thus, for the remainder of this chapter, we shall set $a_{\eta_{b(c)}} = 0$. The constraints on the Wilson coefficients of gluonic operators could be obtained either from studying lepton flavor violating η' decays (for μe currents) or from the corresponding tau decays. We use $a_\eta = -0.022 \pm 0.002$ GeV^3 and $a_{\eta'} = -0.057 \pm 0.002$ GeV^3 [64]. The numerical values of the other pseudoscalar decay constants used in the calculations can be found in Table 2.6. For the light quark states, such as η and η' the corresponding expressions are a bit more involved:

$$\begin{aligned}
E_P^{\ell_1\ell_2} = y\frac{m_P}{4\Lambda^2}\Big[&- i f_P^q \kappa_1^P \Big(2\Big(C_{AL}^{q\ell_1\ell_2} + C_{AR}^{q\ell_1\ell_2}\Big) - G_F m_P^2 \Big(C_{PL}^{q\ell_1\ell_2} + C_{PR}^{q\ell_1\ell_2}\Big)\Big) \\
&- i f_P^s \kappa_2^P \Big(2\Big(C_{AL}^{s\ell_1\ell_2} + C_{AR}^{s\ell_1\ell_2}\Big) - G_F m_P^2 \Big(C_{PL}^{s\ell_1\ell_2} + C_{PR}^{s\ell_1\ell_2}\Big)\Big) \\
&+ 9\, G_F a_P \Big(C_{\widetilde{G}L}^{\ell_1\ell_2} + C_{\widetilde{G}R}^{\ell_1\ell_2}\Big)\Big], \\
F_P^{\ell_1\ell_2} = y\frac{m_P}{4\Lambda^2}\Big[&- f_P^q \kappa_1^P \Big(2\Big(C_{AL}^{q\ell_1\ell_2} - C_{AR}^{q\ell_1\ell_2}\Big) - G_F m_P^2 \Big(C_{PL}^{q\ell_1\ell_2} - C_{PR}^{q\ell_1\ell_2}\Big)\Big) \\
&- f_P^s \kappa_2^P \Big(2\Big(C_{AL}^{s\ell_1\ell_2} - C_{AR}^{s\ell_1\ell_2}\Big) - G_F m_P^2 \Big(C_{PL}^{s\ell_1\ell_2} - C_{PR}^{s\ell_1\ell_2}\Big)\Big) \\
&- 9i\, G_F a_P \Big(C_{\widetilde{G}L}^{\ell_1\ell_2} - C_{\widetilde{G}R}^{\ell_1\ell_2}\Big)\Big],
\end{aligned} \tag{2.10}$$

where the index $q = u/d$, $\kappa_1^\eta = 1/\sqrt{3}$, $\kappa_2^\eta = -\sqrt{2/3}$, $\kappa_1^{\eta'} = \sqrt{2/3}$, and $\kappa_2^{\eta'} = 1/\sqrt{3}$. It is important to note that, if observed, simultaneous fit to several light quark meson decays could independently constrain Wilson coefficients of effective operators in Eq. (1.5), as follows from Eq. (2.10).

The resulting constraints on the WCs could be found in Tables 2.7 and 2.8. Note that no experimental constraints on the b and c currents are available, as the corresponding

Wilson coefficient (GeV^{-2})	Leptons $\ell_1\ell_2$	Initial state η_b	η_c	$\eta(u/d)$	$\eta(s)$	$\eta'(u/d)$	$\eta'(s)$
$\lvert C_{AL}^{q\ell_1\ell_2}/\Lambda^2\rvert$	$\mu\tau$	$\cdots$	$\cdots$	FPS	FPS	FPS	FPS
	$e\tau$	$\cdots$	$\cdots$	FPS	FPS	FPS	FPS
	$e\mu$	$\cdots$	$\cdots$	3×10^{-3}	2×10^{-3}	2.1×10^{-1}	1.9×10^{-1}
$\lvert C_{AR}^{q\ell_1\ell_2}/\Lambda^2\rvert$	$\mu\tau$	$\cdots$	$\cdots$	FPS	FPS	FPS	FPS
	$e\tau$	$\cdots$	$\cdots$	FPS	FPS	FPS	FPS
	$e\mu$	$\cdots$	$\cdots$	3×10^{-3}	2×10^{-3}	2.1×10^{-1}	1.9×10^{-1}
$\lvert C_{PL}^{q\ell_1\ell_2}/\Lambda^2\rvert$	$\mu\tau$	$\cdots$	$\cdots$	FPS	FPS	FPS	FPS
	$e\tau$	$\cdots$	$\cdots$	FPS	FPS	FPS	FPS
	$e\mu$	$\cdots$	$\cdots$	2×10^{3}	1×10^{3}	3.9×10^{4}	3.6×10^{4}
$\lvert C_{PR}^{q\ell_1\ell_2}/\Lambda^2\rvert$	$\mu\tau$	$\cdots$	$\cdots$	FPS	FPS	FPS	FPS
	$e\tau$	$\cdots$	$\cdots$	FPS	FPS	FPS	FPS
	$e\mu$	$\cdots$	$\cdots$	2×10^{3}	1×10^{3}	3.9×10^{4}	3.6×10^{4}

Table 2.7: Constraints on the Wilson coefficients from pseudoscalar meson decays. Center dots signify that no experimental data is available to produce a constraint; "FPS" means that the transition is forbidden by available phase space [35].

Wilson coefficient (GeV^{-2})	Leptons $\ell_1\ell_2$	Initial state η_b	η_c	η	η'
$\lvert C_{GL}^{\ell_1\ell_2}/\Lambda^2\rvert$	$e\mu$	$\cdots$	$\cdots$	2×10^{2}	5.0×10^{3}
$\lvert C_{GR}^{\ell_1\ell_2}/\Lambda^2\rvert$	$e\mu$	$\cdots$	$\cdots$	2×10^{2}	5.0×10^{3}

Table 2.8: Constraints on the pseudoscalar gluonic Wilson coefficients. Center dots signify that no experimental data is available to produce a constraint. No data for other lepton species is available [35].

$\ell_1\ell_2$	$\mu\tau$	$e\tau$	$e\mu$
$\mathcal{B}(B_d^0 \to \ell_1\ell_2)$	2.2×10^{-5}	2.8×10^{-5}	1.0×10^{-9}
$\mathcal{B}(B_s^0 \to \ell_1\ell_2)$	$\cdots$	$\cdots$	5.4×10^{-9}
$\mathcal{B}(\bar{D}^0 \to \ell_1\ell_2)$	FPS	$\cdots$	1.3×10^{-8}
$\mathcal{B}(K_L^0 \to \ell_1\ell_2)$	FPS	FPS	4.7×10^{-12}

Table 2.9: Available experimental limits on $\mathcal{B}(P \to \ell_1\bar{\ell}_2)$ [34, 65, 66, 67, 68]. Center dots signify that no experimental data are available; "FPS" means that the transition is forbidden by phase space [36].

State	B_d^0	B_s^0	$\bar{D}^0$	K_L^0
f_P, MeV	186 ± 4	224 ± 4	207.4 ± 3.8	155.0 ± 1.9
Γ_P, 10^{-14} MeV	4330 ± 11	4374 ± 15	16050 ± 60	1.287 ± 0.005
m_P, GeV	5.28	5.37	1.86	0.498

Table 2.10: Pseudoscalar meson decay constants [75, 76], total decay widths, and meson masses [34] used in the calculation of branching ratios $\mathcal{B}(P \to \ell_1\bar{\ell}_2)$ [36].

transitions $\eta_{b(c)} \to \ell_1\bar{\ell}_2$ have not yet been experimentally studied. Also, constraints on the WCs of gluonic operators in Table 2.8 are significantly weaker than those available from tau decays [47]. Again, just as in Section 2.1, large entries in the Tables 2.7 and 2.8 do not imply a breakdown of the EFT description of LFV decays, but signify that existing data does not allow us to place strong constraints on the combination of relevant Wilson coefficients.

2.3 Pseudo-scalar B_q^0, D^0, and K^0 Decays $P \to \ell_1\bar{\ell}_2$

Many studies have focused on rare leptonic decays of B_q^0 mesons, $B_q \to \ell\bar{\ell}$, as both precision tests of the SM and as an opportunity to search for new physics (e.g. [69, 70, 71, 72, 73]). The abundance of produced B_q^0 and $\bar{D}^0$ states at the LHCb, Belle II, and BESIII experiments also allows for studies of lepton-flavor violating decays at these experiments [74, 34]. Such decays were discussed at length previously, mainly in the context of particular models. Here we shall review these transitions emphasizing the possibility to constrain Wilson coefficients of the axial and pseudoscalar operators of the effective Lagrangian in

Wilson coefficient	Leptons	Initial state			
GeV^{-2}	$\ell_1\ell_2$	$B_d^0\left(d\bar{b}\right)$	$B_s^0\left(s\bar{b}\right)$	$\bar{D}^0\left(u\bar{c}\right)$	$K_L^0\left(\left(d\bar{s}-s\bar{d}\right)/\sqrt{2}\right)$
	$\mu\tau$	2.3×10^{-8}	$\cdots$	FPS	FPS
$\lvert C_{AL}^{q_1q_2\ell_1\ell_2}/\Lambda^2\rvert$	$e\tau$	2.6×10^{-8}	$\cdots$	$\cdots$	FPS
	$e\mu$	2.3×10^{-9}	4.4×10^{-9}	2.4×10^{-8}	5.0×10^{-12}
	$\mu\tau$	2.3×10^{-8}	$\cdots$	FPS	FPS
$\lvert C_{AR}^{q_1q_2\ell_1\ell_2}/\Lambda^2\rvert$	$e\tau$	2.6×10^{-8}	$\cdots$	$\cdots$	FPS
	$e\mu$	2.3×10^{-9}	4.4×10^{-9}	2.4×10^{-8}	5.0×10^{-12}
	$\mu\tau$	7.1×10^{-5}	$\cdots$	FPS	FPS
$\lvert C_{PL}^{q_1q_2\ell_1\ell_2}/\Lambda^2\rvert$	$e\tau$	8.0×10^{-5}	$\cdots$	$\cdots$	FPS
	$e\mu$	7.1×10^{-6}	1.3×10^{-5}	5.9×10^{-4}	1.7×10^{-6}
	$\mu\tau$	7.1×10^{-5}	$\cdots$	FPS	FPS
$\lvert C_{PR}^{q_1q_2\ell_1\ell_2}/\Lambda^2\rvert$	$e\tau$	8.0×10^{-5}	$\cdots$	$\cdots$	FPS
	$e\mu$	7.1×10^{-6}	1.3×10^{-5}	5.9×10^{-4}	1.7×10^{-6}

Table 2.11: Constraints on the Wilson coefficients from pseudoscalar meson decays. Note the K_L^0 results only include short distance effects. Center dots signify that no experimental data are available to produce a constraint; "FPS" means that the transition is forbidden by phase space. Particle masses and other input parameters are from [36, 34, 65, 66, 67, 68].

Eq. (1.5). Note that these studies are complementtary to those discussed in Sect. 2.2, as here we allow for flavor changes in the quark currents as well. These decays would provide information about $C_{PL}^{q_1q_2\ell_1\ell_2}(C_{PR}^{q_1q_2\ell_1\ell_2})$ and/or $C_{AL}^{q_1q_2\ell_1\ell_2}(C_{AR}^{q_1q_2\ell_1\ell_2})$ in Eq. (1.8).

Here the most general expression for the $P\to\ell_1\overline{\ell}_2$ decay amplitude is the same as Eq. (2.6) of Sect. 2.2, which leads to the same form for the branching ratio found in Eq. (2.7) [35]. We once again neglect the mass of the lighter lepton and set $y=m_2/m_P$. Calculating $E_P^{\ell_1\ell_2}$ and $F_P^{\ell_1\ell_2}$ for $P=B_d^0$ ($q_1q_2=db$), B_s^0 ($q_1q_2=sb$), $\bar{D}^0$ ($q_1q_2=cu$), and , K_L^0 ($q_1q_2=ds$), the coefficients are

$$\begin{aligned}
E_P^{\ell_1\ell_2} &= \kappa_P\frac{m_Pf_Py}{2\Lambda^2}\left[\left(C_{AL}^{q_1q_2\ell_1\ell_2}+C_{AR}^{q_1q_2\ell_1\ell_2}\right)+m_P^2G_F\left(C_{PL}^{q_1q_2\ell_1\ell_2}+C_{PR}^{q_1q_2\ell_1\ell_2}\right)\right],\\
F_P^{\ell_1\ell_2} &= i\kappa_P\frac{m_Pf_Py}{2\Lambda^2}\left[\left(C_{AL}^{q_1q_2\ell_1\ell_2}-C_{AR}^{q_1q_2\ell_1\ell_2}\right)+m_P^2G_F\left(C_{PL}^{q_1q_2\ell_1\ell_2}-C_{PR}^{q_1q_2\ell_1\ell_2}\right)\right].
\end{aligned}\tag{2.11}$$

The decay constant in Eq. (2.11) is defined in Eq. (2.9). The constant κ_P is 1 for B_q^0, $\bar{D}^0$, and K^0; and $1/\sqrt{2}$ for $K^0_{L(S)}$. The experimental limits and numerical values of the pseudo-scalar decay constants used in the calculations can be found in Tables 2.9 and 2.10. The resulting constraints on the Wilson coefficients are found in Table 2.11.

2.4 Scalar quarkonium decays $S \to \ell_1 \overline{\ell}_2$

Scalar quarkonium decays would ideally allow one to probe the Wilson coefficients of the scalar operators in Eq. (1.8). The corresponding p-wave states χ_{q0}, where $q = b, c$ could be effectively produced either directly in gluon-gluon fusion at the LHC, or in the radiative decays of $\Upsilon(2S)$, $\Upsilon(3S)$, or corresponding ψ states. It is important to note that the corresponding branching ratios for, say, $\psi(2S) \to \gamma\chi_{c0}$ are rather large, of the order of 10%. Finally, they could also be produced in B-decays at flavor factories.

Since Wilson coefficients of other operators could be better probed in the processes discussed in Sect. 2.1-2.2, in this section we shall concentrate on the contributions of operators that could not be probed in the decays of vector or pseudoscalar quarkonium states.

The most general expression for the $S \to \ell_1 \overline{\ell}_2$ decay amplitude looks exactly like Eq. (2.6), with obvious modifications for the scalar decay:

$$\mathcal{A}(S \to \ell_1 \overline{\ell}_2) = \overline{u}(p_1, s_1) \left[E_S^{\ell_1 \ell_2} + i F_S^{\ell_1 \ell_2} \gamma_5 \right] v(p_2, s_2). \tag{2.12}$$

$E_S^{\ell_1 \ell_2}$ and $F_S^{\ell_1 \ell_2}$ are dimensionless constants. The branching ratio, which follows from Eq. (2.12), is

$$\mathcal{B}(S \to \ell_1 \overline{\ell}_2) = \frac{m_S}{8\pi\Gamma_S} \left(1 - y^2\right)^2 \left[\left| E_S^{\ell_1 \ell_2} \right|^2 + \left| F_S^{\ell_1 \ell_2} \right|^2 \right]. \tag{2.13}$$

Here Γ_S is the total width of the scalar state and $y = m_2/m_S$. The coefficients $E_S^{\ell_1 \ell_2}$ and

State	$\chi_{c0}(1P)$	$\chi_{b0}(1P)$	$\chi_{b0}(2P)$
m_S, MeV	3414.75 ± 0.31	9859.44 ± 0.52	10232.5 ± 0.6
Γ_S, MeV	10.5 ± 0.6	(1.35)	(0.247 ± 0.097)
f_S, MeV	≈ 887	≈ 423	≈ 421

Table 2.12: Decay constants of Eq. (2.9) for the scalar quarkonium decays [35], derived from the quark model calculation of [77]. We follow [77] and do not assign uncertainty to the quark model estimates of the decay constants. Masses and measured widths are from [34], and unmeasured widths (in brackets) are calculated as in [77, 78].

$F_S^{\ell_1\ell_2}$ are

$$\begin{aligned} E_S^{\ell_1\ell_2} &= y\frac{m_S G_F}{4\Lambda^2}\left[2if_S m_S m_q\left(C_{SL}^{ql_1l_2}+C_{SR}^{ql_1l_2}\right)+9a_S\left(C_{GL}^{ql_1l_2}+C_{GR}^{ql_1l_2}\right)\right], \\ F_S^{\ell_1\ell_2} &= y\frac{m_S G_F}{4\Lambda^2}\left[2f_S m_S m_q\left(C_{SL}^{ql_1l_2}-C_{SR}^{ql_1l_2}\right)-9ia_S\left(C_{GL}^{ql_1l_2}-C_{GR}^{ql_1l_2}\right)\right]. \end{aligned} \tag{2.14}$$

The hadronic matrix elements in Eq. (2.14) are defined as

$$\begin{aligned} &\langle 0|\bar{q}q|S(p)\rangle = -im_S f_S\ , \\ &\langle 0|\frac{\alpha_s}{4\pi}G^{a\mu\nu}G^a_{\mu\nu}|S(p)\rangle = a_S\,. \end{aligned} \tag{2.15}$$

Note that we introduced an extra minus sign and a factor of m_S compared to [77] for the scalar quark density to have uniform units for all matrix elements of quark currents. For the same reasons as in the pseudoscalar case, one expects that the gluonic matrix elements in Eq. (2.14) for the heavy quark states χ_{c0} or χ_{b0} are small, so we set $a_S = 0$ from now on. This means that the Wilson coefficients of the gluonic operators are better probed in LFV tau decays, where the low energy theorems [47] or experimental data [42] could be used to constrain relevant gluonic matrix elements.

Finally, we note that no constraints on the Wilson coefficients of the scalar currents in $\mathcal{L}_{\text{eff}}$ are available, as the corresponding transitions $\chi_{b(c)0} \to \ell_1\bar{\ell}_2$ have not yet been experimentally studied.

CHAPTER 3: THREE-BODY LEPTON FLAVOR VIOLATING DECAYS

3.1 Radiative Vector Quarkonium Decays $V \to \gamma\ell_1\overline{\ell}_2$

Addition of a photon to the final state certainly reduces the number of the events available for studies of LFV decays, especially since no compensating mechanisms seem to be present (*c.f.* [79]). However, it also makes it possible for other operators in $\mathcal{L}_{\rm eff}$, that were not considered in two-body decays of vector quarkonium, to contribute. For this reason the analysis of RLFV decays is a worthwhile exercise, especially for the decays of the vector quarkonium states.

3.1.1 Resonant transitions $V \to \gamma(M \to \ell_1\overline{\ell}_2)$

The resonant two-body radiative transitions of vector states $V \to \gamma(M \to \ell_1\overline{\ell}_2)$ could be used to study two-body decays considered above, provided the corresponding branching ratios for the radiative decays are large enough. Since vector states are abundantly produced in e^+e^- annihilation, these decays could provide a powerful tool to study LFV transitions at flavor factories.

If the soft photon[1] can be effectively tagged at B-factories and $(p_{\ell_1} + p_{\ell_2})^2 \approx m_M^2$, the combined branching ratio factorizes[2] and can be written as

$$\mathcal{B}(V \to \gamma\ell_1\overline{\ell}_2) = \mathcal{B}(V \to \gamma M)\mathcal{B}(M \to \ell_1\overline{\ell}_2), \tag{3.1}$$

where the scalar decays ($M = \chi_{q0}$) $\mathcal{B}(\chi_{q0} \to \ell_1\overline{\ell}_2)$ have been studied in Sect. 2.4, while the corresponding pseudoscalar transitions ($M = \eta_q$) $\mathcal{B}(\eta_q \to \ell_1\overline{\ell}_2)$ have been studied in Sect. 2.2.

The resonant RLFV decays are quite useful for studies of scalar heavy meson decays, as

[1] The photon is relatively soft because the resonance mass is close to the mass of the meson that produced it.

[2] This equation implicitly assumes that the state M is narrow, which is an excellent approximation for the scalar heavy quarkonium states considered here (see Table 2.12). A complete Dalitz plot analysis would be required for wider states.

the corresponding branching ratios are large, of order of a few percent [34]. In charm,

$$\mathcal{B}(\psi(2S) \to \gamma\chi_{c0}(1P)) = 9.99 \pm 0.27\% \ ,$$
$$\mathcal{B}(\psi(3770) \to \gamma\chi_{c0}(1P)) = 0.73 \pm 0.09\% \ .$$

The corresponding radiative transitions in beauty sector are also rather large,

$$\begin{aligned} \mathcal{B}(\Upsilon(2S) \to \gamma\chi_{b0}(1P)) &= 3.8 \pm 0.4\% \ , \\ \mathcal{B}(\Upsilon(3S) \to \gamma\chi_{b0}(1P)) &= 0.27 \pm 0.04\% \ , \\ \mathcal{B}(\Upsilon(3S) \to \gamma\chi_{b0}(2P)) &= 5.9 \pm 0.6\% \ . \end{aligned} \tag{3.2}$$

A rough estimate for SuperKEKB [77] shows that with the integrated luminosity of $\mathcal{L} = 250$ fb^{-1} the number of produced χ_b states could reach tens of millions. Thus, studies of LFV transitions of χ_b states could result in a solid bound on the Wilson coefficients of the scalar operators in $\mathcal{L}_{\text{eff}}$.

Similar radiative transitions to the pseudoscalar states are generally smaller. However, since the pseudoscalar 0^{-+} states are lighter than the 1^{--} ones, the radiative transition rates could still reach a percent level in charm:

$$\mathcal{B}(J/\psi \to \gamma\eta_c) = 1.7 \pm 0.4\% \ ,$$
$$\mathcal{B}(\psi(2S) \to \gamma\eta_c) = 0.34 \pm 0.05\% \ .$$

The corresponding branching ratios in b sector are in a sub permille level and cannot be effectively used to study LFV decays of the η_b states.

3.1.2 Non-resonant transitions

Non-resonant three-body radiative decays of vector states $V \to \gamma\ell_1\bar{\ell}_2$ could be used to constrain the scalar operators, which are not accessible in the two-body decays of vector or

pseudoscalar states. Since the final state now includes the photon, it is no longer possible to express all of the hadronic effects in terms of the decay constants. The constraints would then depend on a set of $V \to \gamma$ form factors that are not well known. We will discuss those in a future publication [80].

Here we would provide information about $C_{SL}^{q\ell_1\ell_2}(C_{SR}^{q\ell_1\ell_2})$, but at the expense of introducing model dependence. We shall calculate the transition $V \to \gamma\ell_1\bar{\ell}_2$ choosing a particular model to describe the effective quark-antiquark distribution function [79].

In principle, besides the Wilson coefficients of the scalar operators, non-resonant RLFV decays could be used to obtain information about vector, axial, pseudoscalar, and tensor operators and thus $C_{VL}^{q\ell_1\ell_2}(C_{VR}^{q\ell_1\ell_2})$, $C_{AL}^{q\ell_1\ell_2}(C_{AR}^{q\ell_1\ell_2})$, $C_{PL}^{q\ell_1\ell_2}(C_{PR}^{q\ell_1\ell_2})$, and $C_{TL}^{q\ell_1\ell_2}(C_{TR}^{q\ell_1\ell_2})$. However, because these operators can be constrained using much simpler two-body decays of vector and pseudoscalar states (see Sec. 2.1-2.2) without significant model dependence, and with better statistics, we shall focus here mainly on the scalar operators, leaving the other constraints to the future work [80]. In principle, a calculation of the amplitude $\mathcal{A}(V \to \gamma\ell_1\bar{\ell}_2)$ involves evaluation of the eight diagrams shown in Fig. 3.1. Since the initial state is a 1^{--} vector meson, the contributions of the axial, scalar, and pseudoscalar are contained in diagrams 3.1(a) and 3.1(b). The diagrams 3.1(c) and 3.1(d) contain the vector and tensor operator contributions and 3.1(e)-3.1(h) are generated by the dipole operator contributions. By the same arguments as above, we shall also ignore these vector, tensor, and dipole operators in this section.

A calculation of $\mathcal{A}(V \to \gamma\ell_1\bar{\ell}_2)$ presented in this section involves a model to describe the quark-antiquark wave function of the quarkonium state [79]. We choose to follow [79, 81, 82, 83] and write it as

$$\Psi_V = \frac{I_c}{\sqrt{6}}\Phi_V(x)\left(m_V\gamma^\alpha + ip^\beta\sigma^{\alpha\beta}\right)\epsilon^\alpha(p). \tag{3.3}$$

Here the momentum of the vector meson is p, the momentum fraction of the quarkonium

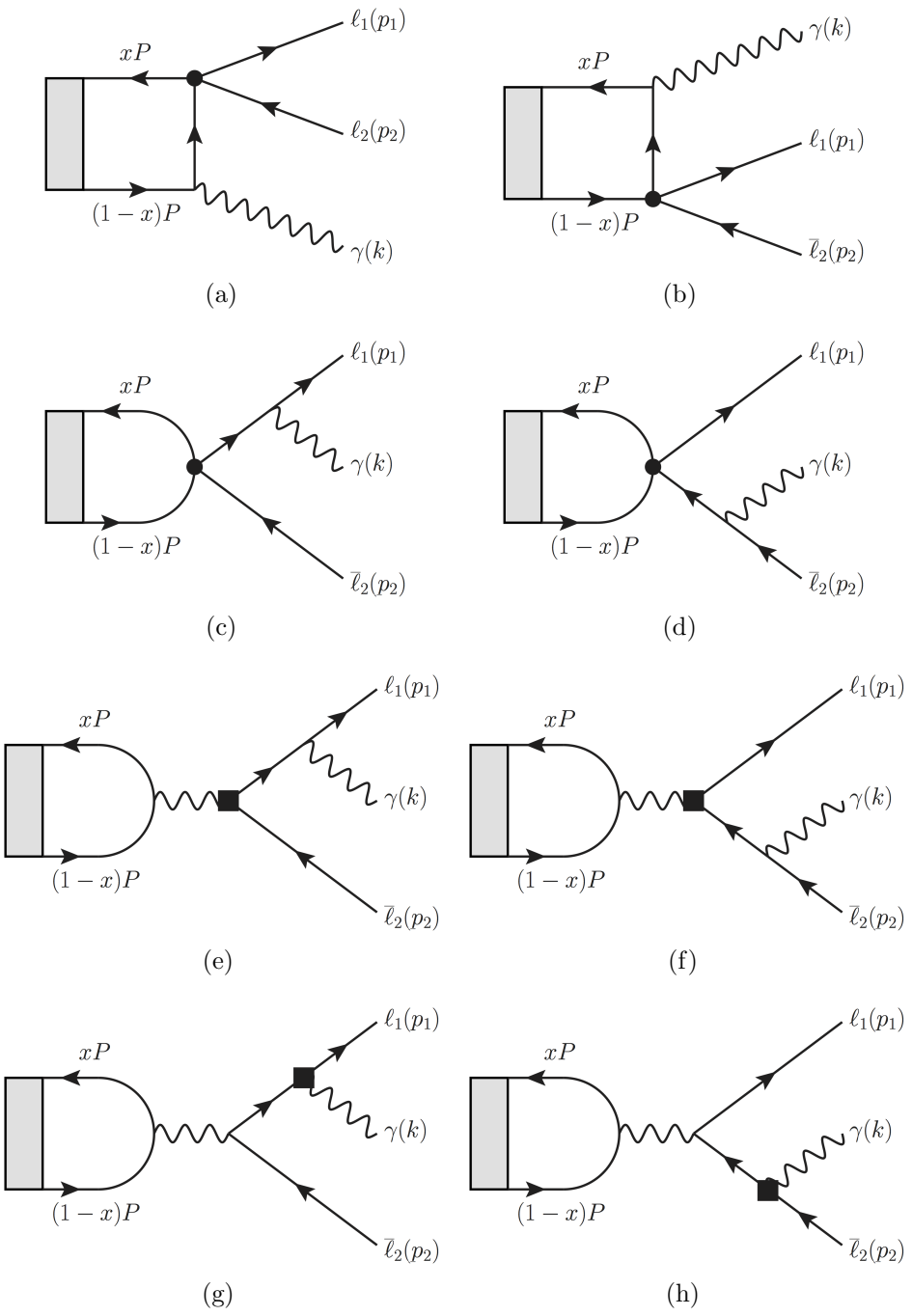

Figure 3.1: Feynman diagrams for $\mathcal{A}(V \to \gamma\ell_1\overline{\ell}_2)$. The black circles represent the four fermion LFV vertex, the black boxes represent the dipole LFV vertex, and the grey boxes represent the quarkonium bound state [35].

carried by one of the constituent quarks is x and the color space identity matrix is I_c. The distribution amplitude, $\Phi_V(x)$, in Eq. (3.3) is defined as

$$\Phi_V(x) = \frac{f_V}{2\sqrt{6}}\delta(x - 1/2), \tag{3.4}$$

where f_V is a decay constant defined in Eq. (2.4). We chose the simplest wave function which makes the approximation that each constituent quark carries half the meson's momentum, which is a good approximation for the heavy quark states made of the same flavor quarks $q\bar{q}$ such as $\Upsilon(nS)$ or J/ψ. The non-local matrix element that is relevant for the radiative transition is then expressed in terms of an integral over momentum fraction:

$$\langle 0|\bar{q}\Gamma^\mu q|V\rangle = \int_0^1 \mathrm{Tr}[\Gamma^\mu \Psi_V]dx. \tag{3.5}$$

We can now calculate the total and differential decay rates. Assuming single operator dominance, the axial, scalar, and pseudoscalar operators lead to the following differential decay rates:

$$\begin{aligned}
\frac{d\Gamma^A_{V\to\gamma\ell_1\bar{\ell}_2}}{dm^2_{12}} &= \frac{1}{9}\frac{\alpha Q_q^2}{(4\pi)^2}\frac{f_V^2}{\Lambda^4}\left(C^2_{AL}+C^2_{AR}\right)\frac{(m_V^2-m_{12}^2)\,(2m_V^2y^2+m_{12}^2)\,(m_V^2y^2-m_{12}^2)^2}{m_V m_{12}^6},\\
\frac{d\Gamma^S_{V\to\gamma\ell_1\bar{\ell}_2}}{dm^2_{12}} &= \frac{1}{24}\frac{\alpha Q_q^2}{(4\pi)^2}\frac{f_V^2 G_F^2 m_V}{\Lambda^4}\left(C^2_{SL}+C^2_{SR}\right)\frac{y^2\,(m_V^2-m_{12}^2)\,(m_V^2y^2-m_{12}^2)^2}{m_{12}^2},\\
\frac{d\Gamma^P_{V\to\gamma\ell_1\bar{\ell}_2}}{dm^2_{12}} &= \frac{1}{24}\frac{\alpha Q_q^2}{(4\pi)^2}\frac{f_V^2 G_F^2 m_V}{\Lambda^4}\left(C^2_{PL}+C^2_{PR}\right)\frac{y^2\,(m_V^2-m_{12}^2)\,(m_V^2y^2-m_{12}^2)^2}{m_{12}^2}.
\end{aligned} \tag{3.6}$$

Here y is defined to be the same as in Sect. 2.1 and we follow the usual definition of the Mandelstam variable $m_{12}^2 = (p_1+p_2)^2$ [34], where momentum p_1 and p_2 correspond to ℓ_1 and ℓ_2. Note that in writing Eqs. (3.6) and (3.7) we suppressed some of the indices of the Wilson coefficients (i.e. $C_{SL}^{q\ell_1\ell_2} \to C_{SL}$) for brevity. The total decay rates for the RLFV transitions

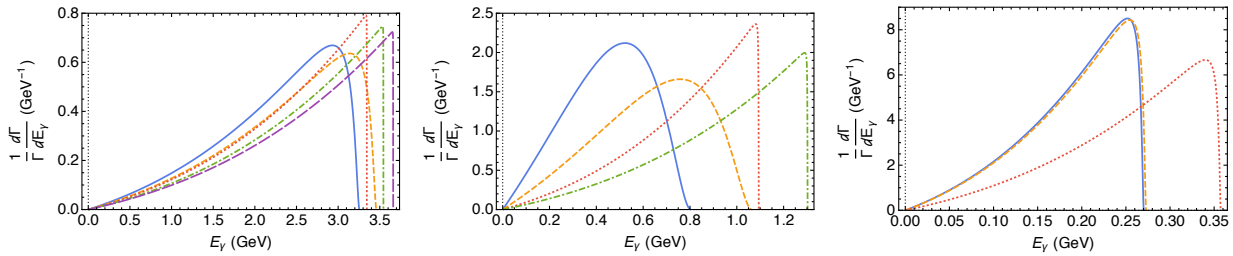

(a) (b) (c)

Figure 3.2: Differential decay rates as functions of photon energy E_γ for axial operators. Plotted decay rates are for (a) $\Upsilon(1S) \to \gamma\mu\tau$ or $\gamma e\tau$ (solid blue), $\Upsilon(2S) \to \gamma\mu\tau$ or $\gamma e\tau$ (short-dashed gold), $\Upsilon(3S) \to \gamma\mu\tau$ or $\gamma e\tau$ (dotted red), $\Upsilon(1S) \to \gamma e\mu$ (dot-dashed green), $\Upsilon(2S) \to \gamma e\mu$ and $\Upsilon(3S) \to \gamma e\mu$ (long-dashed purple); (b) $J\psi \to \gamma\mu\tau$ or $\gamma e\tau$ (solid blue), $\psi(2S) \to \gamma\mu\tau$ or $\gamma e\tau$ (short-dashed gold), $J\psi \to \gamma e\mu$ (dotted red), $\psi(2S) \to \gamma e\mu$ (dot-dashed green); (c) $\rho \to \gamma e\mu$ (solid blue), $\omega \to \gamma e\mu$ (short-dashed gold), $\phi \to \gamma e\mu$ (dotted red) [35].

can be found by integrating Eq. (3.6) over m_{12}^2, which gives

$$\begin{aligned}
\Gamma_A(V \to \gamma\ell_1\bar{\ell}_2) &= \frac{1}{18}\frac{\alpha Q_q^2}{(4\pi)^2}\frac{f_V^2 m_V^3}{\Lambda^4}\left(C_{AL}^2 + C_{AR}^2\right) f(y^2), \\
\Gamma_S(V \to \gamma\ell_1\bar{\ell}_2) &= \frac{1}{144}\frac{\alpha Q_q^2}{(4\pi)^2}\frac{f_V^2 G_F^2 m_V^7}{\Lambda^4}\left(C_{SL}^2 + C_{SR}^2\right) y^2 f(y^2), \\
\Gamma_P(V \to \gamma\ell_1\bar{\ell}_2) &= \frac{1}{144}\frac{\alpha Q_q^2}{(4\pi)^2}\frac{f_V^2 G_F^2 m_V^7}{\Lambda^4}\left(C_{PL}^2 + C_{PR}^2\right) y^2 f(y^2),
\end{aligned} \tag{3.7}$$

where $f(y^2) = 1 - 6y^2 - 12y^4 \log(y) + 3y^4 + 2y^6$. We may use Eq. (3.7) to normalize differential decay distributions, so that they are independent of the unknown Wilson coefficients and plot the normalized decay distributions under the assumption of single operator dominance. We show differential photon spectra in $V \to \gamma\ell_1\bar{\ell}_2$ decay in Fig. 3.2 for the axial operators, and in Fig. 3.3 for the scalar or pseudoscalar ones.

Since no experimental constraints are available for the RLFV decays of vector quarkonia, we cannot yet place any constraints on the Wilson coefficients from those transitions.

3.2 Radiative Pseudoscalar Meson Decays $P \to \gamma\ell_1\bar{\ell}_2$

Similarly to the $B_s^0 \to \mu^+\mu^-\gamma$ transition [84, 85, 86, 87, 88], addition of a photon to the $\ell_1\bar{\ell}_2$ final state allows one to probe operators of the effective Lagrangian that do not

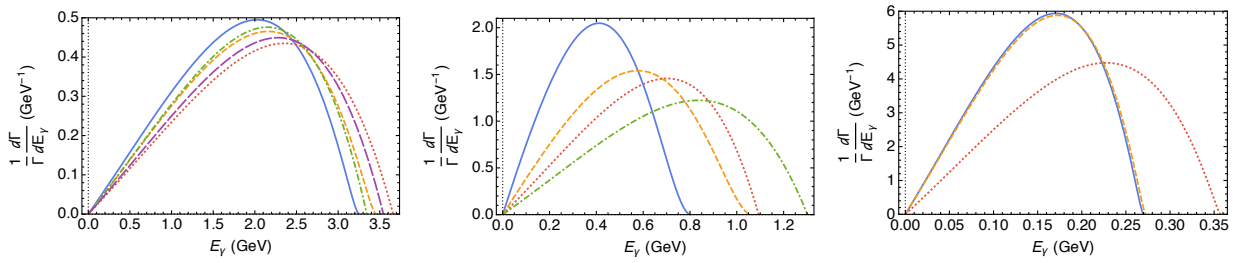

(a) (b) (c)

Figure 3.3: Differential decay rates as functions of photon energy E_γ for scalar/pseudoscalar operators. Plotted decay rates are for (a) $\Upsilon(1S) \to \gamma\mu\tau$ or $\gamma e\tau$ (solid blue), $\Upsilon(2S) \to \gamma\mu\tau$ or $\gamma e\tau$ (short-dashed gold), $\Upsilon(3S) \to \gamma\mu\tau$, $\gamma e\tau$, or $\gamma e\mu$ (dotted red), $\Upsilon(1S) \to \gamma e\mu$ (dot-dashed green), $\Upsilon(2S) \to \gamma e\mu$ (long-dashed purple); (b) $J\psi \to \gamma\mu\tau$ or $\gamma e\tau$ (solid blue), $\psi(2S) \to \gamma\mu\tau$ or $\gamma e\tau$ (short-dashed gold), $J\psi \to \gamma e\mu$ (dotted red), $\psi(2S) \to \gamma e\mu$ (dot-dashed green); (c) $\rho \to \gamma e\mu$ (solid blue), $\omega \to \gamma e\mu$ (short-dashed gold), $\phi \to \gamma e\mu$ (dotted red) [35].

contribute to $P \to \ell_1\bar{\ell}_2$ transition. This was pointed out for the LFV decays in [35], and, more importantly in [89] (for a calculation of $B_s^0 \to \ell_1\bar{\ell}_2\gamma$ in the model of [90]). In addition, $P \to \ell_1\bar{\ell}_2$ decays suffer from chiral suppression (see Eq. (2.11)), which three-body radiative decays do not neccessarily exhibit. Thus, it is possible that RLFV decays might have larger branching ratios than two-body LFV transitions (see [84, 85, 86, 87, 88] for similar effects in lepton flavor conserving decays). Here we evaluate RLFV decays of the pseudoscalar mesons with the model-independent effective Lagrangian of Eq. (1.5).

It might be theoretically easier to deal with a three-body final state that contains no strongly-interacting composite particles. Still, the calculation of the $P \to \ell_1\bar{\ell}_2\gamma$ decay is more complicated than $P \to \ell_1\bar{\ell}_2$, where all nonperturbative effects are summarized in one decay constant f_P. Further, because of the electromagnetic gauge invariance, it is important to have a good understanding of what kind of constraints the kinematic structure of the decay amplitude imposes on the dynamics of these transitions. Let us now derive the most general amplitude for $P \to \ell_1\bar{\ell}_2\gamma$.

3.2.1 General amplitude and differential decay rate for $P \to \ell_1 \bar{\ell}_2 \gamma$

The most general expression for the $P(p) \to \gamma(k)\ell_1(p_1)\bar{\ell}_2(p_2)$ decay amplitude can be obtained using the Bardeen-Tung formalism which we modify to include LFV decays [91]. The decay amplitude may be written as

$$A(P(p) \to \gamma(k)\ell_1(p_1)\bar{\ell}_2(p_2)) = \overline{u}(p_1, s_1)\ M^{\mu}(p, k, q)\ v(p_2, s_2)\ \varepsilon^*_{\mu}(k), \tag{3.8}$$

where $\overline{u}(p_1, s_1)$ and $v(p_2, s_2)$ are spinors for ℓ_1 and $\bar{\ell}_2$, $q = \frac{1}{2}(p_1 - p_2)$, and $\varepsilon^*_{\mu}(k)$ is the polarization vector of the photon. The function $M^{\mu}(p, k, q)$, which we seek to parameterize, transforms as a tensor under Lorentz transformations. This function should only contain dynamical singularities, so particular care should be taking by writing it in such a way that it does not contain kinematical ones[3]. The most general expression for the $M^{\mu}(p, k, q)$ from Eq. (3.8) can be written by expanding it into simpler Lorentz structures $\ell_i^{\mu}(p, q, k)$ multiplied by the invariant functions $M_i^{P\ell_1\ell_2}$, which only depend on Lorentz invariants,

$$M^{\mu}(p, k, q) = \sum_i \ell_i^{\mu}(p, q, k) M_i^{P\ell_1\ell_2}(p^2, ...)\ . \tag{3.9}$$

The most general parameterization of Eq. (3.9) contains twelve form-factors,

$$\begin{aligned} M^{\mu}(p, k, q) &= \gamma^{\mu}\left(M_1^{P\ell_1\ell_2} + \not{k} M_2^{P\ell_1\ell_2}\right) + i\gamma_5\gamma^{\mu}\left(M_3^{P\ell_1\ell_2} + \not{k} M_4^{P\ell_1\ell_2}\right) \\ &+ q^{\mu}\left(M_5^{P\ell_1\ell_2} + \not{k} M_6^{P\ell_1\ell_2}\right) + i\gamma_5 q^{\mu}\left(M_7^{P\ell_1\ell_2} + \not{k} M_8^{P\ell_1\ell_2}\right) \\ &+ p^{\mu}\left(M_9^{q\ell_1\ell_2} + \not{k} M_{10}^{q\ell_1\ell_2}\right) + i\gamma_5 p^{\mu}\left(M_{11}^{P\ell_1\ell_2} + \not{k} M_{12}^{P\ell_1\ell_2}\right)\ . \end{aligned} \tag{3.10}$$

In writing of Eq. (3.10) we used the equation of motion for the lepton spinors, and rewrote terms containing $\sigma^{\mu\nu}$ in terms of components, e.g. $i\sigma^{\mu\nu}q_{\nu} = q^{\mu} - \gamma^{\mu}\not{q}$. Note the terms proportional to $\not{q}$ can be expressed as terms proportional to $\not{k}$ using momentum conservation

[3]Kinematic singularities occur when a scalar product such as $p \cdot k$ can go to zero in the denominator of a term in the function. This differs from a dynamic singularity, which occurs in the denominator of a propagator for example like $1/(q^2 - m^2)$ when $q^2 \to m^2$.

and equations of motion. Next, terms proportional to the $\epsilon^{\mu\nu\alpha\beta}$ tensor, such as $\epsilon^{\mu\nu\alpha\beta}\gamma_\nu p_\alpha k_\beta$, can be written in terms of the existing form factors of Eq. (3.10) using the relation

$$i\epsilon^{\mu\nu\alpha\beta}\gamma_\beta = \gamma^\mu\gamma^\nu\gamma^\alpha\gamma_5 - g^{\mu\nu}\gamma^\alpha\gamma_5 - g^{\nu\alpha}\gamma^\mu\gamma_5 + g^{\mu\alpha}\gamma^\nu\gamma_5 \tag{3.11}$$

and the equations of motion. Finally, all possible terms in Eq. (3.10) proportional to k^μ trivially vanish by gauge invariance.

The set of Eq. (3.10) is still not minimal, as the condition of gauge invariance $k_\mu M^\mu(p,k,q) = 0$ implies that some of the $M_i^{P\ell_1\ell_2}$ in Eq. (3.10) are not independent. An elegant way of finding the minimal set of gauge-invariant Lorentz structures has been given in [91], which we shall apply to our analysis. To get the minimal set, it is most convenient to apply a projection operator

$$P^{\mu\nu} = g^{\mu\nu} - \frac{p^\mu k^\nu}{(p\cdot k)} \tag{3.12}$$

to $M^\mu(p,k,q)$. Since $P^{\mu\nu}M_\nu = M^\mu$ and $k_\mu P^{\mu\nu} = 0$, $P^{\mu\nu}$ does indeed project out gauge-invariant structures in $M^\mu(p,k,q)$. Applying $P^{\mu\nu}$ to Eq. (3.10) we find $P_\nu P^{\mu\nu} = 0$ and so terms proportional to p^μ do not give contributions to the minimal set and should be dropped, leaving the number of independent amplitudes at eight[4]. Applying the condition $k_\mu \ell_i^\mu = 0$ fwe write the Lorentz structures L_i^μ for the set of amplitudes as

$$M^\mu(p,k,q) = \sum_i L_i^\mu(p,q,k) A_i^{P\ell_1\ell_2}(p^2,...), \tag{3.13}$$

which are defined in a manner that removes all kinematical singularities. The $A_i^{P\ell_1\ell_2}(p^2,...)$

[4]There is a simple argument presented in Refs. [92, 93] which calculates the number of independent amplitudes. The number of independent amplitudes is the number N of possible helicity amplitudes as calculated by $N_i = \prod(2s_i+1)$. Here i is the index of the particle in the process and s_i is the spin of the particle. In the case of $P \to \gamma\ell_1\bar{\ell}_2$ we would naively calculate $N = 1\times 3\times 2\times 2 = 12$ because $s_P = 0$, $s_\gamma = 1$, and $s_{\ell_{1,2}} = 1/2$. This is incorrect because the formula over counts the number of helicity states for the photon, which is 2. Correcting for this we find $N = 1\times 2\times 2\times 2 = 8$, which exactly the number of independent amplitudes we found.

are new scalar form factors, while L_i^μ are

$$\begin{aligned}
L_1^\mu &= \gamma^\mu \not{k}, \\
L_2^\mu &= i\gamma_5 \gamma^\mu \not{k}, \\
L_3^\mu &= (p\cdot k)\, q^\mu - (k\cdot q)\, p^\mu, \\
L_4^\mu &= i\gamma_5 \left[(p\cdot k)\, q^\mu - (k\cdot q)\, p^\mu\right], \\
L_5^\mu &= (p\cdot k)\, \gamma^\mu - p^\mu \not{k}, \\
L_6^\mu &= i\gamma_5 \left[(p\cdot k)\, \gamma^\mu - p^\mu \not{k}\right], \\
L_7^\mu &= q^\mu \not{k} - (k\cdot q)\, \gamma^\mu, \\
L_8^\mu &= i\gamma_5 \left[q^\mu \not{k} - (k\cdot q)\, \gamma^\mu\right].
\end{aligned} \tag{3.14}$$

This implies that the decay amplitude can be written as

$$A(P(p) \to \gamma(k)\ell_1(p_1)\bar{\ell}_2(p_2)) = \sum_i A_i^{P\ell_1\ell_2}(p^2, ...)\ \overline{u}(p_1, s_1)\ L_i^\mu(p, q, k)\ v(p_2, s_2)\ \varepsilon_\mu^*(k). \tag{3.15}$$

Using this general amplitude for a three-body pseudoscalar decay, $P \to \gamma\ell_1\bar{\ell}_2$, we calculate Eq. (3.16), which is a general differential decay rate that depends on the same scalar functions $A_i^{P\ell_1\ell_2}(p^2, ...)$. In Eq. (3.16) the Mandelstam variables have the usual definitions: $m_{12}^2 = (p_1 + p_2)^2$, $m_{13}^2 = (p_1 + k)^2$, $m_{23}^2 = (p_2 + k)^2$, where $p_{1,2}$ is the $\ell_{1,2}$ lepton momentum and k is the γ photon momentum. They are related to the pseudoscalar momentum, p, by $p = p_1 + p_2 + k$. The mass m_P is the pseudoscalar mass, m_2 is the heavier lepton mass, and $y = m_2/m_P$. The superscript of $P\ell_1\ell_2$ on the scalar functions $A_i^{P\ell_1\ell_2}(p^2, ...)$ is dropped for brevity in Eq. (3.16). We introduce a photon mass, m_γ, to regulate the infrared divergences that will appear via bremsstrahlung diagrams. We use a value of $m_\gamma = 60$ MeV as our

cut-off, which is near the final state invariant mass resolution of experiments [89].

$$
\begin{aligned}
\frac{d\Gamma}{dm_{12}^2 dm_{23}^2} = \frac{1}{(2\pi)^3}\frac{1}{384 m_P^3}\Big[& -16\left(A_1^2+A_2^2\right)\left(m_{13}^2\left(m_P^2y^2-m_{23}^2\right)+m_\gamma^2 m_P^2\left(1-y^2\right)\right) \\
& +2\left(A_3^2+A_4^2\right)\left(m_P^2y^2-m_{12}^2\right)\Big\{m_{13}^2\left(m_P^4y^2-m_{12}^2m_{23}^2\right) \\
& \qquad +m_\gamma^2\left(m_{13}^2m_{23}^2-\tfrac{1}{4}\left(m_P^2-m_{12}^2+m_\gamma^2\right)^2\right)\Big\} \\
& +4\left(A_5^2+A_6^2\right)\Big\{2m_P^6y^4+m_{12}^2\left(\left(m_P^2y^2-m_{13}^2\right)^2+m_{23}^4\right) \\
& \qquad -m_P^2y^2\left(m_P^2+m_{12}^2\right)\left(m_P^2y^2+m_{23}^2-m_{13}^2\right)\Big\} \\
& -\left(A_7^2+A_8^2\right)\Big\{\left(2m_P^2y^2-m_{12}^2\right)\left(\left(m_P^2y^2-m_{23}^2\right)^2+m_{13}^4\right) \\
& \qquad +m_P^2y^2\left(m_P^2-m_{12}^2\right)\left(m_P^2y^2-m_{23}^2+m_{13}^2\right)\Big\} \\
& -8Re\left[A_1A_3^*+A_2A_4^*\right]\Big\{m_{13}^2\left(m_P^4y^2-m_{12}^2m_{23}^2\right) \\
& \qquad -\tfrac{1}{2}m_\gamma^2\left(m_P^2+m_\gamma^2-m_{12}^2\right)\left(m_P^2y^2-m_{12}^2\right)\Big\} \\
& -16Re\left[A_1A_5^*+A_2A_6^*\right]m_Pym_{13}^2\left(m_P^2-m_{12}^2\right) \\
& +8Re\left[A_1A_7^*+A_2A_8^*\right]m_Pym_{13}^2\left(m_P^2y^2-m_{23}^2+m_{13}^2\right) \\
& +8Re\left[A_3A_5^*+A_4A_6^*\right]m_Pym_{13}^2\left(m_P^4y^2-m_{12}^2m_{23}^2\right) \\
& +4Re\left[A_3A_7^*+A_4A_8^*\right]m_Pym_{13}^2\left(m_P^4y^2-m_{12}^2m_{23}^2\right) \\
& +4Re\left[A_5A_7^*+A_6A_8^*\right]\left(m_P^2-m_{12}^2\right)\left(m_P^2y^2-m_{12}^2\right)\left(m_P^2y^2-m_{23}^2+m_{13}^2\right)\Big].
\end{aligned}
\tag{3.16}
$$

3.2.2 Scalar functions $A_i^{P\ell_1\ell_2}$ for B_q^0, $\bar{D}^0$, and K^0 mesons

The scalar functions $A_i^{P\ell_1\ell_2}(p^2,...)$ introduced in Eq. (3.13) can only depend on kinematical invariants and form factors. These functions can be calculated on the lattice or using other non-perturbative methods. Examining the four-fermion Lagrangian of Eq. (1.8) one can find that the contributions of Figs. (3.4), (3.6), and (3.7) to $A_i^{P\ell_1\ell_2}$ could be written in terms of the form factors for $P(p)\to\gamma(k)$ transitions used to parameterize lepton flavor conserving decays, such as $P^+\to\gamma\ell^+\bar{\nu}$ or $P^0\to\gamma\ell\bar{\ell}$. The definitions of the form factors are

[85, 86, 87, 89]

$$\begin{aligned}
\langle\gamma(k)|\overline{q}_1\gamma^\mu\gamma_5 q_2|P(p)\rangle &= i\sqrt{4\pi\alpha}\;\varepsilon^*_\alpha(k)\left[g^{\alpha\mu}p\cdot k - p^\alpha k^\mu\right] f_A^P[Q^2,k^2], && (3.17)\\
\langle\gamma(k)|\overline{q}_1\gamma^\mu q_2|P(p)\rangle &= \sqrt{4\pi\alpha}\;\varepsilon^*_\nu(k)\epsilon^{\mu\nu\alpha\beta}p_\alpha k_\beta f_V^P[Q^2,k^2], && (3.18)\\
\langle\gamma^*(k)|\overline{q}_1\sigma^{\mu\nu}q_2|P(p)\rangle &= i\sqrt{4\pi\alpha}\;\varepsilon^*_\alpha(k)\Bigg[\epsilon^{\mu\nu\alpha\beta}k_\beta f_{T1}^P[Q^2,k^2]\\
&\quad+\left(p^\alpha-\frac{p\cdot k}{k^2}k^\alpha\right)\epsilon^{\mu\nu\rho\beta}p_\rho k_\beta f_{T2}^P[Q^2,k^2] && (3.19)\\
&\quad+\left(\epsilon^{\mu\nu\alpha\rho}p_\rho+\frac{k^\alpha}{k^2}\epsilon^{\mu\nu\rho\beta}p_\rho k_\beta\right)f_{T3}^P[Q^2,k^2]\Bigg].
\end{aligned}$$

Here $Q = p - k$ and the tensor form factors are defined for an off-shell photon. The tensor form factors $f^P_{T1,2,3}[k_1^2, k_2^2]$ are functions of two variables: k_1, which is the momentum flowing from a vertex associated with the tensor current, and k_2, which is the momentum of the photon emitted from the valence quark of the meson. Note that for the on-shell photon $k^2 = 0$, there exist a relationship between f^P_{T2} and f^P_{T3}. Gauge invariance implies that $f^P_{T3}[Q^2, 0] = (p\cdot k) f^P_{T2}[Q^2, 0]$, so the tensor matrix element simplifies to [85]

$$\begin{aligned}
\langle\gamma(k)|\overline{q}_1\sigma_{\mu\nu}q_2|P(p)\rangle = i\sqrt{4\pi\alpha}\;\varepsilon^{*\alpha}(k)\Big[&\epsilon_{\mu\nu\alpha\beta}k^\beta f_{T1}^P[Q^2,0]\\
&+\left(p_\alpha\epsilon_{\mu\nu\rho\beta}p^\rho k^\beta + p\cdot k\epsilon_{\mu\nu\alpha\beta}p^\beta\right)f_{T2}^P[Q^2,0]\Big].
\end{aligned} \qquad (3.20)$$

Using Eqs. (3.17), (3.18), and (3.20) we can calculate the scalar function contributions of the axial, vector, and tensor operators from the Lagrangian in Eq. (1.8) of type $\mathcal{O} \sim (\ell_1\overline{\ell}_2)(\overline{q}_1 q_2)$ where $q_1 \neq q_2$, which are found in Fig. (3.4). To calculate these and the other diagrams that follow one must understand that the amplitudes of the individual diagrams factorize into a part described by the matrix elements that define the form factors and a part that can be found by calculating the Feynman rules for the new physics effective interaction. In Fig. (3.4) these new physics effective interactions are described in Eq. (1.8).

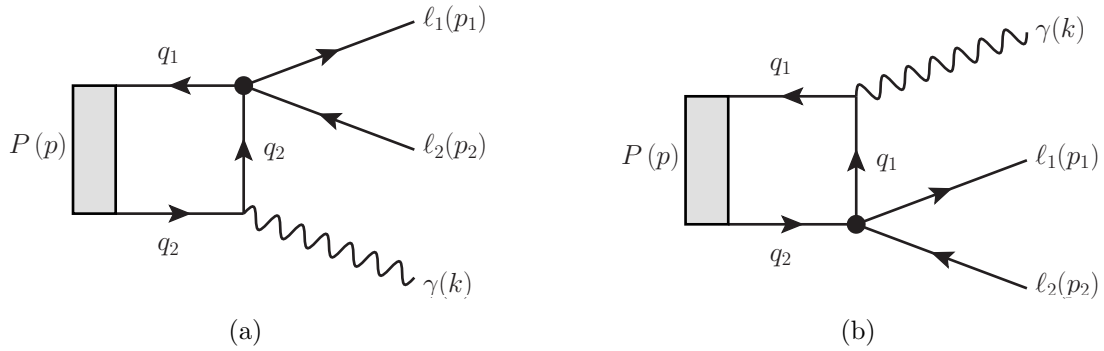

Figure 3.4: Four-fermion interaction diagrams for $\mathcal{A}(P \to \gamma\ell_1\overline{\ell}_2)$ for operators of type $\mathcal{O} \sim (\ell_1\overline{\ell}_2)(\overline{q}_1 q_2)$ where $q_1 \neq q_2$ with photon $\gamma(k)$ attached to the valence quark. The black circles represent the four-fermion LFV vertex defined in $\mathcal{L}_{eff}$ of Eq. (1.8) [36].

The contributions of these diagrams to the scalar functions $A_i^{P\ell_1\ell_2}$ are

$$\begin{aligned}
A_1^{3.4ab} = &\quad \tfrac{\sqrt{4\pi\alpha}}{2\Lambda^2}\left(C_{VR}^{q_1q_2\ell_1\ell_2} - C_{VL}^{q_1q_2\ell_1\ell_2}\right) y m_P f_V^P[m_{12}^2, 0] \\
&- \tfrac{\sqrt{4\pi\alpha}}{\Lambda^2}\left(C_{TR}^{q_1q_2\ell_1\ell_2} - C_{TL}^{q_1q_2\ell_1\ell_2}\right) y m_P m_H G_F \left(f_{T1}^P[m_{12}^2, 0] + \tfrac{m_P^2 - m_{12}^2}{2} f_{T2}^P[m_{12}^2, 0]\right), \\
A_3^{3.4ab} = &- \tfrac{2\sqrt{4\pi\alpha}}{\Lambda^2}\left(C_{TR}^{q_1q_2\ell_1\ell_2} - C_{TL}^{q_1q_2\ell_1\ell_2}\right) y m_P m_H G_F f_{T2}^P[m_{12}^2, 0], \\
A_5^{3.4ab} = &- \tfrac{\sqrt{4\pi\alpha}}{2\Lambda^2}\left(C_{AR}^{q_1q_2\ell_1\ell_2} + C_{AL}^{q_1q_2\ell_1\ell_2}\right) f_A^P[m_{12}^2] \\
&+ \tfrac{\sqrt{4\pi\alpha}}{\Lambda^2}\left(C_{TR}^{q_1q_2\ell_1\ell_2} - C_{TL}^{q_1q_2\ell_1\ell_2}\right) y^2 m_P^2 m_H G_F f_{T2}^P[m_{12}^2, 0], \text{ and} \\
A_7^{3.4ab} = &\quad \tfrac{\sqrt{4\pi\alpha}}{\Lambda^2}\left(C_{VR}^{q_1q_2\ell_1\ell_2} - C_{VL}^{q_1q_2\ell_1\ell_2}\right) f_V^P[m_{12}^2, 0].
\end{aligned} \tag{3.21}$$

Note that in this section (e.g. in writing Eq. (3.21)) we suppressed the previously used superscript of $P\ell_1\ell_2$ in favor of a superscript related to the associated diagrams, which consists of the figure number and sub-figure letters (i.e. $3.4ab$). We only show the odd subscript scalar function equations. The even subscript equations can be found from the odd subscript equations by replacing the left-handed WCs by their negative magnitudes (i.e. $C_{VL} \to -C_{VL}$, $C_{AL} \to -C_{AL}$, etc.) and multiplying the odd subscript scalar function by the imaginary constant i. This may be used to find A_2 from A_1, A_4 from A_3, A_6 from A_5, and A_8 from A_7 and is true throughout this section.

There is no contribution in Fig. (3.4) from the pseudoscalar operators of the Lagrangian

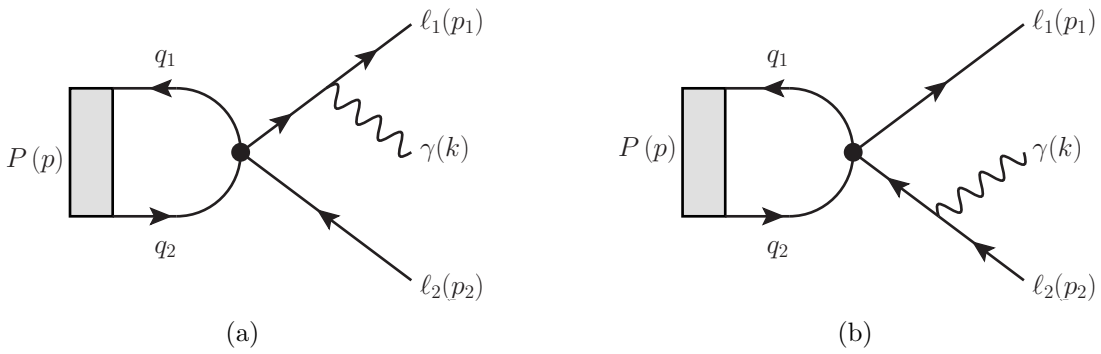

Figure 3.5: Bremsstrahlung diagrams for $\mathcal{A}(P \to \gamma\ell_1\bar{\ell}_2)$ for operators of type $\mathcal{O} \sim (\ell_1\bar{\ell}_2)(\bar{q}_1 q_2)$ where $q_1 \neq q_2$. The black circles represent the four-fermion LFV vertex defined in $\mathcal{L}_{eff}$ of Eq. (1.8) [36].

in Eq. (1.8). This can be seen by taking the divergence of the matrix element for the axial current to relate the axial and pseudoscalar matrix elements,

$$\langle\gamma(k)|\bar{q}_1\gamma_5 q_2|P(p)\rangle = -\frac{1}{m_{q_1}+m_{q_2}}p^\mu\langle\gamma(k)|\bar{q}_1\gamma_\mu\gamma_5 q_2|P(p)\rangle, \tag{3.22}$$

and using Eq. (3.17) to get

$$\langle\gamma(k)|\bar{q}_1\gamma_5 q_2|P(p)\rangle = 0. \tag{3.23}$$

A similar argument can be made to prove that the scalar operators also do not give form factor contributions.

The bremsstrahlung diagrams of Fig. (3.5) are calculated similarly to the two-body decays of Sect. 2.3 using the matrix element of Eq. (2.9). We have given the photon a small mass, m_γ, to regulate the infrared divergences. This divergence only appears in the quark flavor changing axial and pseudoscalar operator terms of the scalar functions, Eq. (3.24), so the photon mass is set to zero for the non-divergent terms. The same is true for the differential decay rate in Eq. (3.16). The axial and pseudoscalar operator scalar function terms are defined here as

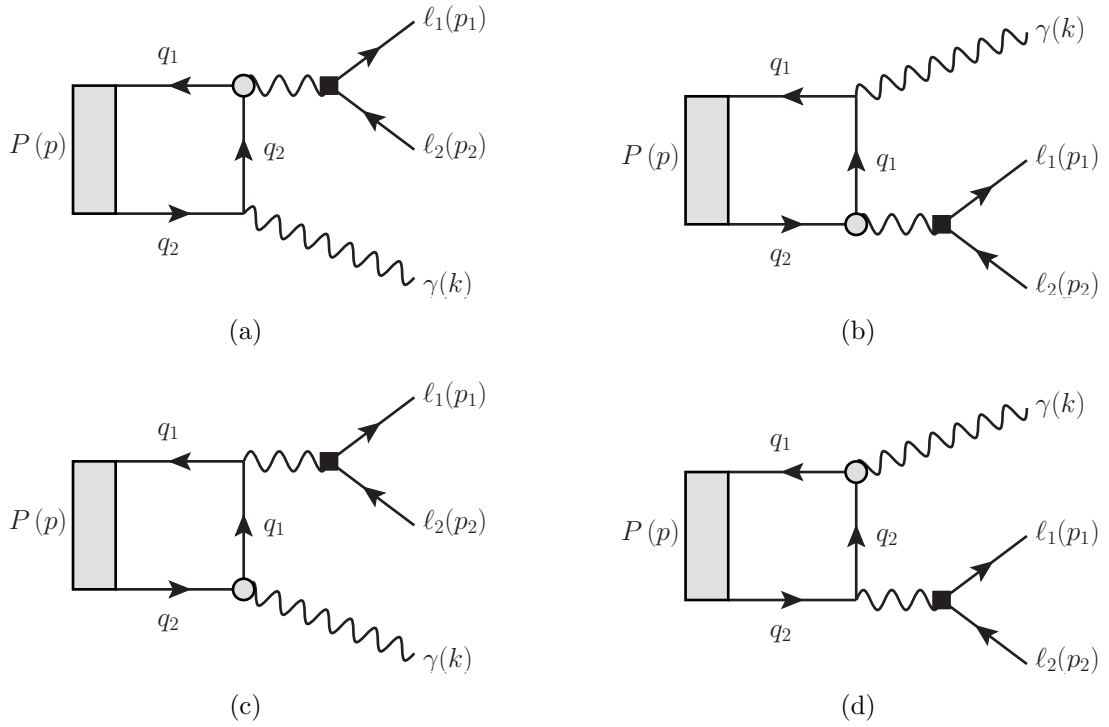

Figure 3.6: Dipole operator diagrams for $\mathcal{A}(P \to \gamma \ell_1 \bar{\ell}_2)$. The grey circles with the black border represent the SM dipole penguin vertex (Eq. (1.7)) and the black boxes represent the dipole LFV vertex (Eq. (1.6)). Note that the contributions of these diagrams are severely constrained by already available data on $\ell_1 \to \ell_2 \gamma$ decays [36].

$$A_1^{3.5ab} = \frac{\sqrt{4\pi\alpha}}{2\Lambda^2}\left(C_{AR}^{q_1q_2\ell_1\ell_2} + C_{AL}^{q_1q_2\ell_1\ell_2} + m_P^2 G_F\left(C_{PR}^{q_1q_2\ell_1\ell_2} + C_{PL}^{q_1q_2\ell_1\ell_2}\right)\right)\frac{y m_P f_P\left(m_P^2+m_\gamma^2-m_{12}^2\right)}{m_{13}^2\left(m_{23}^2-m_P^2 y^2\right)},$$
$$A_3^{3.5ab} = \frac{2\sqrt{4\pi\alpha}}{\Lambda^2}\left(C_{AR}^{q_1q_2\ell_1\ell_2} - C_{AL}^{q_1q_2\ell_1\ell_2} + m_P^2 G_F\left(C_{PR}^{q_1q_2\ell_1\ell_2} - C_{PL}^{q_1q_2\ell_1\ell_2}\right)\right)\frac{y m_P f_P}{m_{13}^2\left(m_{23}^2-m_P^2 y^2\right)}. \quad (3.24)$$

The diagrams in Fig. (3.6) contain both the dipole operators of Eq. (1.6) and contributions from the SM dipole penguin operator, Eq. (1.7). This is directly related to both the on and off-shell tensor matrix elements in Eqs. (3.19) and (3.20) from which we need to write matrix elements of the form $\langle \gamma(k)|\overline{q}_1 \sigma^{\mu\nu}(1 \pm \gamma_5) q_2|P(p)\rangle$. These can be found by using the

relation $\sigma_{\mu\nu}\gamma_5 = -\frac{i}{2}\epsilon_{\mu\nu\alpha\beta}\sigma^{\alpha\beta}$, which yields:

$$\begin{aligned}\langle\gamma(k)|\overline{q}_1\sigma^{\mu\nu}(1\pm\gamma_5)q_2|P(p)\rangle Q_\nu = i\sqrt{4\pi\alpha}\;\varepsilon^*_\alpha(k)\big\{\;&\left(f_{T1}^P[Q^2,0]+p\cdot k f_{T2}^P[Q^2,0]\right)\epsilon^{pk\alpha\mu}\\ &\pm i\left(f_{T1}^P[Q^2,0]+p\cdot Q f_{T2}^P[Q^2,0]\right)\left(g^{\alpha\mu}p\cdot k - p^\alpha k^\mu\right)\big\},\end{aligned} \tag{3.25}$$

$$\begin{aligned}\langle\gamma^*(Q)|\overline{q}_1\sigma^{\mu\nu}(1\pm\gamma_5)q_2|P(p)\rangle k_\nu = fi\sqrt{4\pi\alpha}\;\varepsilon^*_\alpha(Q)\left\{\epsilon^{pk\mu\alpha}\pm i\left(g^{\alpha\mu}p\cdot k - p^\mu k^\alpha\right)\right\}\\ \times\left(f_{T1}^P[0,Q^2]+f_{T3}^P[0,Q^2]\right).\end{aligned} \tag{3.26}$$

The on-shell matrix element in Eq. (3.25) contributes to Figs. 3.6(a) and 3.6(b). While the off-shell matrix element in Eq. (3.26) is necessary for calculating the dipole operator contributions of the diagrams in Figs. 3.6(c) and 3.6(d). In these diagrams, the lepton current is attached to the photon coming from the meson's valence quarks and so $Q \leftrightarrow k$ when we calculate Eq. (3.26). Using these matrix elements we find the dipole operator components of the scalar functions which are

$$\begin{aligned}A_1^{3.6abcd} &= -\tfrac{1}{\Lambda^2}\left(C_{DR}^{\ell_1\ell_2}-C_{DL}^{\ell_1\ell_2}\right)\tfrac{4\pi\alpha}{\pi^2}\;y m_P m_H\tfrac{G_F}{\sqrt{2}}C_{7\gamma}\sum_q\lambda_q^P\;f_{T,I}^P,\\ A_3^{3.6abcd} &= \;\tfrac{2}{\Lambda^2}\tfrac{4\pi\alpha}{\pi^2}\tfrac{y m_P m_H}{m_{12}^2}\tfrac{G_F}{\sqrt{2}}C_{7\gamma}\sum_q\lambda_q^P\left(\left(C_{DR}^{\ell_1\ell_2}-C_{DL}^{\ell_1\ell_2}\right)f_{T,\mathrm{I}}^P-\left(C_{DR}^{\ell_1\ell_2}+C_{DL}^{\ell_1\ell_2}\right)f_{T,\mathrm{II}}^P\right),\\ A_5^{3.6abcd} &= -\tfrac{1}{\Lambda^2}\tfrac{4\pi\alpha}{\pi^2}\tfrac{y^2 m_P^2 m_H}{m_{12}^2}\tfrac{G_F}{\sqrt{2}}C_{7\gamma}\sum_q\lambda_q^P\left(\left(C_{DR}^{\ell_1\ell_2}-C_{DL}^{\ell_1\ell_2}\right)f_{T,\mathrm{I}}^P-\left(C_{DR}^{\ell_1\ell_2}+C_{DL}^{\ell_1\ell_2}\right)f_{T,\mathrm{II}}^P\right),\end{aligned} \tag{3.27}$$

where we have used the shorthand notations $f_{T,\mathrm{I}}^P$ and $f_{T,\mathrm{II}}^P$ that we define as

$$\begin{aligned}f_{T,\mathrm{I}}^P &= f_{T1}^P[m_{12}^2,0]+f_{T1}^P[0,m_{12}^2]+\tfrac{m_P^2-m_{12}^2}{2}f_{T2}^P[m_{12}^2,0]+f_{T3}^P[0,m_{12}^2]\text{ and}\\ f_{T,\mathrm{II}}^P &= f_{T1}^P[m_{12}^2,0]+f_{T1}^P[0,m_{12}^2]+\tfrac{m_P^2+m_{12}^2}{2}f_{T2}^P[m_{12}^2,0]+f_{T3}^P[0,m_{12}^2].\end{aligned} \tag{3.28}$$

Here $\lambda_q^P = V_{qq_2}V_{qq_1}^*$, which are the appropriate CKM matrix elements for the calculation.

So far we have not addressed the contributions of the diagrams in Fig. (3.7). These diagrams contain contributions from the axial, vector, and tensor operators from the Lagrangian in Eq. (1.8) of type $\ell_1\overline{\ell}_2\overline{q}q$, where the quarks are both the same flavor. As was the case for

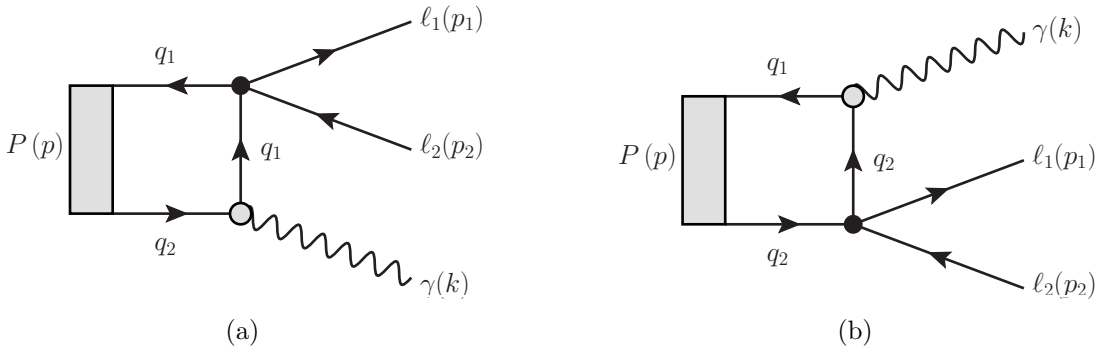

Figure 3.7: Four-fermion interaction diagrams for $\mathcal{A}(P \to \gamma \ell_1 \bar{\ell}_2)$ for operators of type $\mathcal{O} \sim (\ell_1 \bar{\ell}_2)(\bar{q}q)$ with photon $\gamma(k)$ attached to the SM dipole penguin vertex. The black circles represent the four-fermion LFV vertex (Eq. (1.8)) and the grey circles with the black border represent the SM dipole penguin vertex (Eq. (1.7)) [36].

the four-fermion operators that had a flavor change on both the quark side and lepton side, the scalar and pseudoscalar operators do not contribute. We can calculate the contributions of the vector operators using the same tensor matrix element as in Eq. (3.26), but with one important modification. The form factors are the sum of two form factors related to each quark flavor, $f_{Ti} = \tilde{f}_{Ti}^{q_1} + \tilde{f}_{Ti}^{q_2}$ (e.g. see [94]). Because it is convenient we will use a definition with the quark charge explicitly included in the formula, $f_{Ti} = Q_{q_1} f_{Ti}^{q_1} + Q_{q_2} f_{Ti}^{q_2}$. This is important because in the case of Fig. 3.7(a) we only have contributions from $f_{Ti}^{q_1}$ and in Fig. 3.7(b) we only have $f_{Ti}^{q_2}$.

$$
\begin{aligned}
A_1^{3.7ab} &= -\tfrac{\sqrt{4\pi\alpha}}{\pi^2\Lambda^2} \sum_{j=1}^{2} \left(C_{VR}^{q_j \ell_1 \ell_2} - C_{VL}^{q_j \ell_1 \ell_2} \right) \tfrac{y m_P}{2} \tfrac{G_F}{\sqrt{2}} C_{7\gamma} \sum_q \lambda_q^P \left(f_{T1}^{P,q_j}[0, m_{12}^2] + f_{T3}^{P,q_j}[0, m_{12}^2] \right), \\
A_5^{3.7ab} &= \tfrac{\sqrt{4\pi\alpha}}{\pi^2\Lambda^2} \sum_{j=1}^{2} \left(C_{VR}^{q_j \ell_1 \ell_2} + C_{VL}^{q_j \ell_1 \ell_2} \right) \tfrac{m_H}{2} \tfrac{G_F}{\sqrt{2}} C_{7\gamma} \sum_q \lambda_q^P \left(f_{T1}^{P,q_j}[0, m_{12}^2] + f_{T3}^{P,q_j}[0, m_{12}^2] \right), \\
A_7^{3.7ab} &= -\tfrac{\sqrt{4\pi\alpha}}{\pi^2\Lambda^2} \sum_{j=1}^{2} \left(C_{VR}^{q_j \ell_1 \ell_2} - C_{VL}^{q_j \ell_1 \ell_2} \right) m_H \tfrac{G_F}{\sqrt{2}} C_{7\gamma} \sum_q \lambda_q^P \left(f_{T1}^{P,q_j}[0, m_{12}^2] + f_{T3}^{P,q_j}[0, m_{12}^2] \right).
\end{aligned}
\tag{3.29}
$$

Applying this information to the decays of B_q^0, $\bar{D}^0$, and K^0 mesons shown in Figs. (3.4)–

(3.7), we find that each scalar function $A_i^{P\ell_1\ell_2}$ is written as

$$A_i^{P\ell_1\ell_2}(p^2,...) = A_i^{3.4ab} + A_i^{3.5ab} + A_i^{3.6abcd} + A_i^{3.7ab} \quad (i = 1\text{–}8)\,, \tag{3.30}$$

which are functions of model independent form factors and decay constants.

3.2.3 Results

Unfortunately, no experimental limits on the branching ratios of radiative lepton-flavor violating decays exist to constrain any of the applicable Wilson coefficients of the effective Lagrangian of Eq. (1.5). We encourage our colleagues from the LHC and KEK to study these decays. However, some information about Wilson coefficients is available from other transitions, such as two-body decays discussed in Chap. 2. In this section we use this information, along with the assumption of single operator dominance to derive the expectations for the size of the radiative LFV decays, if driven by those operators. These upper limits are presented in Tables 3.1 and 3.2 and the differential decay rates are plotted in Figs. (3.8)–(3.11) of Section 3.2.3.1.

All of the form factors and numerical constants, unless previously mentioned, used to obtain the results in this section may be found in the Appendix. In some cases where form factors are currently unknown, we apply a constituent quark model to estimate the relevant contribution. The quark model approach and results may be found in Sect. 3.2.4.

3.2.3.1 Spectra

Inputting the scalar functions of Eq. (3.30) in the differential decay rate, Eq. (3.16), and integrating over the Mandelstam variables m_{23}^2 and m_{12}^2, we calculate the differential decay rate, $d\Gamma/dm_{12}^2$, and total decay rate, $\Gamma\left(P \to \gamma\ell_1\bar{\ell}_2\right)$. Using these results we may predict the differential decay spectra for individual operators, $(1/\Gamma)\,(d\Gamma/dE_\gamma)$. Where we make the variable change from m_{12}^2 to E_γ, the photon energy in the meson rest frame, and normalize to the total decay rate. This analysis requires the practical assumption of single operator dominance so that the unknown WCs of individual operators will cancel between

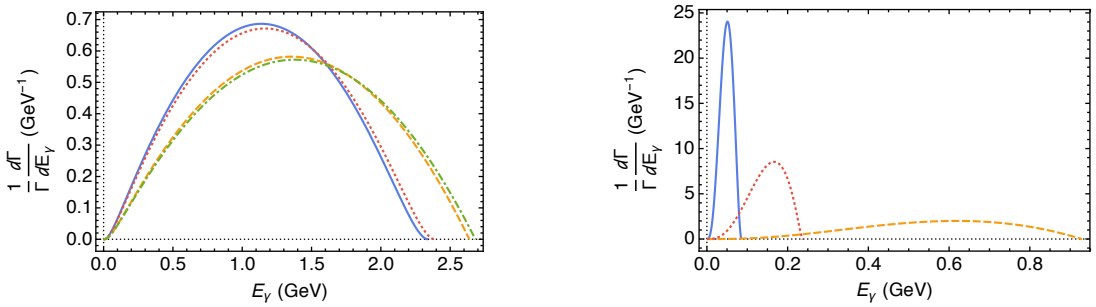

(a) (b)

Figure 3.8: Vector operator ($\mathcal{O} \sim (\ell_1\bar{\ell}_2)(\bar{q}_1 q_2)$ where $q_1 \neq q_2$) differential decay plots as functions of photon energy E_γ: (a) $B_d \to \gamma\mu\tau$ or $\gamma e\tau$ (solid blue curve), $B_d \to \gamma e\mu$ (short-dashed gold curve), $B_s \to \gamma\mu\tau$ or $\gamma e\tau$ (dotted red curve), $B_s \to \gamma e\mu$ (dot-dashed green curve); (b) $D \to \gamma e\tau$ (solid blue curve), $D \to \gamma e\mu$ (short-dashed gold curve), $K \to \gamma e\mu$ (dotted red curve) [36].

the differential and total decay rates.

The differential decay rates for the vector and tensor operators of type $\mathcal{O} \sim (\ell_1\bar{\ell}_2)(\bar{q}_1 q_2)$ where $q_1 \neq q_2$ are

$$\frac{d\Gamma_V^{q_1 q_2 \ell_1 \ell_2}}{dm_{12}^2} = \frac{C_{VR}^2 + C_{VL}^2}{\Lambda^4}\frac{4\pi\alpha}{(2\pi)^3}\frac{1}{576 m_P^2}\left(m_P^2 - m_{12}^2\right)^3\left(2m_{12}^2 - 3m_P^2 y^2\right) f_V^P[m_{12}^2, 0], \tag{3.31}$$

$$\begin{aligned}\frac{d\Gamma_T^{q_1 q_2 \ell_1 \ell_2}}{dm_{12}^2} = \frac{C_{TR}^2 + C_{TL}^2}{\Lambda^4}\frac{4\pi\alpha}{(2\pi)^3}\frac{y^2 m_{q_\mathrm{H}}^2 G_F^2}{288 m_P^2}\left(m_P^2 - m_{12}^2\right)^3 \\ \times\left(\left(2f_{T1}^P[m_{12}^2,0] + m_P^2 f_{T2}^P[m_{12}^2,0]\right)^2 + m_{12}^2\left(f_{T2}^P[m_{12}^2,0]\right)^2\right).\end{aligned} \tag{3.32}$$

Here we have suppressed the superscripts of the WCs for brevity (e.g. $C_{VR}^{q_1 q_2 \ell_1 \ell_2} \to C_{VR}$). We drop terms higher in order than y^2, which is a good approximation in most cases as the ratio y is small. The vector and tensor operators with flavor change on both the quark and lepton side are of particular importance to our analysis. They cannot be constrained via two-body decays and so the three-body decay channels present us with a unique opportunity to place limits on the associated WCs. The vector operators also have an advantage over the tensor operators because they are not chirally suppressed by quark and lepton masses.

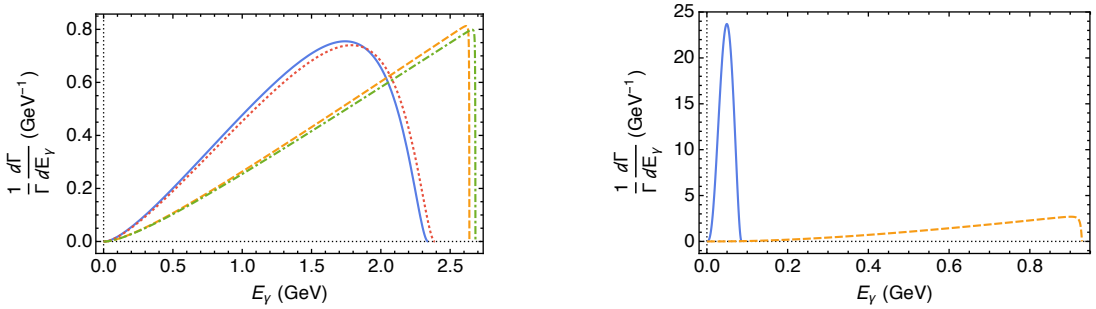

(a) (b)

Figure 3.9: Tensor operator ($\mathcal{O} \sim (\ell_1\bar{\ell}_2)(\bar{q}_1 q_2)$ where $q_1 \neq q_2$) differential decay plots as functions of photon energy E_γ: (a) $B_d \to \gamma\mu\tau$ or $\gamma e\tau$ (solid blue curve), $B_d \to \gamma e\mu$ (short-dashed gold curve), $B_s \to \gamma\mu\tau$ or $\gamma e\tau$ (dotted red curve), $B_s \to \gamma e\mu$ (dot-dashed green curve); (b) $D \to \gamma e\tau$ (solid blue curve), $D \to \gamma e\mu$ (short-dashed gold curve) [36].

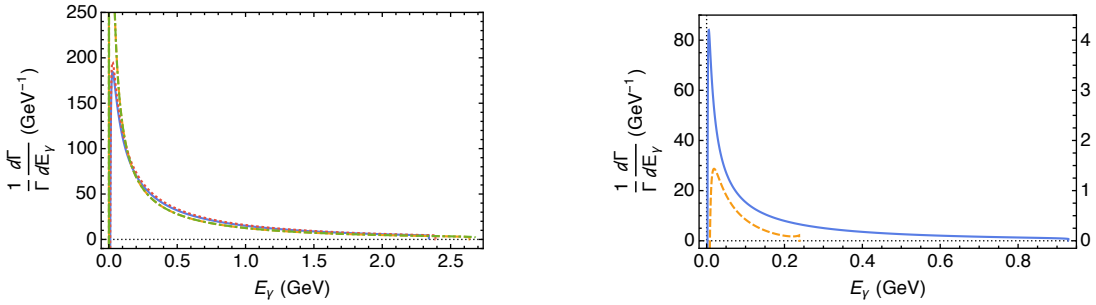

(a) (b)

Figure 3.10: Axial operator ($\mathcal{O} \sim (\ell_1\bar{\ell}_2)(\bar{q}_1 q_2)$ where $q_1 \neq q_2$) differential decay plots as functions of photon energy E_γ: (a) $B_d \to \gamma\mu\tau$ or $\gamma e\tau$ (solid blue curve), $B_d \to \gamma e\mu$ (short-dashed gold curve), $B_s \to \gamma\mu\tau$ or $\gamma e\tau$ (dotted red curve), $B_s \to \gamma e\mu$ (dot-dashed green curve); (b) left scale $D \to \gamma e\mu$ (solid blue curve), right scale $K \to \gamma e\mu$ (short-dashed gold curve) [36].

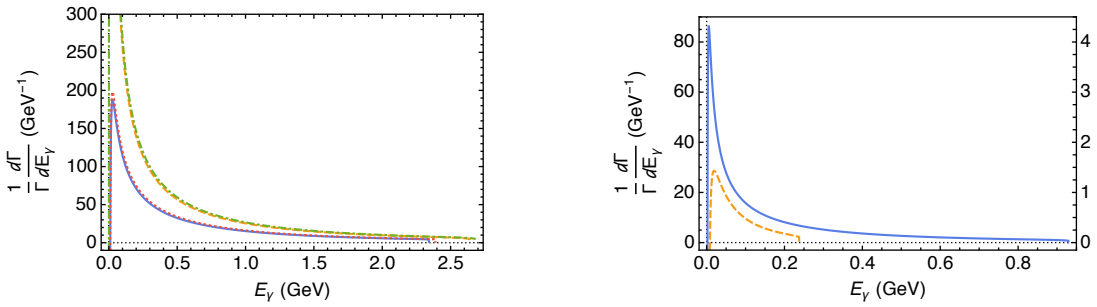

(a) (b)

Figure 3.11: Pseudoscalar operator ($\mathcal{O} \sim (\ell_1\bar{\ell}_2)(\bar{q}_1 q_2)$ where $q_1 \neq q_2$) differential decay plots as functions of photon energy E_γ: (a) $B_d \to \gamma\mu\tau$ or $\gamma e\tau$ (solid blue curve), $B_d \to \gamma e\mu$ (short-dashed gold curve), $B_s \to \gamma\mu\tau$ or $\gamma e\tau$ (dotted red curve), $B_s \to \gamma e\mu$ (dot-dashed green curve); (b) left scale $D \to \gamma e\mu$ (solid blue curve), right scale $K \to \gamma e\mu$ (short-dashed gold curve) [36].

Assuming WCs are of similar size, this means the vector operators would give a larger contribution to the overall decay rate and conversely are better constrained by experimental limits. The differential spectra given in Eqs. (3.31)–(3.32) are shown in Figs. (3.8)–(3.9).

The three-body decays considered here also provide complementary access to the axial and pseudoscalar operators of type $\mathcal{O} \sim (\ell_1\bar{\ell}_2)(\bar{q}_1 q_2)$ where $q_1 \neq q_2$. We do not provide the equations for the individual differential decay rates as they are more cumbersome than their vector and tensor counterparts and they are better constrained via two-body decays. Their differential spectra are plotted in Figs. (3.10)–(3.11) We demonstrate how well constrained these and other operators are in Sects. 3.2.3.2 and 3.2.4.2.

3.2.3.2 Limits

Using the available limits on Wilson coefficients from Sect. 2.3 with the form factors of the Appendix, we predict the upper threshold experiments must reach to potentially see LFV in the $P \to \gamma\ell_1\bar{\ell}_2$ decays involving the axial and pseudoscalar operators of type $\mathcal{O} \sim (\ell_1\bar{\ell}_2)(\bar{q}_1 q_2)$ where $q_1 \neq q_2$ and dipole operators. These upper bounds are presented in Table 3.1 for B_q^0 decays and in Table 3.2 for $\bar{D}^0$ and K_L^0 decays. K_L^0 is used in lieu of K^0 for the limits on the branching ratios due to a lack of experimental information on the total decay rate of K^0.

Wilson	Upper limits			
coefficient	$\mathcal{B}(B_d^0 \to \gamma\mu\tau)$	$\mathcal{B}(B_d^0 \to \gamma e\tau)$	$\mathcal{B}(B_d^0 \to \gamma e\mu)$	$\mathcal{B}(B_s^0 \to \gamma e\mu)$
$C_{AR}^{qb\ell_1\ell_2}$	9.2×10^{-7}	1.2×10^{-6}	6.5×10^{-11}	3.7×10^{-10}
$C_{AL}^{qb\ell_1\ell_2}$	9.2×10^{-7}	1.2×10^{-6}	6.5×10^{-11}	3.7×10^{-10}
$C_{PR}^{qb\ell_1\ell_2}$	9.0×10^{-7}	1.2×10^{-6}	3.2×10^{-11}	1.7×10^{-10}
$C_{PL}^{qb\ell_1\ell_2}$	9.0×10^{-7}	1.2×10^{-6}	3.2×10^{-11}	1.7×10^{-10}

Table 3.1: Upper limits on $B_q^0 \to \gamma\ell_1\bar{\ell}_2$ branching ratios from known Wilson coefficient constraints using form factors for four-fermion axial and pseudoscalar operators of type $\mathcal{O} \sim (\ell_1\bar{\ell}_2)(\bar{q}_1 q_2)$ where $q_1 \neq q_2$ [36].

Wilson	Upper limits	
coefficient	$\mathcal{B}(\bar{D}^0 \to \gamma e\mu)$	$\mathcal{B}(K_L^0 \to \gamma e\mu)_{SD}$
$C_{AR}^{q_1q_2\ell_1\ell_2}$	2.2×10^{-10}	2.3×10^{-14}
$C_{AL}^{q_1q_2\ell_1\ell_2}$	2.2×10^{-10}	2.3×10^{-14}
$C_{PR}^{q_1q_2\ell_1\ell_2}$	4.5×10^{-9}	2.2×10^{-14}
$C_{PL}^{q_1q_2\ell_1\ell_2}$	4.5×10^{-9}	2.2×10^{-14}

Table 3.2: Upper limits on $\bar{D}^0\,(u\bar{c})$, $K_L^0\left(\left(d\bar{s} - s\bar{d}\right)/\sqrt{2}\right) \to \gamma\ell_1\bar{\ell}_2$ branching ratios from known Wilson coefficient constraints using form factors for four-fermion axial and pseudoscalar operators of type $\mathcal{O} \sim (\ell_1\bar{\ell}_2)(\bar{q}_1 q_2)$ where $q_1 \neq q_2$. Note the K_L^0 results are for short distance (SD) interactions [36].

The normalized differential decay plots of K^0 are the same as K_L^0 because the normalization to the total decay rate cancels out the numerical differences (i.e. a factor of $1/\sqrt{2}$).

The predicted upper limits of the four-fermion axial and pseudoscalar operators for radiative pseudoscalar decays $P \to \gamma\ell_1\bar{\ell}_2$ in Tables 3.1 and 3.2 demonstrate that these operators ultimately are better constrained by their two-body decay counterparts. When we compare the predicted upper bounds of three-body rates in Tables 3.1 and 3.2 to the two-body experimental limits in Table 2.9 we see they are one to two orders of magnitude smaller. Therefore the three-body decays could still provide complimentary access to these operators.

The tensor form factors in the Appendix also allow us to analyze the contributions of the dipole operators from Eq. (1.6). The dipole operators are best constrained via radiative

Leptons $\ell_1\ell_2$	Wilson coefficient [35] (GeV^{-2})		Predicted upper limits $\mathcal{B}(B_d^0 \to \gamma\ell_1\bar{\ell}_2)$	$\mathcal{B}(B_s^0 \to \gamma\ell_1\bar{\ell}_2)$	$\mathcal{B}(\bar{D}^0 \to \gamma\ell_1\bar{\ell}_2)$
$\mu\tau$	$\lvert C_{DR}^{\ell_1\ell_2}/\Lambda^2\rvert =$	2.6×10^{-10}	3.1×10^{-28}	1.2×10^{-26}	FPS
$e\tau$		2.7×10^{-10}	3.3×10^{-28}	1.3×10^{-26}	3.8×10^{-38}
$e\mu$		3.1×10^{-7}	5.3×10^{-24}	1.2×10^{-21}	1.4×10^{-27}
$\mu\tau$	$\lvert C_{DL}^{\ell_1\ell_2}/\Lambda^2\rvert =$	2.6×10^{-10}	3.1×10^{-28}	1.2×10^{-26}	FPS
$e\tau$		2.7×10^{-10}	3.3×10^{-28}	1.3×10^{-26}	3.8×10^{-38}
$e\mu$		3.1×10^{-7}	5.3×10^{-24}	1.2×10^{-21}	1.4×10^{-27}

Table 3.3: Upper limits on $B_q^0\left(q\bar{b}\right)$, $\bar{D}^0\left(u\bar{c}\right) \to \gamma\ell_1\bar{\ell}_2$ branching ratios from known dipole Wilson coefficient constraints found in Chap. 2 and using form factors for dipole operators (see the Appendix). FPS stands for "forbidden phase space" [36].

lepton decays $\ell_2 \to \ell_1\gamma$, where $\ell_2 = \tau$, μ and $\ell_1 = \mu$, e. These decays have been the focus of most LFV experiments and therefore have the best constraints: $\mathcal{B}(\tau \to \mu\gamma) = 4.4 \times 10^{-8}$, $\mathcal{B}(\tau \to e\gamma) = 3.3 \times 10^{-8}$, and $\mathcal{B}(\mu \to e\gamma) = 4.2 \times 10^{-13}$ [34, 95, 96]. In Sect. 2.1 we were able to provide complimentary access via two-body vector quarkonium decays $V \to \ell_1\bar{\ell}_2$ [35].

Using the WC constraints obtained from the radiative lepton decays $\ell_2 \to \ell_1\gamma$ in [35], we predict the dipole operator decay upper limits for $P \to \gamma\ell_1\bar{\ell}_2$ in Table 3.3. Here the predicted upper limits range from 10^{-21}–10^{-38}, which is much lower than we would expect to be within experimental reach during the foreseeable future. Despite showing that $P \to \gamma\ell_1\bar{\ell}_2$ is not a useful means to constrain the dipole operators, the results in Table 3.3 are ten or more orders of magnitude smaller than the predictions of the axial and pseudoscalar operators in Tables 3.1 and 3.2. This confirms that $P \to \gamma\ell_1\bar{\ell}_2$ decays are better equiped to constrain four-fermion operators. Indeed the operators in the best position to be constrained are the quark flavor changing four-fermion vector operators, which see no chiral suppression via lepton or quark masses and cannot be constrained via two-body decays.

3.2.4 Quark Model

When the necessary form factors are unavailable to take a model independent approach to the calculation of the four-fermion operator contributions of the diagrams in Fig. (3.7),

Wilson	Leptons	Quark			
coefficient (GeV^{-2})	$\overline{\ell_1}\ell_2$	b	c	s	u/d
$\lvert C^{q\ell_1\ell_2}_{VL(R)}/\Lambda^2\rvert$	$\mu\tau$	3.5×10^{-6}	5.5×10^{-5}	$\cdots$	$\cdots$
$\lvert C^{q\ell_1\ell_2}_{VL(R)}/\Lambda^2\rvert$	$e\tau$	4.1×10^{-6}	1.1×10^{-4}	$\cdots$	$\cdots$
$\lvert C^{q\ell_1\ell_2}_{VL(R)}/\Lambda^2\rvert$	$e\mu$	$\cdots$	1.0×10^{-5}	2.0×10^{-3}	$\cdots$
$\lvert C^{q\ell_1\ell_2}_{AL(R)}/\Lambda^2\rvert$	$e\mu$	$\cdots$	$\cdots$	2.0×10^{-3}	3.0×10^{-3}
$\lvert C^{q\ell_1\ell_2}_{TL(R)}/\Lambda^2\rvert$	$\mu\tau$	2.8×10^{-2}	1.2	$\cdots$	$\cdots$
$\lvert C^{q\ell_1\ell_2}_{TL(R)}/\Lambda^2\rvert$	$e\tau$	3.2×10^{-2}	2.4	$\cdots$	$\cdots$
$\lvert C^{q\ell_1\ell_2}_{TL(R)}/\Lambda^2\rvert$	$e\mu$	$\cdots$	4.8	$\cdots$	$\cdots$

Table 3.4: Known Wilson coefficient limits from Chap. 2 [35]. Note the center dots denote unknown values which could be constrained via $P\to\gamma\ell_1\bar{\ell}_2$ [36].

we may choose a model dependent approach. We again apply a constituent quark model to calculate the contributions of four-fermion vector, axial, and tensor operators of the type $(\ell_1\overline{\ell}_2)(\overline{q}q)$. We constrained both the vector and tensor Wilson coefficients for these operators previously in Chap. 2 [35]. The results are reproduced here in Table 3.4 and can be used to find a predicted upper bound on the branching ratio of $\mathcal{B}\left(P\to\gamma\ell_1\overline{\ell}_2\right)$ for individual operators using the single operator dominance assumption.

3.2.4.1 Consituent Quark Model

The amplitude for the diagrams in Fig. (3.7) using this model is

$$\begin{aligned} i\mathcal{A} = -\frac{i}{\Lambda^2}\varepsilon^{*\mu}(k)\sum_{i=1}^{2}\Big(&\overline{u}_{\ell_1}\Big[\ C^{q_i\ell_1\ell_2}_{VR}\gamma^\alpha P_R + C^{q_i\ell_1\ell_2}_{VL}\gamma^\alpha P_L\ \Big]v_{\ell_2}\langle 0|\,\overline{q}_1\Gamma^{V,q_i}_{\alpha\mu}q_2\,|P(p)\rangle \\ &+\overline{u}_{\ell_1}\Big[\ C^{q_i\ell_1\ell_2}_{AR}\gamma^\alpha P_R + C^{q_i\ell_1\ell_2}_{AL}\gamma^\alpha P_L\ \Big]v_{\ell_2}\langle 0|\,\overline{q}_1\Gamma^{A,q_i}_{\alpha\mu}q_2\,|P(p)\rangle \\ &+m_2m_{q_i}G_F\overline{u}_{\ell_1}\Big[C^{q_i\ell_1\ell_2}_{TR}\sigma^{\alpha\beta}P_L + C^{q_i\ell_1\ell_2}_{TR}\sigma^{\alpha\beta}P_R\Big]v_{\ell_2}\langle 0|\,\overline{q}_1\Gamma^{T,q_i}_{\alpha\beta\mu}q_2\,|P(p)\rangle\Big). \end{aligned} \tag{3.33}$$

This amplitude is dependent on matrix elements of the form $\langle 0|\,\overline{q}_1\Gamma q_2\,|P\rangle$ with the matrices Γ defined for each operator ($\mathcal{O}\sim(\ell_1\overline{\ell}_2)(\overline{q}_iq_i)$, $i=1,2$) as

$$\begin{aligned}
\Gamma^{V,q_1}_{\alpha\mu} &= i\tfrac{G_F}{\sqrt{2}}\tfrac{\sqrt{4\pi\alpha}}{\pi^2} m_{q_1} C_{7\gamma} \sum_q \lambda_q^P \gamma_\alpha \tfrac{x\not{p}-\not{k}+m_{q_1}}{(xp-k)^2-m_{q_1}^2}\sigma_{\mu\nu}\left(1+\gamma_5\right)k^\nu, \\
\Gamma^{A,q_1}_{\alpha\mu} &= i\tfrac{G_F}{\sqrt{2}}\tfrac{\sqrt{4\pi\alpha}}{\pi^2} m_{q_1} C_{7\gamma} \sum_q \lambda_q^P \gamma_\alpha\gamma_5 \tfrac{x\not{p}-\not{k}+m_{q_1}}{(xp-k)^2-m_{q_1}^2}\sigma_{\mu\nu}\left(1+\gamma_5\right)k^\nu, \\
\Gamma^{T,q_1}_{\alpha\beta\mu} &= i\tfrac{G_F}{\sqrt{2}}\tfrac{\sqrt{4\pi\alpha}}{\pi^2} m_{q_1} C_{7\gamma} \sum_q \lambda_q^P \sigma_{\alpha\beta} \tfrac{x\not{p}-\not{k}+m_{q_1}}{(xp-k)^2-m_{q_1}^2}\sigma_{\mu\nu}\left(1+\gamma_5\right)k^\nu,
\end{aligned} \tag{3.34}$$

$$\begin{aligned}
\Gamma^{V,q_2}_{\alpha\mu} &= i\tfrac{G_F}{\sqrt{2}}\tfrac{\sqrt{4\pi\alpha}}{\pi^2} m_{q_2} C_{7\gamma} \sum_q \lambda_q^P \sigma_{\mu\nu}\left(1+\gamma_5\right)k^\nu \tfrac{-(1-x)\not{p}+\not{k}+m_{q_2}}{((1-x)p-k)^2-m_{q_2}^2}\gamma_\alpha, \\
\Gamma^{A,q_2}_{\alpha\mu} &= i\tfrac{G_F}{\sqrt{2}}\tfrac{\sqrt{4\pi\alpha}}{\pi^2} m_{q_2} C_{7\gamma} \sum_q \lambda_q^P \sigma_{\mu\nu}\left(1+\gamma_5\right)k^\nu \tfrac{-(1-x)\not{p}+\not{k}+m_{q_2}}{((1-x)p-k)^2-m_{q_2}^2}\gamma_\alpha\gamma_5, \text{ and} \\
\Gamma^{T,q_2}_{\alpha\beta\mu} &= i\tfrac{G_F}{\sqrt{2}}\tfrac{\sqrt{4\pi\alpha}}{\pi^2} m_{q_2} C_{7\gamma} \sum_q \lambda_q^P \sigma_{\mu\nu}\left(1+\gamma_5\right)k^\nu \tfrac{-(1-x)\not{p}+\not{k}+m_{q_2}}{((1-x)p-k)^2-m_{q_2}^2}\sigma_{\alpha\beta}.
\end{aligned} \tag{3.35}$$

In modeling the quark anti-quark distribution, we again chose to follow [79, 82, 83], where we can write the wave function of the ground state, $P(p)$, as

$$\psi_P = \frac{I_c}{\sqrt{6}}\phi_P[x]\gamma_5\left(\not{p}+m_P g[x]\right). \tag{3.36}$$

The variable x is the fraction of the meson momentum transferred by one of the quarks and I_c is the color space identity matrix. We assigned the momenta in Fig. (3.7) such that the valence quark $\overline{q}_1$ has momentum xP and the valence quark q_2 has momentum $(1-x)P$. The function $g_P[x]$ is $g_H[x] \sim 1$ for high mass mesons and $g_L[x] = 0$ for low mass mesons. The distribution amplitudes used for light and heavy mesons and their normalization are

$$\phi_L \sim\ x\left(1-x\right),\ \ \phi_H \sim\ \left[\frac{m_{q_L}}{M_H}\frac{1}{1-x}+\frac{1}{x}-1\right]^{-2},\ \ \frac{f_P}{2\sqrt{6}} = \int_0^1 \phi[x]\ dx. \tag{3.37}$$

Here m_{q_L} is the mass of the low mass quark and the normalization is proportional to the

Quark	m_u	m_d	m_s	m_c	m_b
Constituent mass (MeV)	335.5	339.5	486	1550	4730

Table 3.5: Constituent quark masses required for calculations of quark model matrix element [97].

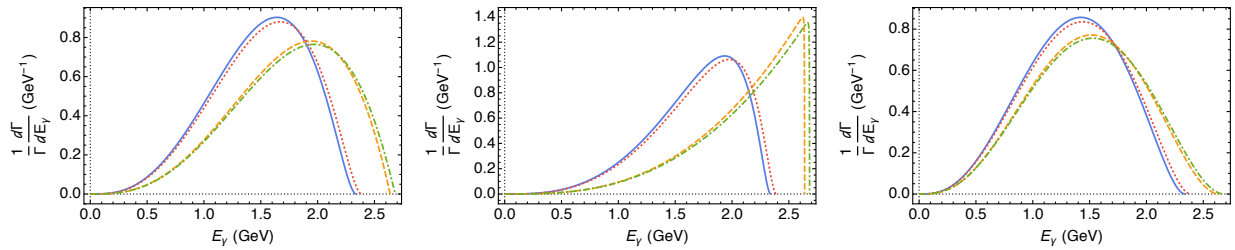

(a) (b) (c)

Figure 3.12: Differential decay plots as functions of photon energy E_γ for (a) vector/axial, (b) left-handed tensor, and (c) right-handed tensor operators of the type $\mathcal{O} \sim (\ell_1 \bar{\ell}_2)(\bar{b}b)$. Plotted decay rates are $B_d \to \gamma\mu\tau$ or $\gamma e\tau$ (solid blue curve), $B_d \to \gamma e\mu$ (short-dashed gold curve), $B_s \to \gamma\mu\tau$ or $\gamma e\tau$ (dotted red curve), $B_s \to \gamma e\mu$ (dot-dashed green curve) [36].

decay constant f_P. We find the matrix element,

$$\langle 0|\, \overline{q}_1 \Gamma^\mu q_2 \,|P\rangle = \int_0^1 \mathrm{Tr}[\Gamma^\mu \psi_P]\; dx, \tag{3.38}$$

by integration of the meson momentum fraction x and taking the trace.

3.2.4.2 Spectra and Limits

Since we applied a constituent quark model to calculate the transition amplitudes we need to define its parameters (constituent quark masses) that are used to calculate the matrix element in Eq. (3.38). These masses are in Table 3.5. Using this matrix element and integrating over the Mandelstam variables m_{23}^2 and m_{12}^2 we can calculate the differential decay rate as a function of the photon energy, E_γ, in the rest-frame of the meson P and the total decay rate. Plots of these differential decay spectra normalized to individual operator total decay rates are in Figs. (3.12)–(3.16), which show the spectra of B_q^0, $\bar{D}^0$, and K^0 decays for the vector, axial, and tensor operators of type $(\ell_1 \bar{\ell}_2)(\bar{q}q)$. The normalization cancels out

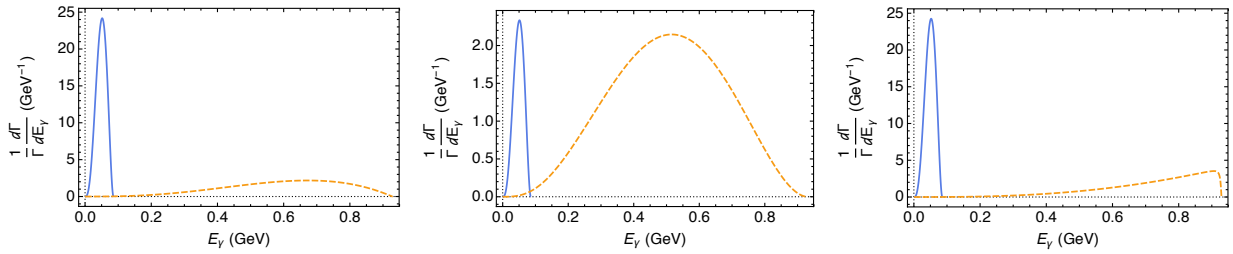

(a) (b) (c)

Figure 3.13: Differential decay plots as functions of photon energy E_γ for (a) vector/axial, (b) left-handed tensor, and (c) right-handed tensor operators of the type $\mathcal{O} \sim \left(\ell_1\bar{\ell}_2\right)(\bar{c}c)$. Plotted decay rates are $D \to \gamma e\tau$ (solid blue curve), $D \to \gamma e\mu$ (short-dashed gold curve).

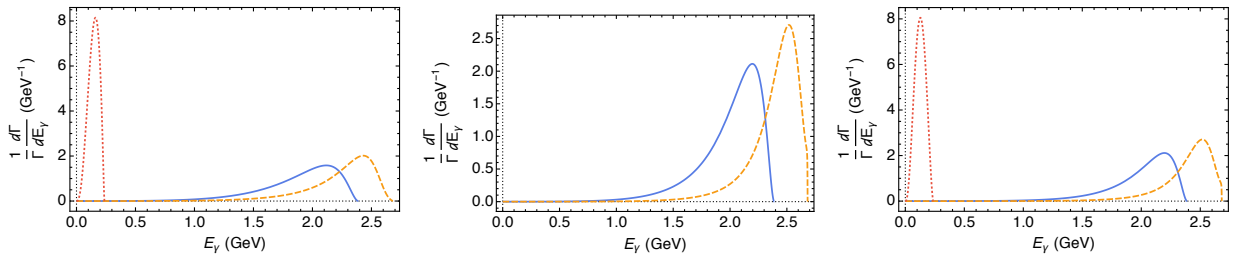

(a) (b) (c)

Figure 3.14: Differential decay plots as functions of photon energy E_γ for (a) vector/axial and (b) left/right-handed tensor operators of the type $\mathcal{O} \sim \left(\ell_1\bar{\ell}_2\right)(\bar{s}s)$. Plotted decay rates are $B_s \to \gamma\mu\tau$ or $\gamma e\tau$ (solid blue curve), $B_s \to \gamma e\mu$ (short-dashed gold curve), and $K \to \gamma e\mu$ (dotted red curve).

sources of uncertainty such as the Wilson coefficients (i.e. $C_{VR(L)}^{q_i\ell_1\ell_2}$) and the CKM matrix element values. As we did in Section 3.2.3.2, we apply known Wilson coefficient constraints from Table. 3.4 and the single operator dominance assumption to the total decay rate to make predictions of the branching ratio upper limit for these operators, which can be found in Tables. 3.6 – 3.8.

These limits range in order of magnitude from 10^{-10}–10^{-28} and therefore many are below experimental reach. It is the spaces between these limits that should draw the reader's attention. There is much opportunity here to constrain the operators whose limits cannot be predicted. Providing limits using these RLFV decays would of course be complementary to two-body LFV decays of quarkonia (e.g. [35]), but would come for free as we constrain

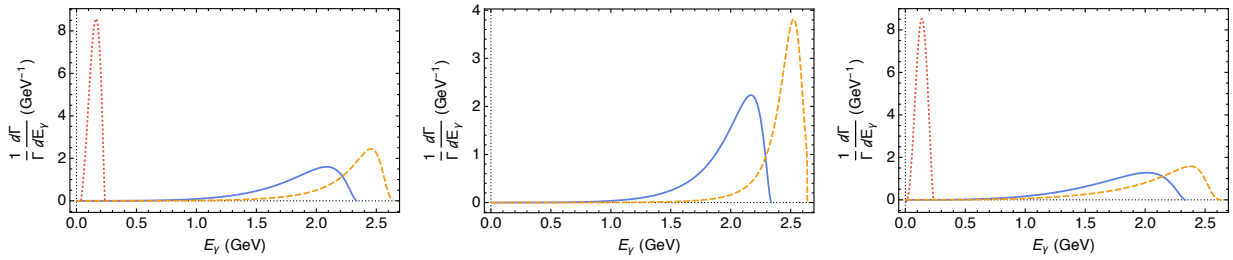

(a) (b) (c)

Figure 3.15: Differential decay plots as functions of photon energy E_γ for (a) vector/axial, (b) left-handed tensor, and (c) right-handed tensor operators of the type $\mathcal{O} \sim \left(\ell_1 \bar{\ell}_2\right)\left(\bar{d}d\right)$. Plotted decay rates are $B_d \to \gamma\mu\tau$ or $\gamma e\tau$ (solid blue curve), $B_d \to \gamma e\mu$ (short-dashed gold curve), and $K \to \gamma e\mu$ (dotted red curve).

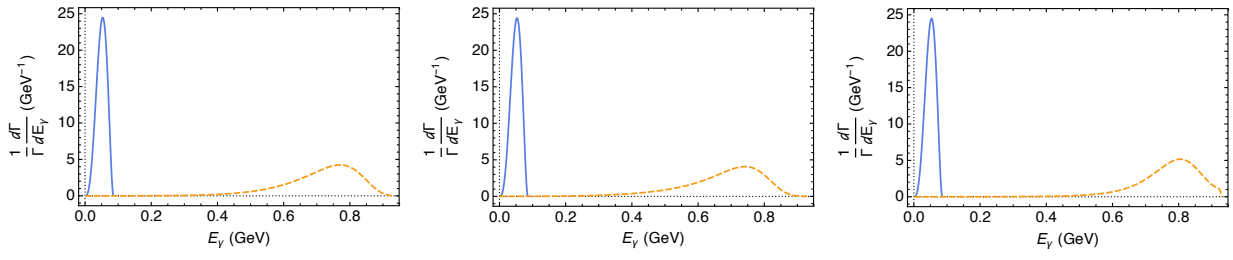

(a) (b) (c)

Figure 3.16: Differential decay plots as functions of photon energy E_γ for (a) vector/axial, (b) left-handed tensor, and (c) right-handed tensor operators of the type $\mathcal{O} \sim \left(\ell_1 \bar{\ell}_2\right)\left(\bar{u}u\right)$. Plotted decay rates are $D \to \gamma e\tau$ (solid blue curve), $D \to \gamma e\mu$ (short-dashed gold curve).

Wilson	Upper limits		
coefficient	$\mathcal{B}(B_d^0 \to \gamma\mu\tau)$	$\mathcal{B}(B_d^0 \to \gamma e\tau)$	$\mathcal{B}(B_d^0 \to \gamma e\mu)$
$C_{VR}^{b\ell_1\ell_2}$	5.7×10^{-20}	7.8×10^{-20}	$\cdots$
$C_{VL}^{b\ell_1\ell_2}$	5.7×10^{-20}	7.8×10^{-20}	$\cdots$
$C_{VR}^{d\ell_1\ell_2}$	$\cdots$	$\cdots$	$\cdots$
$C_{VL}^{d\ell_1\ell_2}$	$\cdots$	$\cdots$	$\cdots$
$C_{AR}^{d\ell_1\ell_2}$	$\cdots$	$\cdots$	2.0×10^{-12}
$C_{AL}^{d\ell_1\ell_2}$	$\cdots$	$\cdots$	2.0×10^{-12}
$C_{TR}^{b\ell_1\ell_2}$	3.9×10^{-21}	5.1×10^{-21}	$\cdots$
$C_{TL}^{b\ell_1\ell_2}$	1.1×10^{-18}	1.5×10^{-18}	$\cdots$

Table 3.6: Upper limits on $B_d^0(d\bar{b}) \to \gamma\ell_1\bar{\ell}_2$ branching ratios from known Wilson coefficient constraints using constituent quark model. The center dots indicate no Wilson coefficient constraints were available for a prediction of an upper bound. Experimental studies of this decay channel would present an opportunity to constrain these Wilson coefficients [36].

Wilson	Upper limits		
coefficient	$\mathcal{B}(B_s^0 \to \gamma\mu\tau)$	$\mathcal{B}(B_s^0 \to \gamma e\tau)$	$\mathcal{B}(B_s^0 \to \gamma e\mu)$
$C_{VR}^{b\ell_1\ell_2}$	1.8×10^{-18}	2.5×10^{-18}	$\cdots$
$C_{VL}^{b\ell_1\ell_2}$	1.8×10^{-18}	2.5×10^{-18}	$\cdots$
$C_{VR}^{s\ell_1\ell_2}$	$\cdots$	$\cdots$	1.3×10^{-10}
$C_{VL}^{s\ell_1\ell_2}$	$\cdots$	$\cdots$	1.3×10^{-10}
$C_{AR}^{s\ell_1\ell_2}$	$\cdots$	$\cdots$	1.5×10^{-11}
$C_{AL}^{s\ell_1\ell_2}$	$\cdots$	$\cdots$	1.5×10^{-11}
$C_{TR}^{b\ell_1\ell_2}$	2.1×10^{-19}	2.8×10^{-19}	$\cdots$
$C_{TL}^{b\ell_1\ell_2}$	3.9×10^{-17}	5.1×10^{-17}	$\cdots$

Table 3.7: Upper limits on $B_s^0(s\bar{b}) \to \gamma\ell_1\bar{\ell}_2$ branching ratios from known Wilson coefficient constraints using constituent quark model. The center dots indicate no Wilson coefficient constraints were available for a prediction of an upper bound. Experimental studies of this decay channel would present an opportunity to constrain these Wilson coefficients [36].

Wilson coefficient	Upper limits $\mathcal{B}(\bar{D}^0 \to \gamma e\tau)$	$\mathcal{B}(\bar{D}^0 \to \gamma e\mu)$
$C_{VR}^{c\ell_1\ell_2}$	5.1×10^{-28}	8.8×10^{-24}
$C_{VL}^{c\ell_1\ell_2}$	5.1×10^{-28}	8.8×10^{-24}
$C_{AR}^{u\ell_1\ell_2}$	$\cdots$	1.3×10^{-16}
$C_{AL}^{u\ell_1\ell_2}$	$\cdots$	1.3×10^{-16}
$C_{TR}^{c\ell_1\ell_2}$	6.0×10^{-28}	2.5×10^{-24}
$C_{TL}^{c\ell_1\ell_2}$	6.2×10^{-27}	3.7×10^{-22}

Table 3.8: Upper limits on $\bar{D}^0\,(u\bar{c}) \to \gamma\ell_1\bar{\ell}_2$ branching ratios from known Wilson coefficient constraints using constituent quark model. The center dots indicate no Wilson coefficient constraints were available for a prediction of an upper bound. Experimental studies of this decay channel would present an opportunity to constrain these Wilson coefficients [36].

the vector and tensor operators with flavor changes on both the quark and lepton sides.

CHAPTER 4: CONCLUSION

Studies of lepton flavor violating transitions are a promising path in the search for new physics. A convenient way to study new physics is to employ effective Lagrangians. All models of new physics that include flavor-violating interactions are encoded in the values of Wilson coefficients of the low energy effective Lagrangian in Eq. (1.5). We argued that Wilson coefficients of this Lagrangian could be effectively probed by studying decays of quarkonium and other meson states with different spin-parity quantum numbers, providing complementary constraints to those obtained from tau and mu decays [37, 98].

The proposed framework allows us to select two-body meson decays in such a way that only operators with particular quantum numbers are probed, significantly reducing the reliance on the single operator dominance assumption that is prevalent in constraining the parameters of the effective LFV Lagrangian. We argued that studies of RLFV decays could provide important complementary access to effective operators probed in two-body decays of type $\mathcal{O} \sim \left(\ell_1 \bar{\ell}_2\right)(\bar{q}q)$ where there is only a FCNC on the lepton side without the need to include a composite strongly-interacting meson to the final state. We also saw that the radiative three-body decays of B_q^0, D^0, and K^0 to $\gamma \ell_1 \bar{\ell}_2$ allowed access to the effective operators in Eq. (1.5) which cannot be probed via any two-body meson decays. Finally, we provide evidence that the dipole operators are so well constrained by radiative LFV transitions $\ell_2 \to \ell_1 \gamma$ that their threshold for contributions to $\mathcal{B}(P \to \gamma \ell_1 \bar{\ell}_2)$ is many orders of magnitude below experimental reach. Thus, their contribution to the sum of amplitudes in Eq. (3.30) can be safely dropped.

As more data is produced by Belle II and the LHCb experiment, we emphatically encourage our experimental colleagues to produce experimental limits on both LFV and radiative LFV decays of the quarkonia and the B_q^0, $\bar{D}^0$, and K^0 mesons discussed in this work.

APPENDIX: FORM FACTORS AND NUMERICAL CONSTANTS

To estimate differential decay rates and the upper limits of the total decay rates of the radiative decays in Section 3.2.3, we must apply the form factors of Eqs. (3.17)–(3.19) and the numerical constants of Tables 1 and 2. Numerical inputs for the CKM matrix elements are found in [34]. Before we can apply these form factors, we must relate them to those calculated in the literature, which are defined as [85, 86, 87, 88, 89]

$$\begin{aligned}
\langle\gamma^*(k_2)|\overline{q}_1\gamma^\mu\gamma_5 q_2|P(p)\rangle &= ie\varepsilon^*_\alpha(k_2)\,(g^{\alpha\mu}k_1\cdot k_2 - k_1^\alpha k_2^\mu)\,\frac{F_A^P[k_1^2,k_2^2]}{m_P},\\
\langle\gamma^*(k_2)|\overline{q}_1\gamma^\mu q_2|P(p)\rangle &= \ e\varepsilon^*_\alpha(k_2)\epsilon^{k_1k_2\mu\alpha}\frac{F_V^P[k_1^2,k_2^2]}{m_P},\\
\langle\gamma^*(k_2)|\overline{q}_1\sigma^{\mu\nu}\gamma_5 q_2|P(p)\rangle k_{1\nu} &= \ e\varepsilon^*_\alpha(k_2)\,(g^{\alpha\mu}k_1\cdot k_2 - k_1^\alpha k_2^\mu)\,F_{TA}^P[k_1^2,k_2^2], \text{ and}\\
\langle\gamma^*(k_2)|\overline{q}_1\sigma^{\mu\nu} q_2|P(p)\rangle k_{1\nu} &= ie\varepsilon^*_\alpha(k_2)\epsilon^{k_1k_2\mu\alpha}F_{TV}^P[k_1^2,k_2^2].
\end{aligned} \tag{1}$$

These form factors are functions of two momenta, k_1, which is emitted from the $q_1 \to q_2$ weak transition current, and k_2, which is emitted from one of the valence quarks of the meson P. Here the photon is off-shell, but the on-shell definitions may be found by assuming $k_2^2 = 0$ and applying the momentum conservation relation $p = k_1 + k_2$.

Assuming $k^2 = 0$ and making the appropriate substitutions of $Q = p - k$ and k for k_1 and k_2 we find the necessary relations between the form factors in Eqs. (3.17)–(3.19) and Eq. (1) as

m_u	m_d	m_c	m_s	m_b
$2.2^{+0.6}_{-0.4}$ MeV	$4.7^{+0.5}_{-0.4}$ MeV	1.28 ± 0.03 GeV	96^{+8}_{-4} MeV	$4.18^{+0.04}_{-0.03}$ GeV

Table 1: $\overline{MS}$ quark masses required for decay calculations [34].

Transition	Scale μ [GeV]	$\lvert C_{7\gamma}\rvert$	Ref.
$b \to d(s)\gamma$	5.0	0.299	[46]
$c \to u\gamma$	1.3	$\frac{0.0025}{4\lvert V_{ub}^* V_{cb}\rvert}$	[60]

Table 2: Penguin operator Wilson coefficients, $C_{7\gamma}$, for decay calculations.

	Parameter	F_V	F_{TV}	F_A	F_{TA}
$B^0_{d,s} \to \gamma$	$\beta\,(\mathrm{GeV}^{-1})$	0.28	0.30	0.26	0.33
	$\Delta\,(\mathrm{GeV})$	0.04	0.04	0.30	0.30

Table 3: Parameters of the $B^0_q \to \gamma$ form factors, as defined in Eq. (3) [85].

$$\begin{aligned} F^P_{V,A}[Q^2,0] &= m_p f^P_{V,A}[Q^2,0], \\ F^P_{TV}[Q^2,0] &= -f^P_{T1}[Q^2,0] - p\cdot k f^P_{T2}[Q^2,0], \\ F^P_{TA}[Q^2,0] &= -f^P_{T1}[Q^2,0] - p\cdot Q f^P_{T2}[Q^2,0], \\ F^P_{TV,TA}[0,Q^2] &= -f^P_{T1}[0,Q^2] - f^P_{T3}[0,Q^2]. \end{aligned} \tag{2}$$

To make use of these relations we employ the parameterizations of [85] for the F_V, F_A, F_{TV}, and F_{TA} form factors. For the $B^0_q \to \gamma$ form factor parameterization when the photon γ is emitted from the valence quarks ($k_1 = Q$, $k_2 = k$) we use

$$F_i^{B_q}[E] = \beta_i \frac{f_P m_P}{\Delta_i + E_\gamma}, \quad i = \mathrm{V},\ \mathrm{A},\ \mathrm{TV},\ \mathrm{TA} \tag{3}$$

where E_γ is the photon energy in the P-meson rest-frame. The constants β and Δ are numerical parameters which can be found in Table 3.

For the parameterization of the $\bar{D}^0$, $K^0 \to \gamma$ form factors when the photon γ is emitted

	Parameter	V	A	TV	TA
$\bar{D}^0 \to \gamma$	$F_i^c(0)$	-0.12	0.14	-0.12	-0.12
	$F_i^u(0)$	-0.37	-0.31	-0.38	-0.38
	M_i (GeV)	2.0	2.3	2.0	2.4
$K^0 \to \gamma$	$F_i^d(0)$	-0.22	0.20	–	–
	$F_i^s(0)$	-0.18	-0.19	–	–
	M_i (GeV)	0.89	0.89	–	–

Table 4: Parameters of the $\bar{D}^0$,$K^0 \to \gamma$ form factors, as defined in Eq. (4) [89, 99]. The K^0 tensor form factors will be calculated elsewhere.

V	$g[0]_+^{B_q^0 \to V}$	$g[0]_+^{\bar{D}^0 \to V}$	f_V (MeV)	m_V (MeV)	Γ_V (MeV)	Refs.
ρ	0.27	-0.66	154	775.26 ± 0.25	147.8 ± 0.9	[34, 88, 100]
ω	-0.27	-0.66	45.3	782.65 ± 0.12	8.49 ± 0.08	[34, 88, 100]
ϕ	-0.38		-58.8	1019.460 ± 0.016	4.247 ± 0.016	[34, 88, 100]

Table 5: Vector meson dominance input parameters for $F_{TV,\,TA}[0, Q^2]$ form factors.

from the valence quarks ($k_1 = Q$, $k_2 = k$) we use

$$F_i^P[m_{12}^2] = \frac{Q_{q_1} F_i^{(q_1)}[0] + Q_{q_2} F_i^{(q_2)}[0]}{1 - \frac{m_{12}^2}{M_i^2}} \ , \quad i = \text{V, A, TV, TA.} \tag{4}$$

Here $Q_{d(s)} = -\frac{1}{3}$, $Q_{u(c)} = \frac{2}{3}$, and the remaining parameters are found in Table 4 [89].

The form factors $F_{TV,\,TA}^P[0, Q^2]$ for B_q^0 and $\bar{D}^0$ decays are parameterized using vector meson dominance in [87, 88], which gives

$$F_{TV,\,TA}^P[0, Q^2] = F_{TV,\,TA}^P[0, 0] - \sum_V 2 f_V g[0]_+^{P \to V} \frac{Q^2/m_V}{Q^2 - m_V^2 + i m_V \Gamma_V}. \tag{5}$$

The vector meson dominance input parameter values are found in Table 5. The ρ and ω mesons are part of the vector meson sum for B_d^0 and $\bar{D}^0$ form factors because of their respective d and u valence quark content. The ϕ meson is part of the vector meson sum for the B_s^0 form factor because of its s valence quark content. The zero momentum values

of the tensor form factors are $F^{B^0_{d,s}}_{TV,\,TA}[0,0] = 0.115$ [85] and $F^{\bar{D}^0}_{TV,\,TA}[0,0] = Q_c f^c_{TV,TA}[0] + Q_u f^u_{TV,TA}[0]$.

Given these form factors and the general input values given in Tables 1 and 2 we are able to plot the normalized differential decay rates and estimate the upper limits for the radiative branching ratios assuming single operator dominance in Section 3.2.3.

BIBLIOGRAPHY

[1] D. Griffiths, "Introduction to elementary particles," Weinheim, Germany: Wiley-VCH (2008) 454 p

[2] R. A. Millikan "A Direct Photoelectric Determination of Planck's h" Phys. Rev. **7**, 355 (1916). doi:10.1103/PhysRev.7.355

[3] C. M. G. Lattes, H. Muirhead, G. P. S. Occhialini and C. F. Powell, "Processes Involving Charged Mesons," Nature **159**, 694 (1947). doi:10.1038/159694a0

[4] R. E. Marshak and H. A. Bethe, "On the Two-Meson Hypothesis," Phys. Rev. **72**, 506 (1947). doi:10.1103/PhysRev.72.506

[5] C. D. Anderson "Early Work on the Positron and Muon" American Journal of Physics **29**, 825 (1961). doi:10.1119/1.1937627

[6] F. Reines and C. L. Cowan, "Detection of the free neutrino," Phys. Rev. **92**, 830 (1953). doi:10.1103/PhysRev.92.830; C. L. Cowan, F. Reines, F. B. Harris, H. W. Kruse, and A. D. McGuire "Detection of the free neutrino: a Confirmation," Science **124**, 103-104 (1956). doi: 10.1126/science.124.3212.103

[7] R. Davis, Jr. and D. S. Harmer, "Attempt to observe the $Cl^{37}(\bar{\nu}e^{-})Ar^{37}$ reaction induced by reactor antineutrinos," Bull. Am. Phys. Soc. **4**, 217 (1959).

[8] E. Nuovo Cim Majorana, "Teoria simmetrica dell'elettrone e del positrone" Il Nuovo Cimento **14**, 171 (1937) doi: 10.1007/BF02961314

[9] E. J. Konopinski and H. M. Mahmoud, "The Universal Fermi interaction," Phys. Rev. **92**, 1045 (1953). doi:10.1103/PhysRev.92.1045

[10] G. Danby, J. M. Gaillard, K. A. Goulianos, L. M. Lederman, N. B. Mistry, M. Schwartz and J. Steinberger, "Observation of High-Energy Neutrino Reactions and the Existence of Two Kinds of Neutrinos," Phys. Rev. Lett. **9**, 36 (1962). doi:10.1103/PhysRevLett.9.36

[11] A. Pais, "Some Remarks on the V-Particles," Phys. Rev. **86**, 663 (1952). doi:10.1103/PhysRev.86.663

[12] M. Gell-Mann, "Isotopic Spin and New Unstable Particles," Phys. Rev. **92**, 833 (1953). doi:10.1103/PhysRev.92.833

[13] T. Nakano and K. Nishijima, "Charge Independence for V-particles," Prog. Theor. Phys. **10**, 581 (1953). doi:10.1143/PTP.10.581

[14] O. W. Greenberg, "Spin and Unitary Spin Independence in a Paraquark Model of Baryons and Mesons," Phys. Rev. Lett. **13**, 598 (1964). doi:10.1103/PhysRevLett.13.598

[15] J. J. Aubert *et al.* [E598 Collaboration], "Experimental Observation of a Heavy Particle J," Phys. Rev. Lett. **33**, 1404 (1974). doi:10.1103/PhysRevLett.33.1404; J. E. Augustin *et al.* [SLAC-SP-017 Collaboration], "Discovery of a Narrow Resonance in e^+e^- Annihilation," Phys. Rev. Lett. **33**, 1406 (1974) [Adv. Exp. Phys. **5**, 141 (1976)]. doi:10.1103/PhysRevLett.33.1406

[16] J. D. Bjorken and S. L. Glashow, "Elementary Particles and SU(4)," Phys. Lett. **11**, 255 (1964). doi:10.1016/0031-9163(64)90433-0

[17] G. Goldhaber *et al.*, "Observation in e+ e- Annihilation of a Narrow State at 1865-MeV/c^2 Decaying to $K\ \pi$ and $K\ \pi\ \pi\ \pi$," Phys. Rev. Lett. **37**, 255 (1976). doi:10.1103/PhysRevLett.37.255; I. Peruzzi *et al.*, "Observation of a Narrow Charged State at 1876-MeV/c^2 Decaying to an Exotic Combination of $K\ \pi\ \pi$," Phys. Rev. Lett. **37**, 569 (1976). doi:10.1103/PhysRevLett.37.569

[18] R. Brandelik *et al.* [DASP Collaboration], "Evidence for the F Meson," Phys. Lett. **70B**, 132 (1977). doi:10.1016/0370-2693(77)90361-6

[19] M. L. Perl *et al.*, "Evidence for Anomalous Lepton Production in $e^+ - e^-$ Annihilation," Phys. Rev. Lett. **35**, 1489 (1975). doi:10.1103/PhysRevLett.35.1489

[20] S. W. Herb *et al.*, "Observation of a Dimuon Resonance at 9.5-GeV in 400-GeV Proton-Nucleus Collisions," Phys. Rev. Lett. **39**, 252 (1977). doi:10.1103/PhysRevLett.39.252

[21] S. Behrends *et al.* [CLEO Collaboration], "Observation of Exclusive Decay Modes of B Flavored Mesons," Phys. Rev. Lett. **50**, 881 (1983). doi:10.1103/PhysRevLett.50.881

[22] F. Abe *et al.* [CDF Collaboration], "Observation of top quark production in $\bar{p}p$ collisions," Phys. Rev. Lett. **74**, 2626 (1995) doi:10.1103/PhysRevLett.74.2626 [hep-ex/9503002].; S. Abachi *et al.* [D0 Collaboration], "Observation of the top quark," Phys. Rev. Lett. **74**, 2632 (1995) doi:10.1103/PhysRevLett.74.2632 [hep-ex/9503003].

[23] S. Weinberg, "A Model of Leptons," Phys. Rev. Lett. **19**, 1264 (1967). doi:10.1103/PhysRevLett.19.1264

[24] F. Halzen and A. D. Martin, "Quarks And Leptons: An Introductory Course In Modern Particle Physics," New York, USA: Wiley (1984) 396p

[25] M. D. Schwartz, "Quantum Field Theory and the Standard Model," Cambridge, UK: Cambridge University Press (2014) 850p

[26] S. Chatrchyan *et al.* [CMS Collaboration], "Observation of a new boson at a mass of 125 GeV with the CMS experiment at the LHC," Phys. Lett. B **716**, 30 (2012) doi:10.1016/j.physletb.2012.08.021 [arXiv:1207.7235 [hep-ex]].;G. Aad *et al.* [ATLAS Collaboration], "Observation of a new particle in the search for the Standard Model Higgs boson with the ATLAS detector at the LHC," Phys. Lett. B **716**, 1 (2012) doi:10.1016/j.physletb.2012.08.020 [arXiv:1207.7214 [hep-ex]].

[27] A. A. Petrov and A. E. Blechman, "Effective Field Theories," Singapore: World Scientific (2016) 303p

[28] M. E. Peskin and D. V. Schroeder, "An Introduction to quantum field theory," Westview Press (1995) 842p

[29] Q. R. Ahmad *et al.* [SNO Collaboration], "Direct evidence for neutrino flavor transformation from neutral current interactions in the Sudbury Neutrino Observatory," Phys. Rev. Lett. **89**, 011301 (2002) doi:10.1103/PhysRevLett.89.011301 [nucl-ex/0204008].

[30] T. P. Cheng and L. F. Li, "$\mu \to e\gamma$ in Theories With Dirac and Majorana Neutrino Mass Terms," Phys. Rev. Lett. **45**, 1908 (1980). doi:10.1103/PhysRevLett.45.1908

[31] T. P. Cheng and L. F. Li, "Gauge Theory Of Elementary Particle Physics," Oxford, Uk: Clarendon (1984) 536 P. (Oxford Science Publications)

[32] T. P. Cheng and L. F. Li, "Nonconservation of Separate mu - Lepton and e - Lepton Numbers in Gauge Theories with v+a Currents," Phys. Rev. Lett. **38**, 381 (1977). doi:10.1103/PhysRevLett.38.381

[33] L. Calibbi and G. Signorelli, arXiv:1709.00294 [hep-ph].

[34] C. Patrignani *et al.* [Particle Data Group], "Review of Particle Physics," Chin. Phys. C **40**, no. 10, 100001 (2016) and 2017 update. doi:10.1088/1674-1137/40/10/100001

[35] D. E. Hazard and A. A. Petrov, "Lepton flavor violating quarkonium decays," Phys. Rev. D **94**, no. 7, 074023 (2016)

[36] D. E. Hazard and A. A. Petrov, "Radiative lepton flavor violating B, D, and K decays," arXiv:1711.05314 [hep-ph].

[37] M. Raidal *et al.*, "Flavour physics of leptons and dipole moments," Eur. Phys. J. C **57**, 13 (2008) doi:10.1140/epjc/s10052-008-0715-2 [arXiv:0801.1826 [hep-ph]].

[38] H. K. Dreiner, G. Polesello and M. Thormeier, "Bounds on broken R parity from leptonic meson decays," Phys. Rev. D **65**, 115006 (2002) doi:10.1103/PhysRevD.65.115006 [hep-ph/0112228].

[39] H. K. Dreiner, M. Kramer and B. O'Leary, "Bounds on R-parity violating supersymmetric couplings from leptonic and semi-leptonic meson decays," Phys. Rev. D **75**, 114016 (2007) doi:10.1103/PhysRevD.75.114016 [hep-ph/0612278].

[40] K. S. Sun, T. F. Feng, T. J. Gao and S. M. Zhao, "Search for lepton flavor violation in supersymmetric models via meson decays," Nucl. Phys. B **865**, 486 (2012) doi:10.1016/j.nuclphysb.2012.08.005 [arXiv:1208.2404 [hep-ph]].

[41] M. Lindner, M. Platscher and F. S. Queiroz, "A Call for New Physics : The Muon Anomalous Magnetic Moment and Lepton Flavor Violation," arXiv:1610.06587 [hep-ph].

[42] A. Celis, V. Cirigliano and E. Passemar, "Model-discriminating power of lepton flavor violating τ decays," Phys. Rev. D **89**, no. 9, 095014 (2014) doi:10.1103/PhysRevD.89.095014 [arXiv:1403.5781 [hep-ph]].

[43] W. Buchmuller and D. Wyler, "Effective Lagrangian Analysis of New Interactions and Flavor Conservation," Nucl. Phys. B **268**, 621 (1986). doi:10.1016/0550-3213(86)90262-2

[44] B. Grzadkowski, M. Iskrzynski, M. Misiak and J. Rosiek, "Dimension-Six Terms in the Standard Model Lagrangian," JHEP **1010**, 085 (2010) doi:10.1007/JHEP10(2010)085 [arXiv:1008.4884 [hep-ph]].

[45] R. Alonso, E. E. Jenkins, A. V. Manohar and M. Trott, "Renormalization Group Evolution of the Standard Model Dimension Six Operators III: Gauge Coupling Dependence and Phenomenology," JHEP **1404**, 159 (2014) doi:10.1007/JHEP04(2014)159 [arXiv:1312.2014 [hep-ph]].

[46] G. Buchalla, A. J. Buras and M. E. Lautenbacher, "Weak decays beyond leading logarithms," Rev. Mod. Phys. **68**, 1125 (1996)

[47] A. A. Petrov and D. V. Zhuridov, "Lepton flavor-violating transitions in effective field theory and gluonic operators," Phys. Rev. D **89**, no. 3, 033005 (2014) doi:10.1103/PhysRevD.89.033005 [arXiv:1308.6561 [hep-ph]].

[48] V. Cirigliano, G. Ecker, H. Neufeld, A. Pich and J. Portoles, "Kaon Decays in the Standard Model," Rev. Mod. Phys. **84**, 399 (2012) doi:10.1103/RevModPhys.84.399 [arXiv:1107.6001 [hep-ph]].

[49] S. Nussinov, R. D. Peccei and X. M. Zhang, "On unitarity based relations between various lepton family violating processes," Phys. Rev. D **63**, 016003 (2001) doi:10.1103/PhysRevD.63.016003 [hep-ph/0004153].

[50] C. X. Yue and J. R. Zhou, "New gauge boson Z? and lepton flavor violating decays and production of vector mesons," Phys. Rev. D **93**, no. 3, 035021 (2016) doi:10.1103/PhysRevD.93.035021 [arXiv:1602.00211 [hep-ph]].

[51] A. Abada, D. Becirevic, M. Lucente and O. Sumensari, "Lepton flavor violating decays of vector quarkonia and of the Z boson," Phys. Rev. D **91**, no. 11, 113013 (2015) doi:10.1103/PhysRevD.91.113013 [arXiv:1503.04159 [hep-ph]].

[52] T. Gutsche, J. C. Helo, S. Kovalenko and V. E. Lyubovitskij, "New bounds on lepton flavor violating decays of vector mesons and the Z0 boson," Phys. Rev. D **83**, 115015 (2011) doi:10.1103/PhysRevD.83.115015 [arXiv:1103.1317 [hep-ph]].

[53] D. Black, T. Han, H. J. He and M. Sher, Phys. Rev. D **66**, 053002 (2002) doi:10.1103/PhysRevD.66.053002 [hep-ph/0206056].

[54] J. P. Lees *et al.* [BaBar Collaboration], "Search for Charged Lepton Flavor Violation in Narrow Upsilon Decays," Phys. Rev. Lett. **104**, 151802 (2010) doi:10.1103/PhysRevLett.104.151802 [arXiv:1001.1883 [hep-ex]].

[55] D. Becirevic, G. Duplancia, B. Klajn, B. Meli and F. Sanfilippo, "Lattice QCD and QCD sum rule determination of the decay constants of η_c, J/ψ and h_c states," Nucl. Phys. B **883**, 306 (2014) doi:10.1016/j.nuclphysb.2014.03.024 [arXiv:1312.2858 [hep-ph]].

[56] B. Colquhoun, R. J. Dowdall, C. T. H. Davies, K. Hornbostel and G. P. Lepage, "Υ and Υ' Leptonic Widths, a_μ^b and m_b from full lattice QCD," Phys. Rev. D **91**, no. 7, 074514 (2015) doi:10.1103/PhysRevD.91.074514 [arXiv:1408.5768 [hep-lat]].

[57] M. S. Maior de Sousa and R. Rodrigues da Silva, "The $\rho(2S)$ and $\psi(2S)$ meson in a double pole QCD Sum Rules," arXiv:1205.6793 [hep-ph].

[58] G. C. Donald *et al.* [HPQCD Collaboration], "V_{cs} from $D_s \to \phi\ell\nu$ semileptonic decay and full lattice QCD," Phys. Rev. D **90**, no. 7, 074506 (2014) doi:10.1103/PhysRevD.90.074506 [arXiv:1311.6669 [hep-lat]].

[59] Y. Chen, A. Alexandru, T. Draper, K. F. Liu, Z. Liu and Y. B. Yang, "Leptonic Decay Constant of ρ at Physical Point," arXiv:1507.02541 [hep-ph]; V. V. Braguta, "The study of leading twist light cone wave functions of J/psi meson," Phys. Rev. D **75**, 094016 (2007) doi:10.1103/PhysRevD.75.094016 [hep-ph/0701234 [HEP-PH]].

[60] A. Khodjamirian, T. Mannel and A. A. Petrov, "Direct probes of flavor-changing neutral currents in e^+ e^--collisions," JHEP **1511**, 142 (2015) doi:10.1007/JHEP11(2015)142 [arXiv:1509.07123 [hep-ph]].

[61] A. A. Petrov and W. Shepherd, "Searching for dark matter at LHC with Mono-Higgs production," Phys. Lett. B **730**, 178 (2014) doi:10.1016/j.physletb.2014.01.051 [arXiv:1311.1511 [hep-ph]].

[62] N. Brambilla *et al.*, "Heavy quarkonium: progress, puzzles, and opportunities," Eur. Phys. J. C **71**, 1534 (2011) doi:10.1140/epjc/s10052-010-1534-9 [arXiv:1010.5827 [hep-ph]].

[63] C. McNeile, C. T. H. Davies, E. Follana, K. Hornbostel and G. P. Lepage, "Heavy meson masses and decay constants from relativistic heavy quarks in full lattice QCD," Phys. Rev. D **86**, 074503 (2012) doi:10.1103/PhysRevD.86.074503 [arXiv:1207.0994 [hep-lat]].

[64] M. Beneke and M. Neubert, "Flavor singlet B decay amplitudes in QCD factorization," Nucl. Phys. B **651**, 225 (2003) doi:10.1016/S0550-3213(02)01091-X [hep-ph/0210085].

[65] B. Aubert *et al.* [BaBar Collaboration], "Searches for the decays $B^0 \to \ell^\pm\tau^\mp$ and $B^+ \to \ell^+\nu$ ($\ell = e,\ \mu$) using hadronic tag reconstruction," Phys. Rev. D **77**, 091104 (2008) doi:10.1103/PhysRevD.77.091104 [arXiv:0801.0697 [hep-ex]].

[66] D. Ambrose *et al.* [BNL Collaboration], "New limit on muon and electron lepton number violation from $K_L^0 \to \mu^\pm e^\mp$ decay," Phys. Rev. Lett. **81**, 5734 (1998) doi:10.1103/PhysRevLett.81.5734 [hep-ex/9811038].

[67] R. Aaij *et al.* [LHCb Collaboration], "Search for the lepton-flavour violating decay $D^0 \to e^\pm\mu^\mp$," Phys. Lett. B **754**, 167 (2016) doi:10.1016/j.physletb.2016.01.029 [arXiv:1512.00322 [hep-ex]].

[68] R. Aaij *et al.* [LHCb Collaboration], "Search for the lepton-flavour violating decays $B^0_{(s)} \to e^\pm\mu^\mp$," arXiv:1710.04111 [hep-ex].

[69] W. Altmannshofer, C. Niehoff and D. M. Straub, "$B_s \to \mu^+\mu^-$ as current and future probe of new physics," JHEP **1705**, 076 (2017) doi:10.1007/JHEP05(2017)076 [arXiv:1702.05498 [hep-ph]].

[70] M. Beneke, C. Bobeth and R. Szafron, "Enhanced electromagnetic correction to the rare B-meson decay $B_{s,d} \to \mu^+\mu^-$," arXiv:1708.09152 [hep-ph].

[71] T. Blake, G. Lanfranchi and D. M. Straub, "Rare B Decays as Tests of the Standard Model," Prog. Part. Nucl. Phys. **92**, 50 (2017) doi:10.1016/j.ppnp.2016.10.001 [arXiv:1606.00916 [hep-ph]].

[72] C. Bobeth, M. Gorbahn, T. Hermann, M. Misiak, E. Stamou and M. Steinhauser, "$B_{s,d} \to l^+l^-$ in the Standard Model with Reduced Theoretical Uncertainty," Phys. Rev. Lett. **112**, 101801 (2014) doi:10.1103/PhysRevLett.112.101801 [arXiv:1311.0903 [hep-ph]].

[73] C. Bobeth, M. Gorbahn and E. Stamou, "Electroweak Corrections to $B_{s,d} \to \ell^+\ell^-$," Phys. Rev. D **89**, no. 3, 034023 (2014) doi:10.1103/PhysRevD.89.034023 [arXiv:1311.1348 [hep-ph]].

[74] Y. Amhis *et al.*, "Averages of b-hadron, c-hadron, and τ-lepton properties as of summer 2016," arXiv:1612.07233 [hep-ex].

[75] R. J. Dowdall *et al.* [HPQCD Collaboration], "B-Meson Decay Constants from Improved Lattice Nonrelativistic QCD with Physical u, d, s, and c Quarks," Phys. Rev. Lett. **110**, no. 22, 222003 (2013) doi:10.1103/PhysRevLett.110.222003 [arXiv:1302.2644 [hep-lat]].

[76] N. Carrasco *et al.*, "Leptonic decay constants f_K, f_D, and f_{D_s} with $N_f = 2 + 1 + 1$ twisted-mass lattice QCD," Phys. Rev. D **91**, no. 5, 054507 (2015) doi:10.1103/PhysRevD.91.054507 [arXiv:1411.7908 [hep-lat]].

[77] S. Godfrey and H. E. Logan, "Probe of new light Higgs bosons from bottomonium χ_{b0} decay," Phys. Rev. D **93**, no. 5, 055014 (2016) doi:10.1103/PhysRevD.93.055014 [arXiv:1510.04659 [hep-ph]].

[78] S. Godfrey and K. Moats, "Bottomonium Mesons and Strategies for their Observation," Phys. Rev. D **92**, no. 5, 054034 (2015) doi:10.1103/PhysRevD.92.054034 [arXiv:1507.00024 [hep-ph]].

[79] Y. G. Aditya, K. J. Healey and A. A. Petrov, "Searching for super-WIMPs in leptonic heavy meson decays," Phys. Lett. B **710**, 118 (2012) doi:10.1016/j.physletb.2012.02.042 [arXiv:1201.1007 [hep-ph]].

[80] D. E. Hazard and A. A. Petrov, to be published

[81] Z. Dziembowski and L. Mankiewicz, "Light Meson Distribution Amplitude: A Simple Relativistic Model," Phys. Rev. Lett. **58**, 2175 (1987). doi:10.1103/PhysRevLett.58.2175

[82] A. Szczepaniak, E. M. Henley and S. J. Brodsky, "Perturbative QCD Effects in Heavy Meson Decays," Phys. Lett. B **243**, 287 (1990). doi:10.1016/0370-2693(90)90853-X

[83] G. P. Lepage and S. J. Brodsky, "Exclusive Processes in Perturbative Quantum Chromodynamics," Phys. Rev. D **22**, 2157 (1980). doi:10.1103/PhysRevD.22.2157

[84] Y. G. Aditya, K. J. Healey and A. A. Petrov, "Faking $B_s \to \mu^+\mu^-$," Phys. Rev. D **87**, 074028 (2013) doi:10.1103/PhysRevD.87.074028 [arXiv:1212.4166 [hep-ph]].

[85] F. Kruger and D. Melikhov, "Gauge invariance and form-factors for the decay $B \to \gamma l^+ l^-$," Phys. Rev. D **67**, 034002 (2003) doi:10.1103/PhysRevD.67.034002 [hep-ph/0208256].

[86] D. Melikhov, A. Kozachuk and N. Nikitin, "Rare FCNC radiative leptonic decays $B \to \gamma \ell^+ \ell^-$," PoS (EPS-HEP2017) 228 [arXiv:1710.02719 [hep-ph]].

[87] A. Kozachuk, D. Melikhov and N. Nikitin, "Rare radiative leptonic B-decays," EPJ Web Conf. **125**, 02015 (2016) doi:10.1051/epjconf/201612502015 [arXiv:1609.06491 [hep-ph]].

[88] D. Melikhov and N. Nikitin, "Rare radiative leptonic decays $B(d,s) \to l^+ l^- \gamma$," Phys. Rev. D **70**, 114028 (2004) doi:10.1103/PhysRevD.70.114028 [hep-ph/0410146].

[89] D. Guadagnoli, D. Melikhov and M. Reboud, "More Lepton Flavor Violating Observables for LHCb's Run 2," Phys. Lett. B **760** (2016) 442 doi:10.1016/j.physletb.2016.07.028 [arXiv:1605.05718 [hep-ph]].

[90] S. L. Glashow, D. Guadagnoli and K. Lane, "Lepton Flavor Violation in B Decays?," Phys. Rev. Lett. **114**, 091801 (2015) doi:10.1103/PhysRevLett.114.091801 [arXiv:1411.0565 [hep-ph]].

[91] W. A. Bardeen and W. K. Tung, "Invariant amplitudes for photon processes," Phys. Rev. **173**, 1423 (1968) Erratum: [Phys. Rev. D **4**, 3229 (1971)]. doi:10.1103/PhysRevD.4.3229, 10.1103/PhysRev.173.1423

[92] H. W. Fearing, G. R. Goldstein and M. J. Moravcsik, "Amplitude structure of off-shell processes," Phys. Rev. D **29**, 2612 (1984). doi:10.1103/PhysRevD.29.2612

[93] M. D. Scadron and H. F. Jones, "Covariant M functions for higher spin," Phys. Rev. **173**, 1734 (1968). doi:10.1103/PhysRev.173.1734

[94] M. Beyer, D. Melikhov, N. Nikitin and B. Stech, "Weak annihilation in the rare radiative $B \to \rho\gamma$ decay," Phys. Rev. D **64**, 094006 (2001) doi:10.1103/PhysRevD.64.094006 [hep-ph/0106203].

[95] A. M. Baldini *et al.* [MEG Collaboration], "Search for the lepton flavour violating decay $\mu^+ \to e^+\gamma$ with the full dataset of the MEG experiment," Eur. Phys. J. C **76**, no. 8, 434 (2016) doi:10.1140/epjc/s10052-016-4271-x [arXiv:1605.05081 [hep-ex]].

[96] B. Aubert *et al.* [BaBar Collaboration], "Searches for Lepton Flavor Violation in the Decays $\tau^\pm \to e^\pm\gamma$ and $\tau^\pm \to \mu^\pm\gamma$," Phys. Rev. Lett. **104** (2010) 021802 doi:10.1103/PhysRevLett.104.021802 [arXiv:0908.2381 [hep-ex]].

[97] M. D. Scadron, R. Delbourgo and G. Rupp, "Constituent quark masses and the electroweak standard model," J. Phys. G **32**, 735 (2006) doi:10.1088/0954-3899/32/5/009 [hep-ph/0603196].

[98] R. Bruser, T. Feldmann, B. O. Lange, T. Mannel and S. Turczyk, "Angular analysis of new physics operators in polarized $\tau \to 3\ell$ decays," JHEP **1510**, 082 (2015) doi:10.1007/JHEP10(2015)082 [arXiv:1506.07786 [hep-ph]].

[99] D. Melikhov "$D \to \gamma$ Form Factors" (Personal Communication)

[100] D. Melikhov and B. Stech, "Weak form-factors for heavy meson decays: An Update," Phys. Rev. D **62**, 014006 (2000) doi:10.1103/PhysRevD.62.014006 [hep-ph/0001113].

ABSTRACT

APPLICATIONS OF EFFECTIVE FIELD THEORIES TO NEW PHYSICS

by

DEREK E. HAZARD

May 2018

Advisor: Dr. Alexey A. Petrov

Major: Physics

Degree: Doctor of Philosophy

We apply an effective field theory approach and argue that lepton flavor violating (LFV) decays $M \to \ell_1 \bar{\ell}_2$ of meson states M with different quantum numbers could be used to put constraints on the Wilson coefficients of effective operators describing LFV interactions at low energy scales. We note that the restricted kinematics of the two-body decay of quarkonium or a heavy quark meson allows us to select operators with particular quantum numbers, significantly reducing the reliance on the *single operator dominance* assumption that is prevalent in constraining parameters of the effective LFV Lagrangian. We shall also argue that studies of radiative lepton flavor violating $M \to \gamma \ell_1 \bar{\ell}_2$ decays could provide important complementary access to those effective operators in addition to primary access to operators that cannot be constrained via two-body decays.

AUTOBIOGRAPHICAL STATEMENT

Name: Derek E. Hazard

Education:
M.Sc. Physics, Wayne State University, Detroit, MI, 2014
B.Sc. Applied Physics, Kettering University, Flint, MI, 2011
B.Sc. Applied Mathematics, Kettering University, Flint, MI, 2011

Professional Experience:
Teaching Assistant, Dept. of Physics and Astronomy, Wayne State University, 2016–2017
Research Assistant, Dept. of Physics and Astronomy, Wayne State University, 2013–2016
Teaching Assistant, Dept. of Physics and Astronomy, Wayne State University, 2012–2013
Cooperative Education Student, Umicore Autocat, Auburn Hills, MI, 2008–2011

Publications:
Radiative lepton flavor violating B, D, and K decays
D. E. Hazard & A. A. Petrov
e-print Archive: arXiv:1711.05314 [hep-ph].

Lepton flavor violating meson decays
Talk presented at the APS Division of Particles and Fields Meeting (DPF 2017), July 31-August 4, 2017, Fermilab. C170731
D. E. Hazard
e-print Archive: arXiv:1710.00117 [hep-ph].

Lepton flavor violating quarkonium decays
D. E. Hazard & A. A. Petrov
Phys. Rev. D**94**, 074023 (2016) 7,
e-print Archive: arXiv:1607.00815 [hep-ph].

Born in Flint, MI in December of 1988, Derek is a mid-westerner through and through. His father worked in the blue collar family business as a water well contractor and his mother was employed in the human resources division of General Motors. They taught him the values of hard work without which he could not have made it through graduate school.

As a young boy he was always fascinated by the world around him and what makes it work. The questions to his father were endless. He carried this curiosity throughout his childhood and into his teenage years where he applied it to his studies.

He excelled in science and mathematics. This drive and curiosity lead him to finish Calculus II and III during his Senior year in high school and to become valedictorian of his class in 2007.

This pace continued throughout his undergraduate studies and allowed him to complete two degrees in four years. Traveling on this academic momentum he decided to immediately enter graduate school to pursue his Ph.D. in physics. After six years of hard work he finished his Ph.D. in December of 2017. He plans to pursue a postdoctoral position.